STUDY OF ELECTROMAGNETIC TRANSITIONS IN ^{37}Ar

by

Charles E. Ragan III

Department of Physics
Duke University

Date: _____

Approved:

_____
N. R. Roberson, Supervisor

_____

_____

_____

_____

A dissertation submitted in partial fulfillment of the requirements for the degree of Doctor of Philosophy in the Department of Physics in the Graduate School of Arts and Sciences of Duke University

1970

ABSTRACT

(Physics)

STUDY OF ELECTROMAGNETIC TRANSITIONS IN ^{37}Ar

by

Charles E. Ragan III

Department of Physics
Duke University

Date: _____

Approved:

_____
N. R. Roberson, Supervisor

_____

_____

_____

_____

An abstract of a dissertation submitted in partial fulfillment of the requirements for the degree of Doctor of Philosophy in the Department of Physics in the Graduate School of Arts and Sciences of Duke University

1970

Abstract

STUDY OF ELECTROMAGNETIC TRANSITIONS
IN ^{37}Ar

The mean lifetimes of the levels of ^{37}Ar below 3.0 MeV excitation energy have been measured using the Doppler shift attenuation method (DSAM). The levels were populated by the endothermic $^{34}S(\alpha,n)^{37}Ar$ reaction (Q_o = -4.629 MeV). A 450 $\mu g/cm^2$ CdS target (enriched to 85.61% in ^{34}S) evaporated onto a 1 μ Ni foil was bombarded with α particles ranging in energy from 7.6 to 8.8 MeV. Gamma rays were detected at 0, 37, 45, 55, 90, and 143° to the beam axis with a 30-cc Ge(Li) detector. The following mean lifetimes were found: τ(1.41-MeV level) = $1.08 \pm {}^{0.17}_{0.13}$ psec, τ(2.22) = 380 ± 50 fsec, τ(2.49) = $775 \pm {}^{105}_{89}$ fsec, and τ(2.80) = 14 ± 11 fsec. Excitation energies for the first five excited states were determined from the ground state transitions. All five levels were found to γ decay 100% to the ground state and upper limits were set on other possible transitions. The angular distributions of the γ rays were measured. Analysis of these distributions for the levels at 1.41, 1.61, and 2.49 MeV gave spins in agreement with previous assignments. On the basis of the angular distribution and the lifetime a most probable spin-parity of $(7/2^+)$ was assigned to the

2.22-MeV level. The mean lives of the positive parity states are in good agreement with those predicted from many particle shell-model calculations. A full description of the DSAM is presented along with a description of the energy loss of heavy ions in matter.

ACKNOWLEDGMENTS

I wish to express my gratitude to my advisor, Dr. N. R. Roberson, for his interest and support during all phases of my graduate career. I am also indebted to Dr. G. E. Mitchell for many helpful discussions and for his assistance in preparing work for publication. I extend my thanks also to Dr. D. R. Tilley for his assistance in data collection and for many helpful discussions. I also wish to thank Dr. C. E. Moss for many helpful discussions in the early phases of this work concerning the design of the experimental apparatus and the analysis of the data. I am indebted to Dr. R. V. Poore for his continued help with computer programing. I also extend my appreciation to Dr. C. R. Gould for his assistance in data collection and for helpful discussions concerning the analysis of the angular distributions.

I wish to thank Drs. E. K. Warburton and J. W. Olness for supplying me with copies of their energy-loss and line-shape analysis codes which were used in the early stages of this investigation. I also wish to thank Dr. A. E. L. Dieperink and Dr. B. H. Wildenthal for providing me with the results of their theoretical calculations. I extend my appreciation

to Mr. G. P. Lamaze and Mr. E. C. Hagen for their assistance in collecting the experimental data. I wish to thank Mr. S. E. Edwards for his help with the electronics and Mr. R. L. Rummel and the entire Nuclear Structure Group for assistance with the accelerator. I am obliged to Mrs. Joseph Bailey who did an excellent job in preparing the illustrations. Thanks are also extended to the Duke University Instrument Shop and especially to Mr. A. W. Lovette for many helpful suggestions concerning the design of the target chamber. I am grateful to Dr. H. W. Newson and Dr. E. G. Bilpuch for providing me with the research assistantship.

Thanks are also extended to Dr. W. E. Anderson and Dr. A. W. Hanson at the Citadel for their encouragement during my academic career. Special thanks are extended to my parents and my wife, Sara, who have offered continued encouragement.

This work was supported in part by the U. S. Atomic Energy Commission.

C. E. R., III

CONTENTS

LIST OF FIGURES

LIST OF TABLES

STUDY OF ELECTROMAGNETIC TRANSITIONS IN ^{37}Ar

Chapter I

INTRODUCTION

A. Historical Background

The basic picture of the composition of the nucleus became established following the discovery of the neutron by Chadwick in 1932 and the suggestion by Heisenberg that the nucleus was composed of neutrons and protons. This advance opened the way for the development of models of nuclear structure. (1-3) The extranuclear structure of atoms provided the basis for an early (1933) independent-particle model of the nucleus involving closed shells for $2(2\ell+1)$ neutrons and protons. The relative stability of nuclei with N or Z equal to 2, 8, and 20 nucleons had been observed experimentally, but there was little additional evidence in support of a nuclear shell model. Successful application of the liquid-drop model (starting in 1935) suggested that the interaction between the nucleons in a nucleus is so strong that shell effects would not be noticeable. (1, 2)

Attention was again turned to the shell model in 1948 when M. Mayer (1, 2) presented a large body of experimental facts in support

of periodic properties of nuclei as a function of N or Z. Mayer and independently Haxel, Jensen, and Suess (1, 2) in 1949 introduced the concept of jj coupling into the independent-particle model. By assuming strong spin-orbit forces for individual nucleons, a sequence of independent-particle states emerged which were able to account for the experimentally known "magic numbers." The nuclear shell model in the form presented by Mayer has enjoyed many successes in explaining nuclear properties. Most of the successes, however, have been concerned with nuclear properties near closed shells. One of the early failures of the independent-particle model was its inability to predict certain collective features of heavy nuclei (A=150-190 and A$\geq$222). The collective model (3) originally proposed by A. Bohr in 1951 and extended by Bohr, Mottelson, and Nilsson (3) was able to explain many nuclear properties in this mass region. In 1956 Litherland et al. (3) used the Nilsson (3) model to successfully explain the low-lying states of ^{25}Al. Since this time the properties of many nuclei near the lower end of the 2s-1d shell have been explained in terms of the collective model.

Theoretical interpretation of the properties of nuclei near the middle and upper end of the 2s-1d shell has been difficult. Some nuclei have been interpreted in terms of the collective model (see for example reference 3), but often this approach has not been successful. Another approach used in the 2s-1d shell is a refinement of the extreme independent particle model -- so-called configuration mixing. This refinement

assumes that the nucleus consists of a "closed core" plus nucleons distributed throughout a number of shell-model states. The "closed core" is usually assumed to be a major shell closure, but in some cases the "closed core" is assumed to be a filled subshell (such as ^{28}Si). Practical problems such as the sizes of computer memories have dictated the number of shell-model states that could be used as the basis states for nuclear wave functions. The number of shell-model states included in the wave function in a given model has increased with the development of larger and faster computers.

Traditionally, the first test of a nuclear model has been to examine whether the model can correctly reproduce the experimentally observed energy levels and their spins and parities. The relative energies of the calculated levels is often insensitive to the details of the wave functions. Thus it is desirable to have a more sensitive means of testing the wave functions provided by the model. The properties of electromagnetic transitions between nuclear levels provide one such test.

The parameters of interest in electromagnetic transitions are the matrix elements of the allowed multipole operators for the states connected by transitions. Since the interaction of the electromagnetic field with the nucleus is a well understood phenomenon, most of the uncertainty in calculating the matrix elements is due to the uncertainty in the wave functions. Electromagnetic matrix elements thus provide a quite sensitive test of nuclear wave functions without any dependence on nuclear forces or

reaction mechanisms.

In general the lifetime [or total width ($\Gamma = \hbar/\tau$)] of a level is not directly related to a matrix element. The magnitude of a matrix element is determined by measuring a partial radiative width. A partial width is usually determined in three steps: First, the lifetime or total width is determined. Next, the fractional decay to a given final level (branching ratio) is determined. This partial width must further be separated into contributions from competing multipoles by measuring the mixing ratio. (There are some exceptions to this procedure for determining a partial width such as Coulomb excitation measurements where the partial width is determined directly.)

B. Techniques for Lifetime Measurements

The lifetimes of excited states of nuclei span a very broad range, and the technique suitable for measuring the lifetime of a given level depends, of course, upon the magnitude of the lifetime. Table I gives some of the most commonly used methods of measuring lifetimes of bound nuclear levels, along with the region of applicability of each method. These regions are not to be considered as absolute but vary with the energy of the de-exciting γ ray and with the reaction used to produce the level. At the present time, however, either limit can usually be reached only under ideal circumstances. The last two methods have the disadvantage that

TABLE I

Methods of Measuring Mean Lifetimes

Method	Range of Mean Lifetimes
Electronic Timing	$\tau \geq 5 \times 10^{-11}$ sec
Doppler Shift Attenuation	$5 \times 10^{-15} \leq \tau \leq 10^{-11}$ sec
Recoil Distance	$10^{-12} \leq \tau \leq 5 \times 10^{-9}$ sec
Resonance Fluorescence	$\tau \leq 10^{-10}$ sec
Coulomb Excitation	$10^{-15} \leq \tau \leq 10^{-8}$ sec

only the lifetimes of levels of stable nuclei can be measured.

The lifetimes of most of the previously measured bound states of nuclei with $A \leq 40$ are in the region 10^{-15} to 10^{-11} seconds. (4) Thus the Doppler shift attenuation method (DSAM) is seen to be the method that would generally be the most applicable in the 2s-1d shell. For lifetimes only slightly outside the upper limit for DSA work, however, the recoil distance method (RDM) is seen to be most applicable. Pioneer work in applying both of these methods was performed by Devons and co-workers. (5-7) In this early work the γ rays were detected with NaI(Tl) crystals which had energy resolutions of $\geq 7\%$. Usually heavy ion beams were used in order to give the excited nuclei large recoil velocities. In the DSA work the recoiling nuclei were assumed to lose energy only to the electrons of the stopping material, and the scattering by the atoms of the stopping material was neglected. In the work done using the RDM, slits were used to define the position at which the nuclei decayed. Neither of these methods was extremely accurate, and the number of states which could be studied was limited. However, this was a first step in measuring lifetimes of levels that could not be measured by any other methods.

Since Devon's initial work, technological improvements have increased the accuracy of both methods. Some improvements have been better amplifiers, larger multi-channel analyzers, and better electronics in general. The largest single factor in improving the accuracy, however, has been the development of lithium-drifted-germanium [Ge(Li)] γ-ray

detectors. (8) The energy resolution of a Ge(Li) detector is typically 0.2% but resolutions better than 0.15% have been obtained. Thus Ge(Li) detectors have meant an improvement of about a factor of 50 in resolution, and the measurable Doppler shifts have, therefore, decreased by this factor. Lower recoil velocities of the excited nuclei can be used, and many more levels have become accessible to study.

C. Objectives of the Present Study

In recent years more and more sophisticated calculations in the 2s-1d shell using complex shell-model wave functions have been made possible by the development of large, high-speed computers. At the same time the techniques for measuring lifetimes have been improving rapidly. In the mass region A = 30-34 a large amount of experimental information on the matrix elements of electromagnetic transitions has been accumulated. Recently Glaudemans et al. (9) have used many particle shell-model wave functions to calculate magnetic dipole and electric quadrupole transition rates and moments as well as β-decay rates in this mass region. General agreement between theory and experiment is very good, and for some nuclei (such as ^{33}S) agreement is excellent.

In view of the good agreement in the region A = 30-34, it is clear that more experimental information is needed near the upper end of the 2s-1d shell. Dieperink and Brussaard (10) have performed calcu-

lations for A =36-39 using the Tabakin (11) interaction for the effective two-body interaction. Nuclear moments were calculated, and where comparison with experiment was possible, electromagnetic transition rates for positive parity states were calculated. At the time of the calculations no transition rates for the positive parity states in ^{37}Ar had been determined experimentally. The main objective in this work was the determination of the lifetimes of the levels of ^{37}Ar. Since lifetimes are not the only properties needed to determine electromagnetic matrix elements, another objective was to study other γ-decay properties of the states. In order to meet these objectives, it was first necessary to develop procedures for measuring lifetimes in the range 10^{-15} to 10^{-10} seconds. As part of this development program, the lifetimes of the low-lying levels of ^{33}S and ^{34}S have been measured and the results published. (12-14) These publications are included in the appendices for completeness. The DSAM and the RDM were used in studying the levels of ^{33}S, but only the DSAM was necessary in studying ^{34}S. A complete description of the DSAM (which was used in measuring the lifetimes in ^{37}Ar) is presented in this dissertation.

D. Notes on ^{37}Ar

The available information on the levels of ^{37}Ar as of 1967 has been summarized by Endt and Van der Leun. (15) Figure 1 shows the

Figure 1. Energy level diagram of ^{37}Ar summarizing the available information at the beginning of this investigation. The excitation energies and uncertainties (in parentheses) in keV are shown along with the ℓ_n-value from the $^{36}Ar(d,p)^{37}Ar$ reaction. All of the information in this Figure is from reference 15 except for the spin assignment for the 2.22-MeV level which is from reference 19.

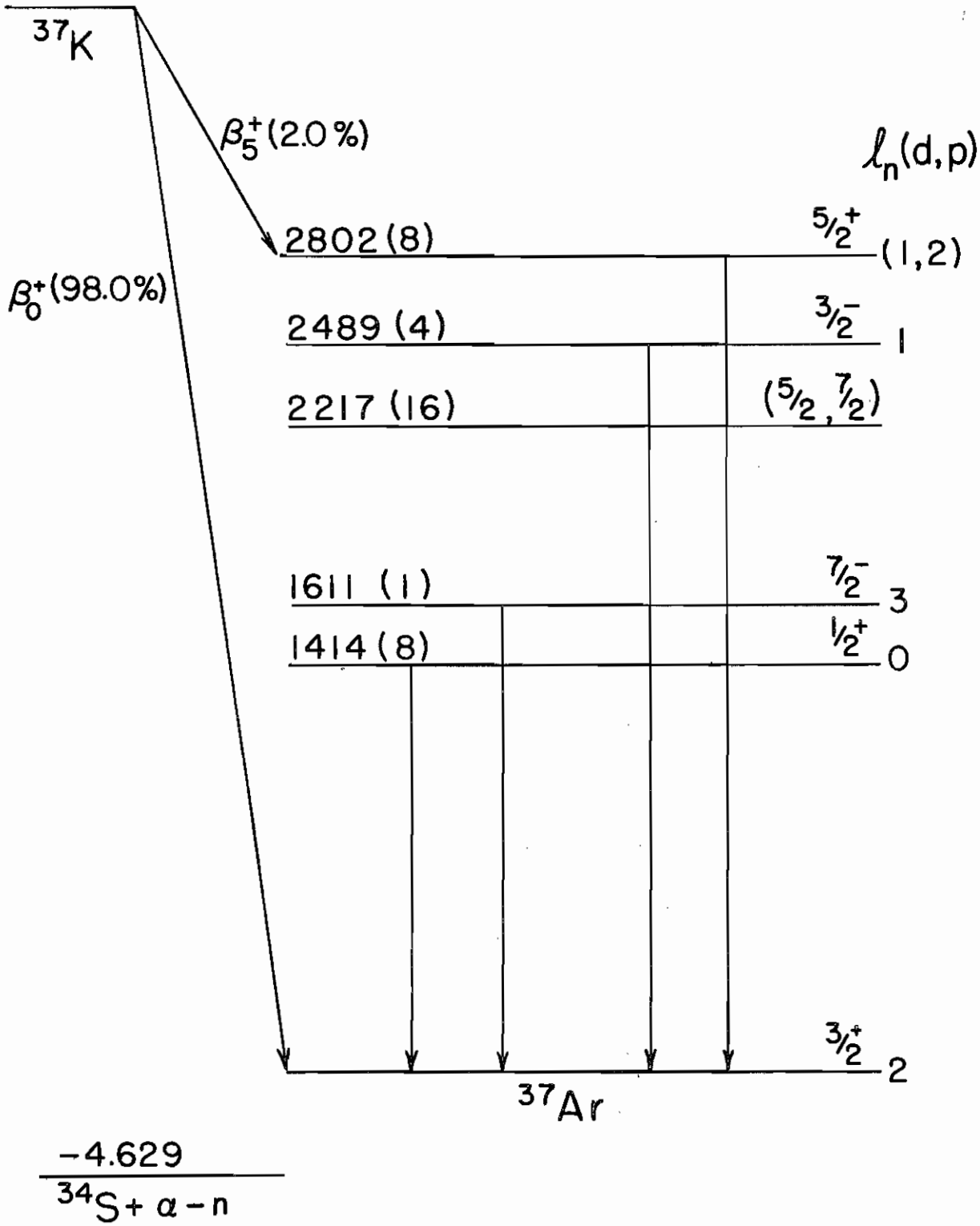
37K
β5+(2.0%)
β0+(98.0%)
ln(d,p)
2802(8)
5/2+
(1,2)
2489(4)
3/2−
1
2217(16)
(5/2, 7/2)
1611(1)
7/2−
3
1414(8)
1/2+
0
3/2+
2
37Ar
−4.629
34S + α − n

information available on the low-lying levels of ^{37}Ar at the beginning of this investigation. The excitation energies and uncertainties (in parentheses) in keV are shown along with the ℓ_n-values determined from the proton angular distribution from the ^{36}Ar(d,p)^{37}Ar reaction. (16)

The only spin assignment which is unambiguous is the value of $J^\pi = 1/2^+$ for the 1.41-MeV level. This spin was determined from the ℓ_n-value of 0 as well as from the fact that the ^{37}Cl(p,$n_1\gamma$)^{37}Ar angular correlation is isotropic. (17) The spin and parity of the 1.61-MeV level was assigned on the basis of the j-dependence of the (d,p) angular distribution (16) and a lifetime measurement. (18) The mean lifetime of this level was determined to be 5.15 ± 0.70 nsec by Goosman and Kavanagh (18) using a simple version of the RDM. This lifetime indicated an E3/M2 transition to the ground state and thus a J^π of $7/2^-$. Naude et al. (19) deduced a most probable spin for the 2.22-MeV level of (5/2, 7/2). This deduction was based on the analysis of ^{39}K(d,α)^{37}Ar cross section using fluctuation analysis and Hauser-Feshbach theory. The spin and parity of the 2.49-MeV level were determined from the j-dependence of the (d,p) angular distribution. (16) The spin and parity of the 2.80-MeV level were determined from the ℓ_n-value and from the β^+ decay of ^{37}K. Glaudemans et al. (20) were able to explain the fast (log ft = 3.8) β decay to this level only for an assignment of $J^\pi = 5/2^+$.

In the present investigation the levels of ^{37}Ar were populated using the ^{34}S(α,n)^{37}Ar reaction (Q_o = -4.629 MeV). The lifetimes of the

levels at 1.41, 2.22, 2.49, and 2.80 MeV were measured using the DSAM. The excitation energies and branching ratios for these levels as well as for the 1.61-MeV level were obtained. Since the levels of ^{37}Ar were populated at bombarding energies near threshold, the reaction is expected to be dominated by outgoing s-wave neutrons. If this is true, then the angular distribution of the γ rays can be analyzed using the method first suggested by Biedenharn, Arfken, and Rose (21) and developed by Litherland and Ferguson (Method II). (22) Angular distributions were, therefore, measured at two bombarding energies. Since the magnetic substates are not truly restricted, the method is not expected to be strictly rigorous. However, tentative checks on previous spin assignments could be made and some mixing ratios determined.

In Chapter II a description of the theory of lifetime measurements is given along with a description of the energy loss of heavy ions in matter. The experimental apparatus and procedure are described in Chapter III. A description of the method in which the data were analyzed is given in Chapter IV along with the results. In Chapter V the measured lifetimes are compared with two sets of theoretical calculations. The calculations by Dieperink (23) were performed using many particle shell-model wave functions with the two-body matrix elements determined from the Tabakin (11) interaction and assumed bare nucleon charges. The calculations by Wildenthal (24) used the Kuo-Brown matrix elements (25) for the two-body matrix elements and assumed $e_n = e_p = 0.5$ for the

electric quadrupole transitions and bare nucleon values for the magnetic dipole transitions. A summary and conclusions are presented in Chapter VI.

Chapter II

THEORY OF LIFETIME MEASUREMENTS

A. General

When sound waves of frequency ν are emitted by a source moving with respect to an observer, the frequency detected by the observer is different from ν. This effect was first pointed out by the Austrian scientist J. C. Doppler (1803-1853). A similar effect is observed for electromagnetic radiation emitted from a moving source. Since the energy of a photon is proportional to the frequency, a change in the frequency is equivalent to a change in the energy. This change in energy (frequency) is termed the Doppler effect, and the shift with respect to the original energy (frequency) is known as the Doppler shift.

Lifetime measurements of nuclear levels using Doppler shift techniques make use of the fact that the energy of a γ ray is proportional to the velocity of the source. If a γ ray is emitted at a time t by a nucleus moving with a velocity $v(t) \ll c$, the energy of the γ ray observed in a stationary detector is given by

$$E_\gamma(t) = E_{\gamma o}\left[1 + \frac{v(t)}{c} \cos \psi(t)\right] \quad , \tag{1}$$

where $E_{\gamma o}$ is the energy of the γ ray when the nucleus is at rest and $\psi(t)$ is the time-dependent angle between the direction of motion of the source and the direction in which the γ ray is detected. The Doppler shift $\Delta E_{\gamma}(t)$ is given by the relation

$$\Delta E_{\gamma}(t) = E_{\gamma}(t) - E_{\gamma o} = E_{\gamma o} \frac{v(t)}{c} \cos \psi(t) \quad . \tag{2}$$

If the velocity of a moving excited nucleus can be changed significantly on a time scale comparable with the nuclear lifetime τ, then a measurement of the Doppler shift is equivalent to measuring the velocity at the time of γ decay. The extraction of a lifetime from this measurement is dependent upon a knowledge of the velocity of the nucleus as a function of time.

In order to change the velocity of a moving nucleus significantly on a time scale comparable with τ, two methods are commonly used. One method is to allow the excited nuclei to recoil into a backing which is either a solid or a gas. This method is known as the Doppler shift attenuation method (DSAM). Typical stopping times for nuclei slowing down in solids are 0.2 - 0.8 psec while typical stopping times in a gas are several orders of magnitude longer but are, of course, strongly dependent upon the gas pressure. Another method is to allow the nuclei to recoil a variable distance in a vacuum, and then stop them abruptly with a solid material. This method is known as the recoil distance method (RDM) and will not be discussed further in this dissertation. The reader is referred to Appendix E and references 14 and 26 for more information on the RDM.

B. DSAM

The DSAM derives its name from the fact that the recoiling nuclei lose energy in some stopping material and the resulting attenuated Doppler shift is measured. There are two primary mechanisms by which the nuclei lose energy: to the atomic electrons of the stopping material through ionization and excitation (electronic part) and to the translational motion of the atoms of the stopping material through elastic scattering processes (atomic or nuclear part). The energy lost to the electrons of the stopping material is essentially a continuous process. For ion velocities less than $v_o Z_1^{2/3}$ where Z_1 is the atomic number of the recoiling nucleus and v_o (=c/137) is the velocity in the first Bohr orbit of hydrogen, the rate of energy loss is approximately proportional to the velocity. (27, 28) The atomic or nuclear part of the energy loss is a discontinuous process in which the recoiling nuclei change direction as well as lose energy. (27) The total rate of energy loss is thus the sum of the continuous electronic part and the discontinuous nuclear part.

In measuring lifetimes of nuclear levels using Doppler shift techniques the recoiling excited nuclei are usually produced in nuclear reactions of the form $M_2(m_1, m_4)M_3^*$ where m_1 is the incident particle, M_2 is the target nucleus, m_4 is the outgoing light particle, and M_3^* is the recoiling excited nucleus. Consider an ensemble of N_o nuclei produced in a reaction of this type at time $t=0$, and assume that these nuclei

all have the same initial velocity v(0) and move along the beam direction (z-axis). (These conditions are usually not exactly true experimentally, but can be closely approached. The experimental methods used to approximate these ideal conditions are discussed later.)

The direction as well as the velocity of the nuclei in the ensemble will change due to the effects of nuclear scattering. Therefore, the angle $\psi(t)$ of Eqs. (1) and (2) can be considered to be composed of two parts: 1) a time-independent part θ which is the angle between the z-axis and the direction of the γ-ray detector and 2) a time-dependent part $\phi(t)$ which is the instantaneous nuclear scattering angle between the z-axis and the direction of motion ($\phi(0) = 0$). A schematic diagram of this geometry is shown in Fig. 2. Thus

$$\cos\psi(t) = \cos[\theta + \phi(t)] = \cos\theta \cdot \cos\phi(t) - \sin\theta \cdot \sin\phi(t). \quad (3)$$

Since the observed γ-ray peak is due to the γ rays emitted by all of the nuclei in the ensemble, it is necessary to average over the time and the ensemble in order to calculate the observed Doppler shift from Eq. (2). Averaging over the ensemble gives the average Doppler shift as a function of time, namely

$$\overline{\Delta E_\gamma(t)} = E_{\gamma o} \overline{\frac{v(t)}{c} \cdot \cos\psi(t)} \quad , \quad (4)$$

and

$$\overline{v(t) \cdot \cos\psi(t)} = \overline{v(t)[\cos\theta \cdot \cos\phi(t) - \sin\theta \cdot \sin\phi(t)]} \quad . \quad (5)$$

The distribution of the nuclei in the ensemble remains symmetric about the z-axis, therefore, the ensemble average of $v(t) \cdot \sin\phi(t)$ is zero, and

Figure 2. A schematic diagram showing the components of $\psi(t) = \theta + \phi(t)$. θ is the angle between the z-axis and the Ge(Li) detector, and $\phi(t)$ is the time-dependent nuclear scattering angle. The velocity at time t along the beam direction is $\vec{v} \cdot \cos\phi(t)$.

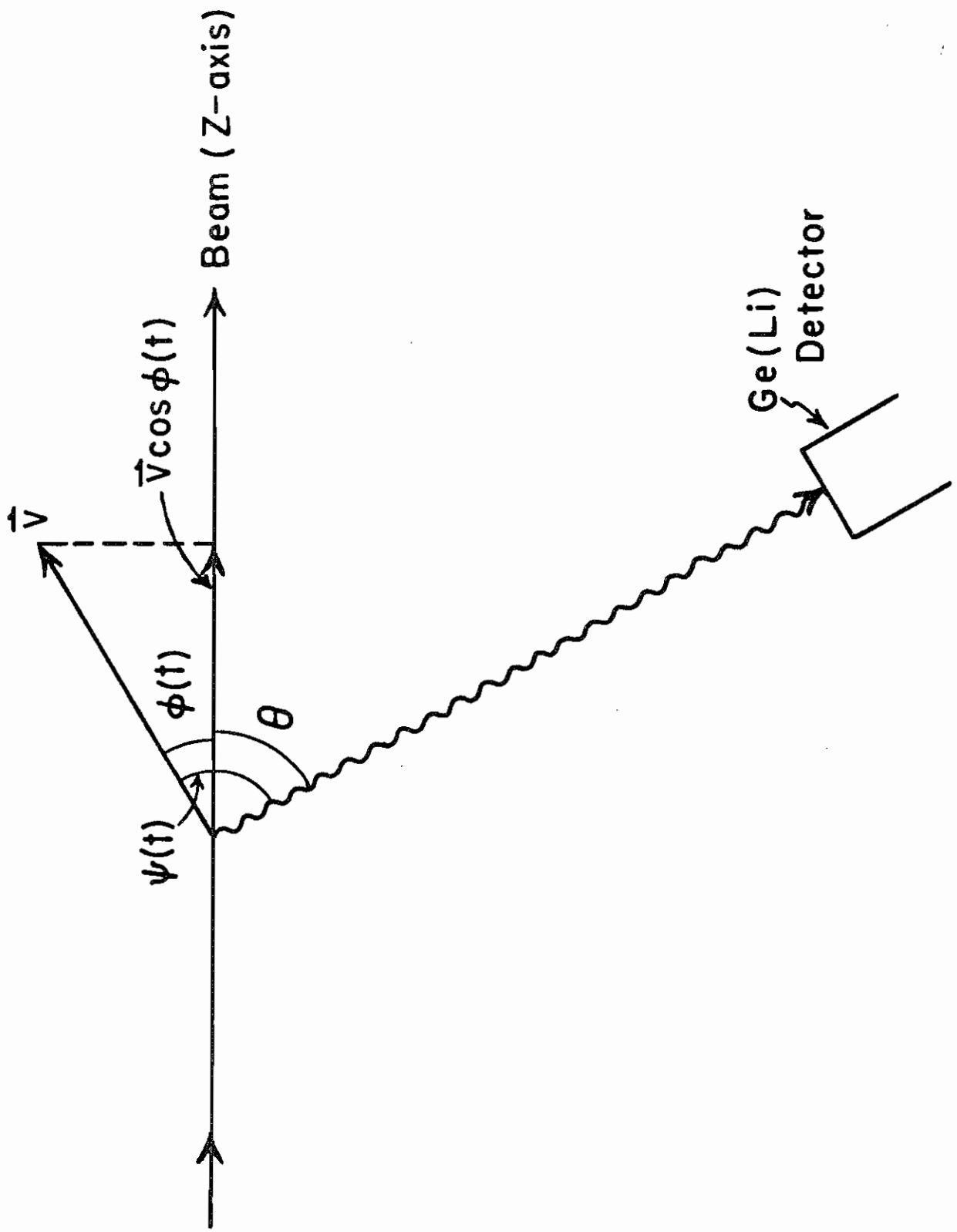
Beam (Z-axis)
Ge(Li)
Detector
$\vec{V}\cos\phi(t)$
$|\vec{V}|$
$\phi(t)$
θ
$\psi(t)$

$$\overline{v(t) \cdot \cos\psi(t)} = \overline{v(t) \cdot \cos\phi(t)} \cdot \cos\theta \qquad (6)$$

since the angle θ does not change and is the same for all the nuclei in the ensemble. Thus Eq. (4) becomes

$$\overline{\Delta E_\gamma(t)} = E_{\gamma o} \frac{v_z(t)}{c} \cos\theta \quad , \qquad (7)$$

where $v_z(t) = \overline{v(t) \cdot \cos\phi(t)}$ is the average recoil velocity of the ensemble along the beam direction at time t.

The number of nuclei dN which decay in a time interval dt is

$$dN = [-N(t)/\tau]\, dt \quad , \qquad (8)$$

where N(t) is the number of nuclei existing at time t. The number remaining at a time t is

$$N(t) = N_o \cdot \exp(-t/\tau) \quad , \qquad (9)$$

and

$$dN(t)/dt = -N_o/\tau \exp(-t/\tau) \, . \qquad (10)$$

The average Doppler shift of the γ rays emitted by the ensemble is, therefore,

$$\Delta E_\gamma = \left[\int_o^\infty \overline{\Delta E_\gamma(t)} \cdot (dN(t)/dt)\, dt\right] \Big/ \left[\int_o^\infty (dN(t)/dt)\, dt\right] \quad . \qquad (11)$$

The maximum possible Doppler shift is obtained if all of the nuclei have the initial recoil velocity v(0), or

$$\Delta E_\gamma^{max} = E_{\gamma o} \frac{v_z(0)}{c} \cos\theta = E_{\gamma o} \frac{v(0)}{c} \cos\theta \quad . \qquad (12)$$

The Doppler shift attenuation factor $F(\tau)$ is defined as the ratio of ΔE_γ

to ΔE_γ^{max}, or using Eqs. (7), (10), (11), and (12)

$$F(\tau) = \frac{1}{v(0)\,\tau} \int_0^\infty v_Z(t) \exp(-t/\tau)\, dt \quad . \tag{13}$$

In order to calculate the attenuation factor for a given lifetime, it is necessary to know $v_Z(t)$ which can be determined from a knowledge of the electronic and nuclear stopping powers. Lindhard, Scharff, and Schiøtt (hereafter referred to as LSS) (27) have used a Thomas-Fermi type of potential to derive general expressions for both of the stopping powers. LSS (27) introduced the universal dimensionless variables ϵ for the energy ρ for the path length traversed by the ion. These variables are defined as

$$\epsilon \equiv \frac{a\,M_2}{Z_1 Z_2 e^2 (M_1 + M_2)}\, E \tag{14}$$

$$\rho \equiv 4\pi a^2 N \frac{M_1 M_2}{(M_1+M_2)^2}\, x \tag{15}$$

where the subscripts 1 and 2 refer to the moving ion and the atoms of the stopping medium, respectively. In these expressions $a = 0.8853\, a_o (Z_1^{2/3} + Z_2^{2/3})^{-1/2}$, a_o is the radius of the first Bohr orbit of hydrogen, e is the charge on the electron, Z is the atomic number, M the atomic mass, N the number of atoms of the stopping material per unit volume, E the energy of the moving ion, and x the distance traveled along its path.

The following equations for the electronic and nuclear parts (denoted by the subscripts e and n, respectively) of the specific energy

loss have been derived by LSS:

$$(d\epsilon / d\rho)_e = k \epsilon^{1/2} \quad , \tag{16}$$

and

$$(d\epsilon / d\rho)_n = \frac{1}{\epsilon} \int_0^{\epsilon} f(q)\, dq \quad , \tag{17}$$

where

$$k = \mathcal{E}_e \frac{0.0793\ Z_1^{1/2} Z_2^{1/2} (A_1 + A_2)^{3/2}}{(Z_1^{2/3} + Z_2^{2/3})^{3/4} A_1^{3/2} A_2^{1/2}} \quad , \tag{18}$$

$\mathcal{E}_e \approx Z_1^{1/6}$, and the function f(q) is given in Fig. A2(a) of Appendix A.

Two different approaches have been used to calculate $v_z(t)$ from the expressions given by LSS. The simplest method is due to Warburton and co-workers. (29-32) In this approach the nuclear part of the energy loss is approximated by the relation $-M_1 (dv_z/dt)_n = K_n (v_z/v_o)^{-1}$, and the total energy loss is expressed as

$$-M_1 (dv_z/dt) = K_e (v_z/v_o) + K_n (v_z/v_o)^{-1} \tag{19}$$

where the constant K_e is determined either from the LSS electronic stopping parameter k or from experimental data, and K_n is determined from the LSS value at $v_z = v_o$. This expression is derived in Appendix B and a comparison between this method and the LSS method for nuclear stopping is given. Equation (19) can be integrated to give $v_z(t)$, and $F(\tau)$ can then be calculated as a function of the mean lifetime. The expressions for $F(\tau)$ are also given in Appendix B.

The other approach to calculate $v_z(t)$ is due to Blaugrund (33)

and includes the effects of nuclear scattering directly. Starting from an expression derived by Lewis (34) for the angular distribution function of an originally parallel beam of ions after traveling a distance x in a scattering material, Blaugrund derives an expression for the ensemble average of $\cos\phi(t)$ (see Appendix C). The product $\overline{v(t)} \cdot \overline{\cos\phi(t)}$ can thus be computed numerically using exact expressions for $(d\epsilon/d\rho)_e$ and $(d\epsilon/d\rho)_n$ given by LSS. This is still an approximation to $v_z(t) = \overline{v(t) \cdot \cos\phi(t)}$, but as pointed out by Blaugrund, the difference is of the order of 5-10% for $A_1/A_2 \equiv r = 1$ and smaller for other values of r. This has been verified by Currie (35) using a Monte Carlo calculation.

A computer program FTAU (13) has been written which evaluates $F(\tau)$ for different values of τ using Blaugrund's approach. In general the excited nucleus is produced in a target of finite thickness and moves some distance before entering a backing which is essentially infinitely thick. The program handles the finite target thickness as well as the fact that the recoiling nuclei slow down in two different stopping materials. The target and backing can be composed of up to three different elements each. Appendix D gives a detailed description of FTAU.

In order to determine the attenuation factor experimentally ($F_{exp}(\tau)$), the ratio $\Delta E_\gamma/\Delta E_\gamma^{max}$ must be calculated from the measured Doppler shift and the maximum possible Doppler shift at a given angle. The maximum Doppler shift can be determined either by allowing the excited nuclei to recoil into a vacuum and measuring the Doppler shift

or by calculating the maximum shift from the reaction kinematics. The second method was used in this investigation.

The average energy of a γ ray can be expressed as $E_\gamma = E_{\gamma o} + \Delta E_\gamma^{exp}$ where $\Delta E_\gamma^{exp} = \Delta E_\gamma^{max} \cdot F_{exp}(\tau)$. Thus E_γ can be expressed as

$$E_\gamma = E_{\gamma o} + M \cdot \cos\theta \quad , \tag{20}$$

where $M = F_{exp}(\tau) \cdot \Delta E^{max}(0^o)$ and $\Delta E^{max}(0^o)$ is the maximum Doppler shift when the γ ray is detected at 0^o. By making a least-squares fit of a straight line to the experimentally measured energy at several angles, the slope M can be determined and $F_{exp}(\tau)$ calculated. Equation (20) also gives the relation

$$F_{exp}(\tau) = \frac{E_\gamma - E_{\gamma o}}{\Delta E_\gamma^{max}(0^o) \cdot \cos\theta} \quad . \tag{21}$$

In reactions of the type $M_2(m_1, m_4)M_3^*$ the center of mass (c.m.) recoil velocity (32) is

$$v_{c.m.} = c\,(2m_1E_1)^{1/2}/(m_1+M_2) \quad , \tag{22}$$

where the masses and energies are in MeV and E_1 is the laboratory bombarding energy. A nucleus M_3^* emitted at an angle $\theta_{c.m.}$ with respect to the beam in the c.m. has a velocity along the z-axis at t = 0 of

$$v_z(0) = v_{c.m.}\,[1 + \gamma^{-1} \cos\theta_{c.m.}] \quad , \tag{23}$$

where γ^{-1} is the ratio of the speed of M_3^* in the c.m. to the speed of the

c.m. in the laboratory. This can be seen schematically from Fig. 3 where an explicit expression for γ^{-1} is given. There is an upper and a lower limit to the velocity along the z-axis. If the distribution of M_3* is symmetric about 90° in the c.m., then the average recoil velocity is just the c.m. velocity. The magnitude of the component of the velocity perpendicular to the z-axis is

$$v_\perp(0) = v_{c.m.}\ \gamma^{-1} \sin\theta_{c.m.}\ , \tag{24}$$

and because of axial symmetry this component of the velocity does not contribute to the average shift.

The average initial recoil velocity along the z-axis is

$$\langle v_z(0)\rangle = v_{c.m.}\ [1 + \gamma^{-1} \langle\cos\theta_{c.m.}\rangle\ ]\ . \tag{25}$$

Warburton et al. (32) have found that a good a priori estimate of $\langle\cos\theta_{c.m.}\rangle$ is 0 ± 0.33, and this can be used to obtain a limit on the spread in the initial recoil velocity, or

$$\langle v_z(0)\rangle = v_{c.m.}\ [1 \pm 0.33\ \gamma^{-1}]\ . \tag{26}$$

At bombarding energies very near threshold, γ^{-1} is small and in the first approximation all of the recoils are along the beam axis. As the energy is raised above threshold, the recoiling nuclei remain confined to a narrow cone about the beam axis. For cone half-angles $\lesssim 10^\circ$, $\cos\theta \gtrsim 0.97$, and the effects of the cone angle can be neglected. That is, the initial direction of the recoils can be assumed to be along the z-axis. In this

Figure 3. A schematic diagram showing the relation between $v_{c.m.}$ (the speed of the c.m.) and v (the speed of the nucleus in the c.m.). γ^{-1} is the ratio of v to $v_{c.m.}$, and the expression for γ^{-1} for reactions of the form $M_1(m_2, m_4)M_3^*$ is given.

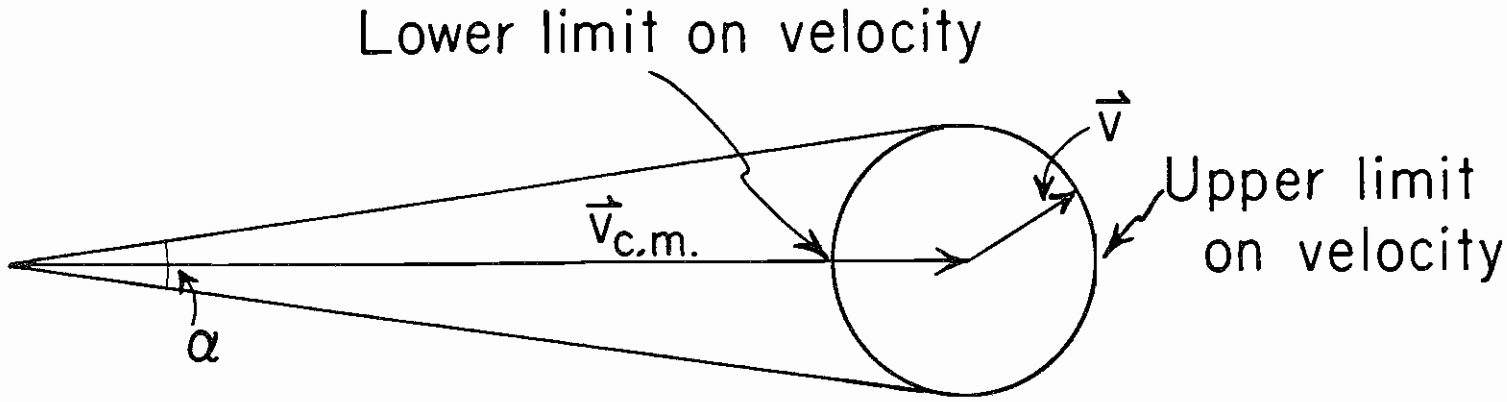

$$\frac{v}{v_{c.m.}} = \gamma^{-1} = \left\{ \frac{M_2 m_4}{m_1 M_3^*} \left[1 + \frac{(m_1 + M_2)}{M_2} \frac{Q}{E_1} \right] \right\}^{1/2}$$

$Q = Q_0 - E_x$

Q_0 = g.s. Q – value

E_x = Excitation energy

α = Cone angle of recoils

investigation bombarding energies were less than 1 MeV above threshold (except for one case when it was 1.3 MeV above threshold) and the cone angles were $\lesssim 10^{\circ}$ (one case of 11.3°). The spread in the recoil velocity was estimated from Eq. (26) and was less than 6% for all cases in this investigation.

Chapter III

EXPERIMENTAL APPARATUS AND PROCEDURE

A. General

States studied in this investigation were populated via α-particle induced endothermic reactions. Reactions of this type are useful in studying lifetimes of nuclear levels for the following reasons: 1) Large recoil velocities are imparted to the excited nuclei, and thus large Doppler shifts are attainable. 2) Low γ-ray backgrounds are present since only a few particle channels are open. 3) Gamma-ray spectra can be recorded in singles rather than coincidence because of the low background. 4) For endothermic reactions the recoil direction can be confined to a narrow cone about the beam axis by using bombarding energies near threshold. 5) An important practical consideration is the low neutron flux in the target area due to the negative Q-value of most (α, n) reactions. Thus the "life" of a Ge(Li) detector is greatly increased because of the reduced neutron radiation damage.

Alpha beams of the desired energy and intensity were obtained from the TUNL FN tandem Van de Graaff accelerator. A $^4He^-$ beam was

obtained by passing $^4He^+$ ions from the duoplasmatron through a lithium vapor. These negative ions were then accelerated to the tandem terminal. In the terminal the electrons were stripped off by an oxygen stripper, and the $^4He^{++}$ beam accelerated to a final energy of three times the terminal voltage.

After magnetic analysis, the beam passed through an opening defined by a set of vertical and horizontal slits. The slit position was adjustable -- a typical opening was 25 mils by 25 mils. The horizontal slits were connected to a feedback network which was used to control the voltage on the terminal. The slits were followed by a magnetic beam deflector, two sets of magnetic quadrupoles, and two additional beam deflectors. These devices were used to focus and steer the beam through the collimators into the scattering chamber. By optimizing the focusing and steering parameters, 50 to 70% of the analyzed beam could be obtained on target. Minimizing the beam on the collimators was desirable in order to reduce background and to prevent overheating resulting in carbon deposits. Beam currents on target were between 200 and 300 nA.

B. Collimating System and Target Chamber

A schematic drawing of the target chamber and the associated collimating system is shown in Fig. 4. The collimating system consisted of three tantalum disks ~6.3 cm apart with a 2.38 mm center hole. The

Figure 4. A schematic drawing of the target chamber showing the beam path to the target, the collimating system, and the 30-cc Ge(Li) detector.

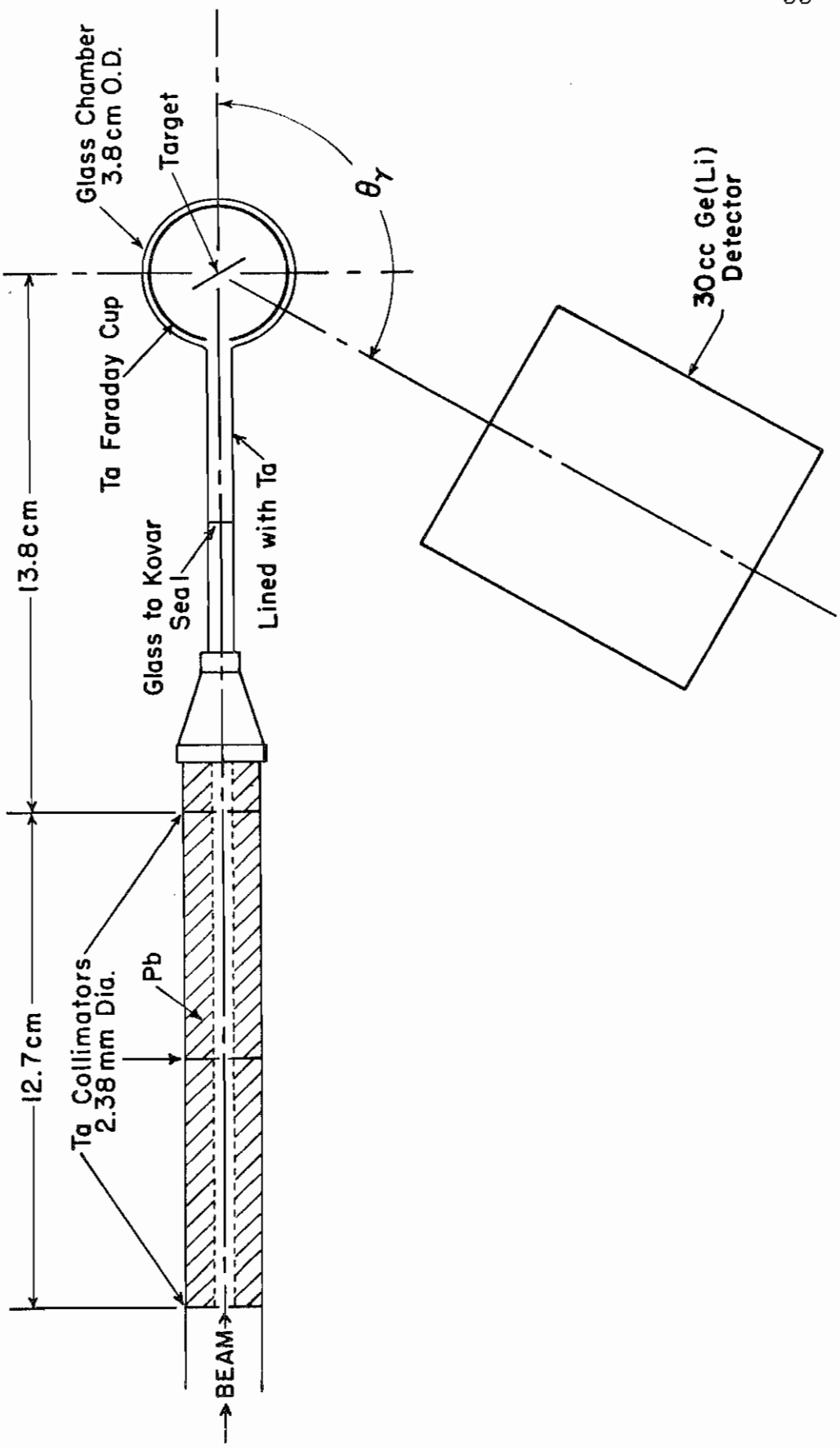
Glass Chamber
3.8cm O.D.
Target
θ_γ
30cc Ge(Li)
Detector
Ta Faraday Cup
Glass to Kovar
Seal
Lined with Ta
13.8cm
12.7cm
Ta Collimators
2.38mm Dia.
Pb
BEAM

collimator nearest the chamber was 13.8 cm from the target. For shielding the space between each pair of collimators was filled with a lead cylinder with a 3.2 mm hole down the center. A lead cylinder ~1 cm long with an 8 mm hole in the center was placed after the collimator nearest the chamber to serve as a shield for the γ rays originating at this collimator. The stainless steel beam pipe immediately before the collimators was lined with tantalum to reduce the γ ray background from particles scattered from the beam pipe.

The target chamber itself was a glass cylinder ~13.5 cm high with an outside diameter (o.d.) of 3.8 cm. A glass chamber was chosen for insulation of the Faraday cup and for ease of construction. It was connected to the beam pipe by a 1 cm o.d. glass tube which was lined with 2 mil tantalum foil. The chamber was lined with a 5 mil piece of tantalum which served as a Faraday cup. A Vac-Ion pump connected to the top of the chamber through a 1 1/2 inch o.d. stainless steel tube maintained a vacuum of 5×10^{-7} mm of Hg in the target chamber. The bottom of the chamber was sealed with a teflon cap with a hole in the center for the target rod. The target rod had positions for three standard target rings, and the desired target could be positioned in the beam path by placing a steel pin in the proper hole in the target rod.

The γ-ray detector was supported by a circular, steel table four feet in diameter positioned below the chamber. The height of the table was adjusted to position the center of the detector at the beam height.

A circular aluminum plate 18 inches in diameter with markings every degree was located at the center of the steel table. The Ge(Li) detector was carried by a flat aluminum cart which pivoted about a pin in the center of the aluminum plate. The cart rolled on ball-bearing wheels and could be locked in position with bolts. The angle of the detector with respect to the beam was indicated by a pointer on the cart and could be determined to $\pm 0.1^{\circ}$. The absolute accuracy of the angle was $\sim 1^{\circ}$.

C. Gamma-Ray Detector, Electronics, and Computer

Gamma rays were detected with a 30-cc, coaxial Ge(Li) detector obtained from Nuclear Diodes, Inc. (36) The cylindrical germanium crystal was 37 mm long by 34 mm in diameter, and the undrifted region down the center was 11 mm in diameter. The efficiency of the detector for the 1.33 MeV γ ray from ^{56}Co was 3.13% relative to a 3 X 3 NaI(Tl) crystal at a 25 cm source-to-detector distance. The resolution of the detector was ~ 2.7 keV full width at half maximum (FWHM) for 1.33-MeV γ rays.

Signals from the Ge(Li) detector were amplified by a Nuclear Diodes, Inc. model 101A charge sensitive preamplifier and by a Camberra model 1417 Spectroscopy Amplifier. (37) These signals were processed by a Northern Scientific (38) analog-to-digital converter (ADC). In the initial runs the zero level of the ADC was adjusted so that only the portion

of the spectrum above $\sim$350 keV was analyzed. This was done so that a dispersion of $\sim$0.73 keV/channel could be maintained while observing γ rays up to 3.3 MeV. In a later run the zero level was set lower so that low-energy γ rays could be observed.

The TUNL on-line computer system (39) operating with the program FORK stored a 4096 channel spectrum during data acquisition and provided an on-line data display. At the end of each run the data was written on magnetic tape for later analysis. The run number and the energy calibration were recorded along with each spectrum. The entire spectrum was also plotted on the line printer to provide a back-up to the tape record. These plots were also useful in comparing data recorded with the Ge(Li) detector at different angles.

D. Target Preparation

^{34}S targets were prepared by evaporating CdS onto 1 μ Ni foils. CdS powder (enriched to 85.61% in ^{34}S with the ^{32}S content being 13.81%) was evaporated from a covered tantalum boat onto Ni foils. The foils were placed at various distances (5-15 cm) from the boat in order to ensure a target of the required thickness. The evaporation was carried out at a vacuum of $\sim 5 \times 10^{-6}$ mm of Hg and at a temperature of $\sim 1100^{\circ}$ C. The targets were allowed to cool for several hours before removal from the evaporator.

E. Target Thickness Measurements

The thickness of the targets was determined from measurements of the energy lost by α particles in the CdS. For these measurements the targets were placed in a 30 inch scattering chamber (designed by E. J. Ludwig) and bombarded with 4 MeV α particles. Scattered particles were detected at back angles with a silicon surface barrier detector. The particles elastically scattered from the Ni were observed as a very broad peak in each spectrum. Spectra were recorded with the Ni foil facing the beam and with the CdS facing the beam. For these two arrangements the upper edges of the Ni peaks differed in energy. This energy difference was due to the energy lost by the α particles entering the CdS target, the difference in energy lost in the elastic scattering from the Ni, and the energy lost coming back through the target. With the detector at an angle of 135° and the target at 90° with respect to the beam, the target thickness is given by

$$\Delta x = (\Delta E)_{Ni} / (\eta \epsilon_i + \epsilon_o \sqrt{2}) \ ,$$

where $(\Delta E)_{Ni}$ is the difference in energy between the Ni elastic edges, ϵ_i is the specific energy loss of the α particles entering the target, and ϵ_o is the specific energy loss of the α particles going back through the target. The factor η depends upon the angle of the detector θ with respect to the beam, and for $\theta = 135^{\circ}$, $\eta = 0.792$. The quantity η takes into account the fact that the energies of the α particles when they reach the Ni foil are

different in the two cases. The specific energy losses ϵ_i and ϵ_o are different since the energy of the particles entering the target is different from the energy of those emerging. This difference is due mainly to the energy lost in the elastic scattering process. The specific energy loss in keV-cm^2/μg was determined from the work of Whaling. (40)

When the target is at an angle of 45° to the beam and facing the surface barrier detector, the thickness is given by

$$\Delta x = (\Delta E)_{Ni} / (\eta \epsilon_i \sqrt{2} + \epsilon_o) \quad .$$

Measurements were made with the targets at angles of 90 and 45° to the beam, and the differences in the target thicknesses were always <10%. Part of this difference was probably due to the uncertainty in locating the Ni edge.

Since the α particles elastically scattered from the Cd are higher in energy than those elastically scattered from Ni, it is possible to use the width of the Cd peak to determine the target thickness. Target thicknesses calculated in this manner were in good agreement with the thicknesses calculated from the difference in the Ni elastic energies. To find a target of the appropriate thickness, several different CdS targets were studied. The target used during this investigation was 390 μg/cm^2 (and when oriented at an angle of 60° with respect to the beam direction was 450 μg/cm^2). The thickness of the natural CdS target used to determine the shape of the peaks from the $^{32}S + \alpha$ reaction was 180 μg/cm^2 when oriented at an angle of 60° with respect to the beam.

F. Procedure

The targets were placed in the glass chamber at an angle of 60° to the beam, and the chamber was evacuated. When a vacuum of $\sim 10^{-5}$ mm of Hg was obtained, the Vac-Ion pump was turned on, and a period of $\sim 1/2$ hour was required to reach a vacuum of $\sim 10^{-6}$ mm of Hg. The Ge(Li) detector was placed on the aluminum cart with its front face ~ 7.5 cm from the target. The axis of the detector was aligned along the axis of the cart so that the pointer accurately indicated the angle of the detector with respect to the beam.

A channel vs energy calibration was obtained by using γ rays of known energy from radioactive sources. The sources most commonly used were ^{60}Co and ^{56}Co. The energies and intensities (41) of the strong γ rays from ^{56}Co are given in Table II. The energies of the single- and double-escape peaks are given for those γ rays with energies greater than 2.5 MeV. The letters S and D denote the single- and double-escape peaks, respectively, and the number in parenthesis with the letter indicates the full-energy peak for that γ ray. The relative intensities were used to determine the efficiency of the Ge(Li) detector.

During the course of several days of data collection, there were slight drifts in the electronics. In order to monitor the long-term drifts, calibration spectra were recorded at periodic intervals. Electronic drifts from one run to the next were monitored using unshifted γ rays originating from the reaction and from the ^{40}K and ThC'' contained in

Table II

Energies and Intensities of Some of the More Intense γ Rays from ^{56}Co

γ Ray Number	Energy (keV)	Relative Intensity [a]	γ Ray Number	Energy (keV)	Relative Intensity [a]
1	787.86 ± 0.04	308	19	2213.91 ± 0.15	377
2	846.79 ± 0.03	100,000	20	2231.61 (33D)	
3	977.46 ± 0.05	1448	21	2251.25 (34D)	
4	1037.91 ± 0.03	14,302	22	2429.55 (35D)	
5	1175.13 ± 0.05	2302	23	2499.22 (30S)	
6	1238.30 ± 0.02	67,638	24	2525.85 (36D)	
7	1360.22 ± 0.03	4340	25	2598.58 ± 0.03	16,851
8	1442.71 ± 0.10	200	26	2691.29 (32S)	
9	1576.57 (25D)		27	2742.61 (33S)	
10	1771.41 ± 0.03	15,778	28	2762.25 (34S)	
11	1810.44 ± 0.58	641	29	2940.55 (35S)	
12	1963.94 ± 0.06	721	30	3010.23 ± 0.23	1009
13	1988.22 (30D)		31	3036.85 (36S)	
14	2015.36 ± 0.03	3095	32	3202.30 ± 0.08	3030
15	2034.92 ± 0.03	7952	33	3253.62 ± 0.04	7392
16	2087.57 (25S)		34	3273.26 ± 0.08	1756
17	2113.81 ± 0.15	387	35	3451.56 ± 0.20	875
18	2180.29 (32D)		36	3547.86 ± 0.15	178

[a] Normalized to the 846.79 keV γ ray.

the concrete walls of the laboratory. Two prominent unshifted γ rays from the long-lived states populated by reactions were from the 1.61-MeV level of ^{37}Ar(τ = 5.15 nsec) (18) and from the 3.16-MeV level of ^{35}Cl($\tau \approx 60$ psec). (42)

Singles spectra were recorded with the Ge(Li) detector at several different angles at each of three bombarding energies. At E_α = 7.63 MeV, spectra were recorded with the Ge(Li) detector at 0, 90, and 143°. This bombarding energy is below the threshold for the production of the 2.22-MeV level of ^{37}Ar, and only the first and second excited states were studied at this energy. At a bombarding energy of 8.10 MeV, spectra were recorded with the detector at 0, 37, 45, 55, 90, and 143°. This bombarding energy is below the threshold for the production of the 280-MeV level of ^{37}Ar. Spectra were also recorded at 0, 37, 55, 90, and 143° at a bombarding energy of 8.75 MeV. From these three sets of data angular distributions, Doppler shifts, branching ratios, and excitation energies were obtained.

In order to determine which γ rays were not from the $^{34}S + \alpha$ reaction, a 1 μ Ni foil and a 180 $\mu g/cm^2$ natural CdS target on a Ni backing were bombarded with α particles. The Ni foil was bombarded with 8.7 MeV α particles, and the γ rays were detected at 90°. The natural CdS target was bombarded with 8.10 MeV α particles and the γ rays were observed at 0, 90, and 143°. To normalize the spectra recorded with the 30-cc detector at different angles, a 20-cc Ge(Li) detector placed at 90°

to the beam was used as a monitor. The spectra recorded with this fixed detector were also written on magnetic tape for later analysis. The total amount of charge collected during a run was recorded along with the live charge (charge collected while the ADC's were not busy). It was found that normalization to the live charge was equivalent to normalizing to the counts in the monitor spectrum.

During the course of the data collection, ^{61}Cu was produced from the (α,p) reaction on the ^{58}Ni in the Ni foil. The nucleus ^{61}Cu has a 3.4 hour half-life and β^+ decays to several levels in ^{61}Ni. The relative intensities of the γ rays following the β decay are known. (43) A spectrum was, therefore, recorded with the beam off shortly after ending a run. The γ rays from the β decay of ^{61}Cu were used to determine the relative efficiency of the detector for low-energy γ rays. Table III gives the γ-ray energies and the number of γ rays per 100 β^+ decays of ^{61}Cu.

Table III

Number of γ Rays Per 100 β^+ Decays of ^{61}Cu

E_γ (keV)	Number of γ Rays Per 100 β^+ Decays
67.40	4.9
282.9	13.0
372.9	1.9
529.4	0.32
588.5	1.2
656.0	9.6
816.8	0.32
841.0	0.23
908.6	1.0
1100.1	0.28
1186.0	3.6

Chapter IV

METHOD OF ANALYSIS AND RESULTS

A. Branching Ratios and Energies

Branching ratios were determined from the spectra recorded at $E_\alpha = 8.75$ MeV with the detector at 55°. This angle is the zero of $P_2(\cos\theta)$; contributions from any $P_4(\cos\theta)$ term in the distribution are expected to be small. The efficiency of the detector was determined from the known intensities (41, 43) of the γ rays from ^{56}Co and from ^{61}Cu. Figure 5 gives the branching ratios and limits on possible branches for the first five excited states of ^{37}Ar. The only transitions definitely observed were to the ground state.

The possible $(3 \rightarrow 2)$ transition had the same energy (807 keV) as both a γ ray observed when a Ni foil was bombarded and also a γ ray that was observed when the beam energy was below the threshold for the production of the third excited state. The number of counts in the 807 keV peak in the Ni + α spectrum, correctly normalized, was subtracted from the counts in the possible $(3 \rightarrow 2)$ transition, and within statistics the difference was found to be zero. The upper limit on this branch re-

Figure 5. Diagram showing the branching ratios determined in this investigation for the first five excited states of ^{37}Ar. All five states were found to decay 100% to the ground state. Limits on other possible branches are also given.

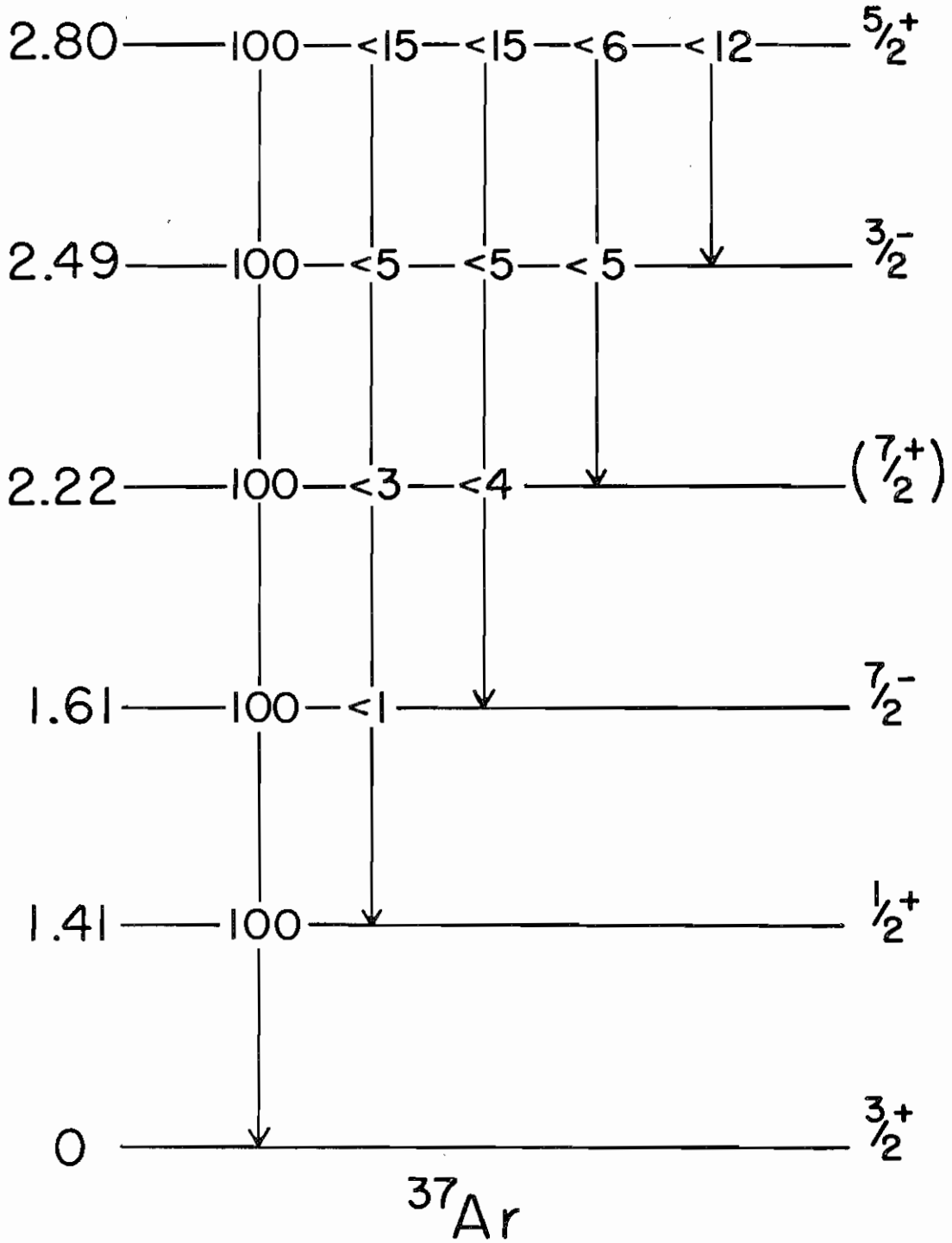
2.80
100
<15
<15
<6
<12
5/2+
2.49
100
<5
<5
<5
3/2-
2.22
100
<3
<4
(7/2+)
1.61
100
<1
7/2-
1.41
100
1/2+
0
3/2+
37Ar

flects the total statistical uncertainty. Gamma rays were also observed in the Ni + α spectrum at the same γ-ray energies as possible (5 → 2), (5 → 3), and (5 → 4) transitions in ^{37}Ar. These γ rays were analyzed in the same manner as the (3 → 2) transition. The upper limits on the other branches were obtained by doubling the statistical error obtained from summing a region of the spectrum where the γ ray was expected.

Excitation energies were obtained from the spectra recorded with the detector at 90° to the beam in the following manner: First, the centroids of the known-energy γ rays from ^{56}Co (see Table II) were calculated as described in section C of this chapter. Next, several sets of three of these γ rays (near the peak whose energy was to be determined) were used to obtain different sets of coefficients (A_i's) in the equation

$$E = A_1 + A_2 x + A_3 x^2 \quad ,$$

where x is the channel number. An energy vs channel listing was then obtained for each set of A_i's, and the known-energy γ rays from the source and the reaction were compared with the prediction of the calibration. This comparison was used to determine the "best" set of coefficients for each energy region and to estimate the accuracy of the calibration. The ground state transition energy for each of the first five excited states was then determined using the "best" coefficients for that energy region. Table IV gives the level energies and uncertainties in keV for these levels.

Table IV

Energies of Excited States of ^{37}Ar

Level Number	E_x (keV)
1	1410 ± 1
2	1611 ± 1
3	2217 ± 1
4	2489 ± 1
5	2796 ± 2

B. Angular Distributions

The angular distributions were normalized to the live charge collected during each run. The charge collection was checked by examining the angular distribution of the γ rays from the first excited state. This state has a spin of 1/2; consequently, an isotropic angular distribution is expected. The yield of this state at 90° at a bombarding energy of 8.10 MeV, unfortunately, was found to be $\sim$8% greater than at the other four angles. The yields of the other γ rays in the 90° spectrum recorded at E_{α} = 8.10 MeV were, therefore, reduced by 8%. Figure 6 shows the experimental angular distribution with the 90° point corrected for the 1.41-MeV γ ray. The solid line represents a least-squares fit to the data (χ^2 = 0.22).

In Method II of Litherland and Ferguson (22) a collinear geometry is used to restrict the population of the magnetic substates in an angular correlation experiment. Similarly, if the bombarding energy is near threshold, the reaction is dominated by outgoing s-wave neutrons, and in the present reaction only m = $\pm$ 1/2 magnetic substates are populated. (The + and - substates are populated equally.) In order to determine the effects of using bombarding energies ranging from 0.1 to 1.1 MeV above threshold, transmission coefficients for neutrons of different ℓ-values were calculated as a function of energy using the computer program ABACUS. (44) The optical model parameters of Perey and Buck (45, 46) were used. The transmission coefficients for s- and p-wave neutrons at

Figure 6. Experimental angular distribution recorded at E_α = 8.10 MeV for the γ rays from the 1.41-MeV level of ^{37}Ar. The solid line represents a least-squares fit to the data using the code M2 and corresponds to a χ^2 of 0.22. The J^π of this level is known to be $1/2^+$. (15)

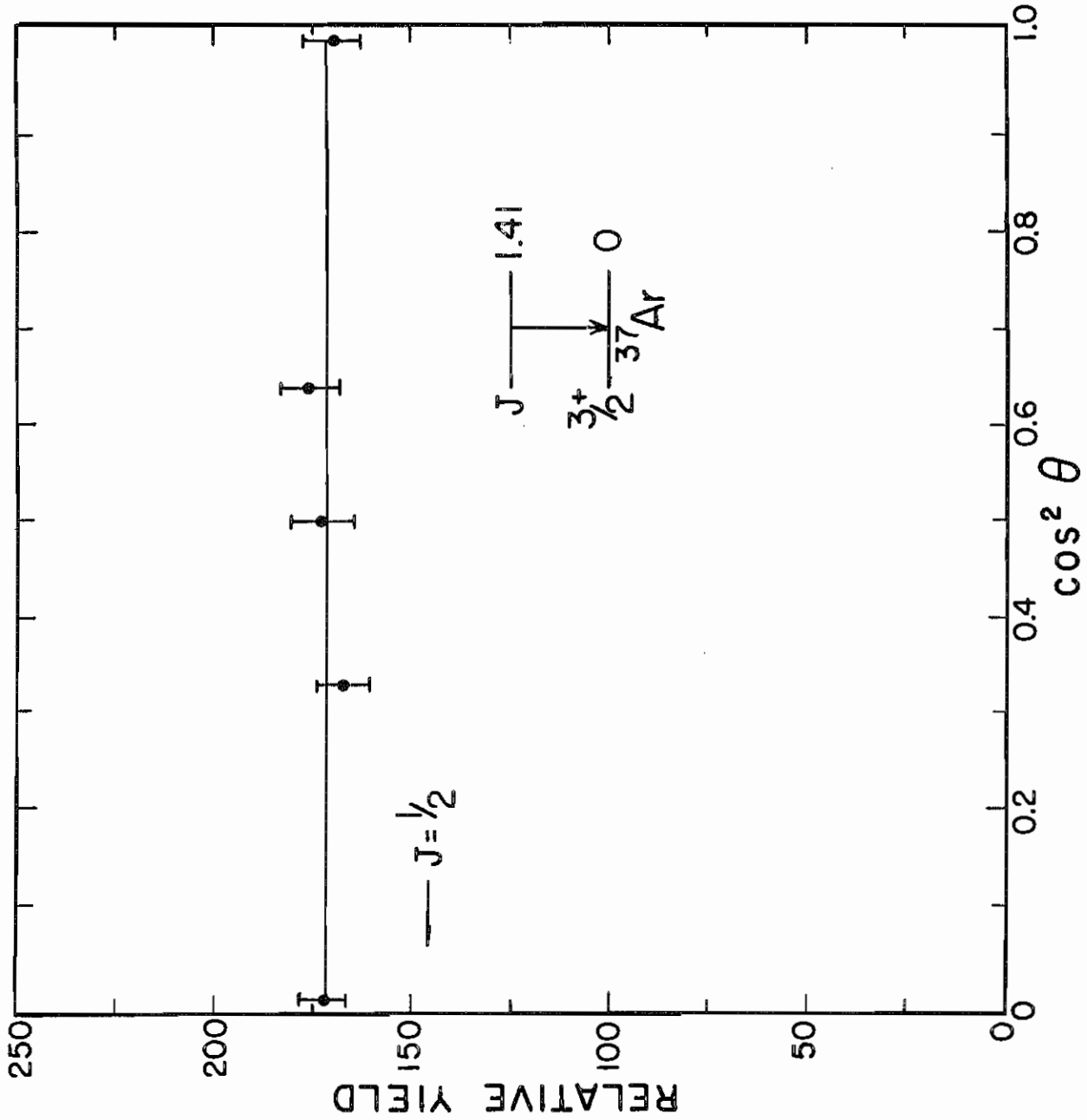
RELATIVE YIELD
250
200
150
100
50
0
0
0.2
0.4
0.6
0.8
1.0
cos² θ
J=½
J
1.41
0
3⁺/2
37Ar

0.4 MeV above threshold were found to be in the ratio of $\sim$3 to 2 while the transmission coefficient for d-wave neutrons was smaller by a factor of 50. The p-wave neutrons could populate both m = 1/2 and 3/2 substates, but no appreciable population of the 5/2 substates was expected due to the small transmission coefficient for the d-wave neutrons.

The angular distribution of the γ rays from a given state depends upon the spin of the initial and final states, the multipole mixing ratio of the transition, and the relative populations [P(m)'s] of the m = 1/2 and 3/2 substates. The computer code M2 written by D. J. Church was used to analyze the angular distributions in terms of these parameters. The code M2 uses the phase convention of Rose and Brink (47) for the mixing ratio. The code was modified so that the population of the $\pm$ 3/2 substates could be restricted to $\leq$ 40% and the population of the $\pm$ 1/2 substates to $\geq$ 60%. This is similar to the method of analysis described in detail by Pilt et al. (48) for (p,n) reactions near threshold. The limits on the population parameters were obtained from the transmission coefficients. For the distributions recorded at two bombarding energies, only the ones at the lower energy were analyzed since the relative transmission for the p-wave neutrons increases as the bombarding energy is increased.

The program M2 performs a least-squares fit of the theoretical angular distribution $W(\theta_i)$ (22) to the experimental distribution. The best fit is determined from the minimum value of X^2, where

$$\chi^2 = \frac{1}{n} \sum_i \left[\frac{Y(\theta_i) - W(\theta_i)}{\Delta Y(\theta_i)} \right]^2 .$$

$Y(\theta_i)$ is the experimental yield at the angle θ_i, $\Delta Y(\theta_i)$ is the experimental error in $Y(\theta_i)$, and n is the number of degrees of freedom. A fit is performed for discrete values of $\tan^{-1}\delta$ where δ is the multipole mixing ratio and for different values of the initial and final spins (J_i and J_f, respectively). For a given J_i, J_f, and δ the population parameters P(1/2) and P(3/2) (with the above noted restrictions) are varied to minimize χ^2.

The attenuation factors (Q_i's) for the Ge(Li) detector were determined from the work of Winn and Sarantites. (49) These factors have an energy dependence, but for γ rays >1.0 MeV the energy dependence is very slight, and the following values were used in the analysis: $Q_0 = 1.0$, $Q_2 = 0.978$, $Q_4 = 0.93$, $Q_6 = 0.87$.

1.61- and 2.49-MeV Levels

The 1.61- and 2.49-MeV levels are populated strongly in the (d,p) reaction. Rosner and Schneid (16) used the j-dependence of the (d,p) angular distribution to assign spins and parities of $7/2^-$ and $3/2^-$ to the 1.61- and 2.49-MeV levels, respectively. A spin and parity of $7/2^-$ for the 1.61-MeV level is supported by the systematics of $7/2^-$ levels in this mass region, the lifetime (18) of 5.15 ± 0.70 nsec, and the large (0.82) spectroscopic factor. (16) The spectroscopic factor (0.45) for the 2.49-

MeV level (16) indicates that it contains $\sim 1/2$ of the $2p_{3/2}$ single particle strength.

The experimental angular distribution of the 1.61-MeV γ rays recorded at $E_a = 8.10$ MeV was analyzed for spins 1/2 through 7/2. Plots of χ^2 vs $\tan^{-1}\delta$ are shown in Fig. 7(a) for the two spins allowed by the ℓ_n-value of 3. Spins 1/2 and 3/2 (not shown) gave values of χ^2 above the 0.1% confidence limit. The spin 7/2 gives the only acceptable fit; the mixing ratios and population parameters at the minima are given in Table V.

The experimental angular distribution of the 2.49-MeV γ rays recorded at $E_a = 8.10$ MeV was analyzed for the spins 1/2 and 3/2 allowed by the ℓ_n-value. Plots of χ^2 vs $\tan^{-1}\delta$ for the $(4 \rightarrow 0)$ transition are shown in Fig. 7(b). The only acceptable fit is for spin 3/2 and for the mixing ratios shown in Table V. Since this level was populated at a bombarding energy only 100 keV above threshold, the angular distribution was analyzed assuming only the $\pm$ 1/2 substates were populated. The dashed lines in Fig. 7(b) show the effect of this assumption on χ^2. The mixing ratios and population parameters at the minimum are given in Table V.

2.22- and 2.80-MeV Levels

The 2.217-MeV γ ray corresponding to the $(3 \rightarrow 0)$ in ^{37}Ar differed in energy by only 15 keV from the γ ray corresponding to the $(1 \rightarrow 0)$ transition in ^{32}S (2.232 MeV). Sample spectra of this doublet recorded at

Figure 7. (a) X^2 plots for the fits to the angular distribution of the 2.22-MeV γ ray corresponding to the $(2 \rightarrow 0)$ transition in ^{37}Ar. Plots are shown for the spins (5/2 and 7/2) allowed by the ℓ_n-value. Only spin 7/2 gives a value of X^2 below the 0.1% confidence limit. The population parameters were allowed to vary with the restriction $P(1/2) \geq 0.60$ and $P(3/2) \leq 0.40$.

(b) X^2 plots for the fits to the angular distribution of the 2.49-MeV γ ray corresponding to the $(4 \rightarrow 0)$ transition in ^{37}Ar. Plots are shown for the spins (1/2 and 3/2) allowed by the ℓ_n-value from (d,p) work. Only spin 3/2 gives a value of X^2 below the 0.1% confidence limit. The solid curve was obtained when the population parameters were allowed to vary with the restriction in (a), and the dashed curve shows the effects of assuming only the $\pm$ 1/2 substates are populated. The data for both γ rays were recorded at $E_d = 8.10$ MeV.

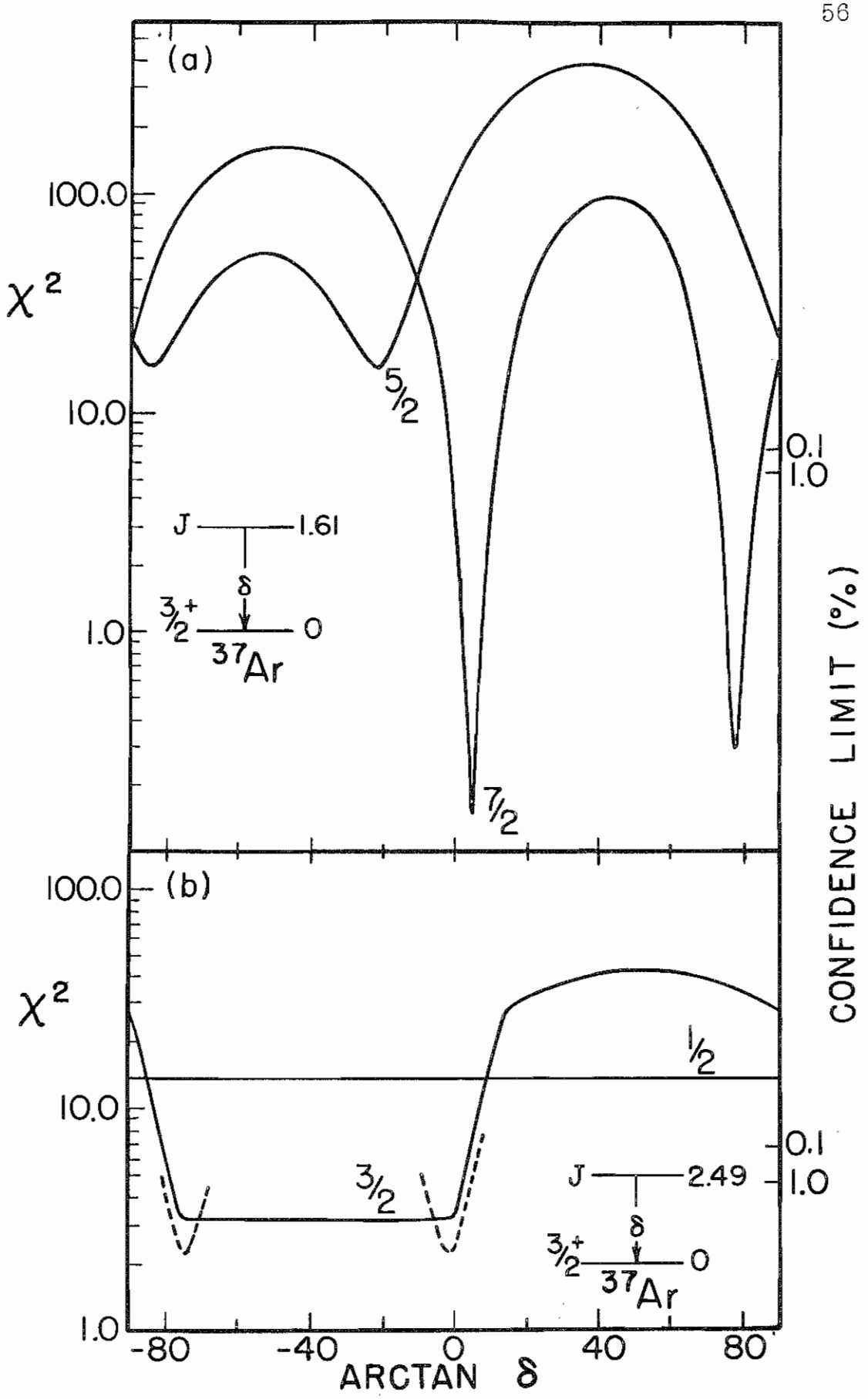
(a)
100.0
χ^2
10.0
1.0
5/2
7/2
J
1.61
δ
3/2+
0
37Ar
0.1
1.0
(b)
100.0
χ^2
10.0
1.0
1/2
3/2
J
2.49
δ
3/2+
0
37Ar
0.1
1.0
-80
-40
0
40
80
ARCTAN δ
CONFIDENCE LIMIT (%)

0, 90, and 143° are shown in Fig. 13(a). The method in which the spectra at these three angles were analyzed to give the number of counts in the 2.22-MeV peaks is described in detail in section C of this chapter. Once the yields of the 2.22-MeV γ rays were known, the yield of the 2.23-MeV γ ray could be determined. The three-point angular distribution of the 2.23-MeV γ ray was then analyzed using the program M2 to obtain the yields at the other two angles. Figure 8 shows two different fits to these three data points. Curve 1 corresponds to a χ^2 of 0.25 and curve 2 corresponds to a χ^2 of 4.27. The two fits were used to obtain some idea of the sensitivity of the data to the method used to unfold the doublet. Using curve 1 of Fig. 8, the contributions due to the 2.23-MeV γ ray were subtracted from the total area of the doublet, and the angular distribution of Fig. 9(a) was obtained. Figure 9(b) shows plots of χ^2 vs $\tan^{-1}\delta$ for spins 1/2 through 7/2 for the $(3 \rightarrow 0)$ transition in ^{37}Ar. The only spin which gives a value of χ^2 below the 0.1% confidence limit is 7/2. The mixing ratios and population parameters at the minima are given in Table V. The solid curve in Fig. 9(a) shows the calculated distribution for $J = 7/2$ and for the smaller of the two mixing ratios. The angular distribution obtained using curve 2 of Fig. 8 gave almost identical plots of χ^2 vs $\tan^{-1}\delta$. On the basis of this analysis the most probable spin of the 2.22-MeV level is 7/2.

The yield for the $(5 \rightarrow 0)$ transition was so low and the statistics so poor that no fit to the angular distribution was attempted.

Table V gives a summary of the mixing ratios determined in

Figure 8. Two different least-squares fits to the three-point angular distribution for the 2.23-MeV γ ray from the first excited state of ^{32}S. Curve 1 corresponds to a χ^2 of 0.25 and curve 2 to a χ^2 of 4.27. These two fits were used to determine the sensitivity of the 2.22-MeV angular distribution to the method used to unfold the 2.23-MeV γ ray from the 2.22-MeV γ ray.

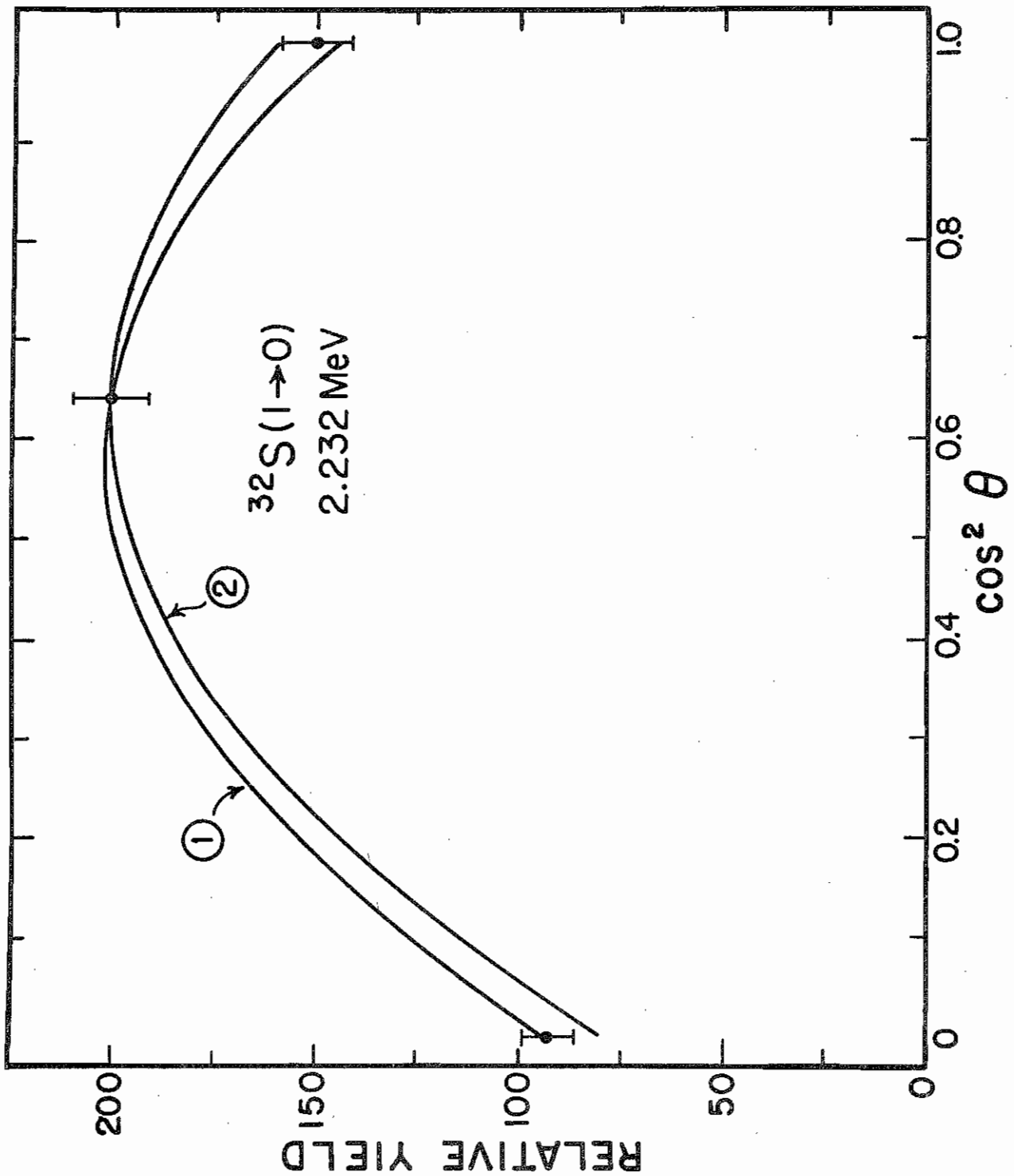
RELATIVE YIELD
200
150
100
50
0
0
0.2
0.4
0.6
0.8
1.0
cos² θ
32S(1→0)
2.232 MeV
①
②

Figure 9. (a) Experimental angular distribution for the 2.22-MeV γ ray and theoretical fits to the data for spin 7/2. These data were obtained at $E_a = 8.10$ MeV using curve 1 of Fig. 8.

(b) Plots of χ^2 vs $\tan^{-1}\delta$ for the $2.22 \rightarrow 0$ transition for spins 1/2, 3/2, 5/2, and 7/2. Only spin 7/2 gives a value of χ^2 below the 0.1% confidence limit. The population parameters were allowed to vary with the restriction $P(1/2) \geq 0.60$ and $P(3/2) \leq 0.40$.

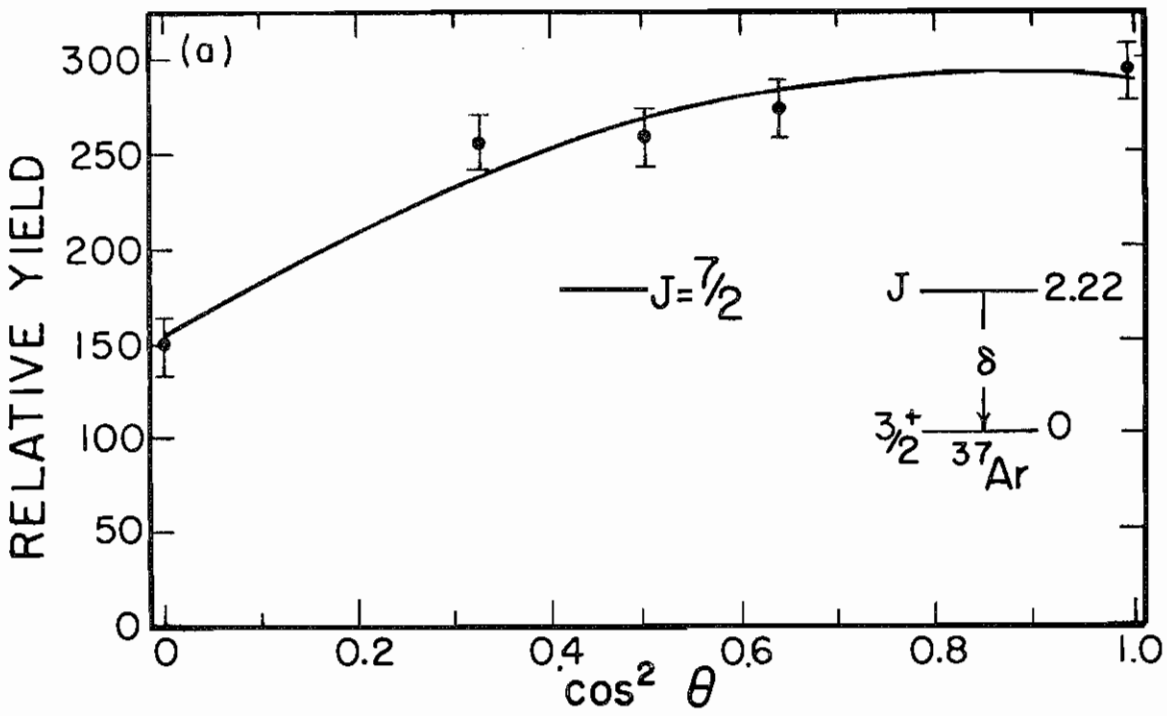
(a)
RELATIVE YIELD
300
250
200
150
100
50
0
0
0.2
0.4
0.6
0.8
1.0
cos² θ
J=7/2
J
2.22
δ
3/2+
0
37Ar

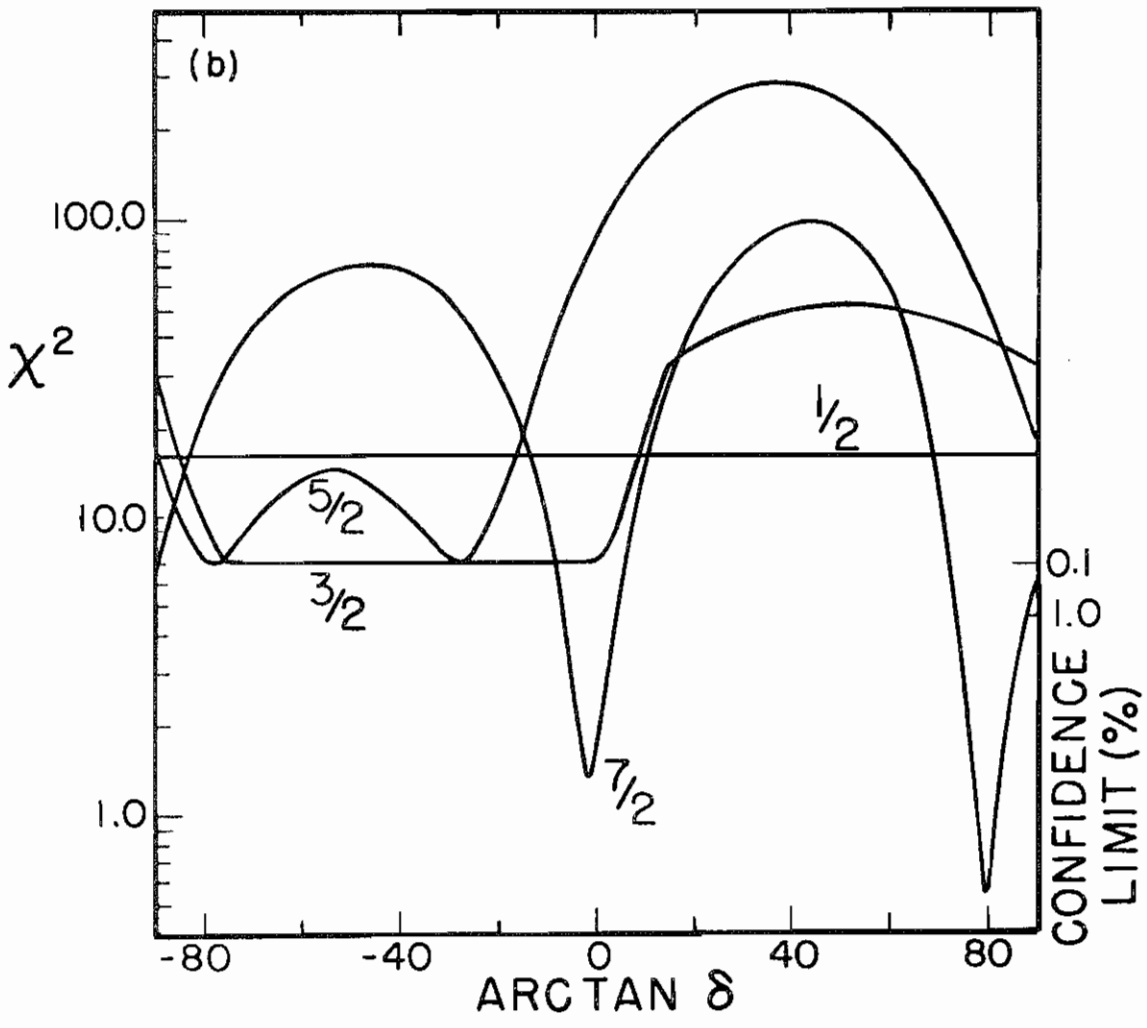
(b)
χ²
100.0
10.0
1.0
1/2
5/2
3/2
7/2
-80
-40
0
40
80
ARCTAN δ
0.1
1.0
CONFIDENCE LIMIT (%)

Table V

Mixing Ratios and Population Parameters in ^{37}Ar

Transition	J_i^π	J_f^π	δ	P(1/2)	P(3/2)
$(2 \rightarrow 0)$	$7/2^-$	$3/2^+$	0.09 ± 0.03	0.60 ± 0.10	0.40 ± 0.10
			$4.54^{+0.79}_{-0.60}$	0.65 ± 0.03	0.35 ± 0.03
$(3 \rightarrow 0)$	$(7/2^+)$	$3/2^+$	-0.03 ± 0.04	0.75 ± 0.15	0.25 ± 0.15
			$5.49^{+1.66}_{-1.05}$	0.74 ± 0.04	0.26 ± 0.04
$(4 \rightarrow 0)$	$3/2^+$	$3/2^+$	$-4.21 \leq \delta \leq 0.06$	-	-
			0.02 ± 0.04 [a]	1.0	0.0
			$-3.57^{+0.48}_{-0.64}$ [a]	1.0	0.0

[a] Determined assuming only the $\pm 1/2$ substates were populated.

this investigation. The populations of the substates are also given. The parity assignment for the 2.22-MeV level will be discussed in Section D of this chapter.

C. Lifetimes

The centroids and areas of the peaks of interest in each spectrum were calculated using the computer program SUNNY. Each spectrum was read back from magnetic tape in 256 channel blocks. A background was calculated under a peak of interest by least-squares fitting a straight line or an exponential to the data in adjacent channels. The channels which were used for the background and for the centroid calculations were chosen with a light pen. Several different backgrounds were usually fitted to the region around each peak, and different channels were included in the centroid and area calculations for each background. These calculations were used to estimate the uncertainty in the calculated areas and centroids and were usually $\sim$the same as the statistical uncertainties. In order to calculate a final value for the centroid of a peak in a given run, the average value of the several centroids was calculated, and the error assigned to this centroid was twice the average statistical error.

In order to determine the experimental Doppler shift attenuation factor $F_{exp}(\tau)$, the maximum possible Doppler shift is needed. The maximum shift was evaluated using the computer program DOPKIN. Since the

CdS target was 100-200 keV thick to the incident α particles, the α-particles energy used in the calculation of the maximum shifts was 50-60 keV less than the incident beam energy. If the angular distribution of the outgoing neutrons is assumed to be symmetric about 90° in the c.m., then the average recoil velocity is just the c.m. velocity (see Eq. (22)). An estimate of the spread in this velocity was obtained from Eq. (26).

The computer program FAVG2 was used to calculate the experimental attenuation factors from the centroids, keV/channel, and maximum shifts. The program first corrected the actual centroids at each angle for any gain or baseline shifts. These shifts were input to the program in the form of baseline shifts and were obtained by noticing how near-by unshifted γ rays and "source" γ rays changed in energy from one run to the next. (Typical shifts were between 0 and 0.3 channels.) A least-squares fit to the channel number of the centroid position at a given angle θ_i was then made with the function (see Chapter II. B.)

$$y_i = a + b \cdot \cos \theta_i \quad . \tag{27}$$

The parameter a, determined from the fit, is the centroid at 90° and $b = F_{exp}(\tau) \cdot M$ where M is the maximum shift at 0° in channels. Figures 12, 14, 15, and 17 show sample plots of the centroid position vs cos θ for some of the γ rays from ^{37}Ar. The solid lines show the fit of Eq. (27) to the data, and the dashed lines show the expected full shift. The values of $F_{exp}(\tau)$ obtained from these fits are also shown.

Theoretical curves of $F(\tau)$ vs τ were calculated using the pro-

gram FTAU described in Appendix D. Several investigators (50 - 53) have found experimentally that for Ar ions in any backing, the electronic stopping parameter k is greater than the LSS value by $\sim$20% (see Appendix A). The electronic stopping parameter was, therefore, increased by 20% in calculating $F(\tau)$. A sample curve plotted from the output of FTAU is shown in Fig. 10 for ^{37}Ar ions recoiling in a 450 $\mu g/cm^2$ $Cd^{34}S$ target on a Ni backing. The mean lifetimes corresponding to values of $F_{exp}(\tau)$ were determined from curves of this type. The statistical errors in τ were determined from the uncertainty in $F_{exp}(\tau)$. The total error in the lifetime was then determined by quadratically adding the errors from the following sources to the statistical errors: a 15% error in the electronic stopping parameter of the target and the backing, a 20% error in the target thickness, and a 6% error in the initial recoil velocity.

1.41-MeV Level

The 1.41-MeV level was studied at two bombarding energies (7.63 and 8.10 MeV). Sample spectra obtained in the investigation of this level at a bombarding energy of 7.63 MeV are shown in Fig. 11, and the Doppler shifts in keV are indicated. Plots of the centroid position vs $\cos\theta$ are shown in Fig. 12 for E_α = 7.63 and 8.10 MeV, and the value of $F_{exp}(\tau)$ is shown for each energy. The weighted average of the mean lifetimes determined at the two energies is $1.08^{+0.17}_{-0.13}$ psec. (See Table VI for

Figure 10. Plot of $F(\tau)$ vs τ in seconds for ^{37}Ar ions recoiling in a 450 $\mu g/cm^2$ $Cd^{34}S$ target and a Ni backing. The incident α-particle bombarding energy was 8.10 MeV. Due to the target thickness of $\sim$100 keV, an effective bombarding energy of 8.05 MeV was used and corresponds to the velocity indicated. This curve was plotted from the output of the code FTAU and is the average of the curves in Fig. D1.

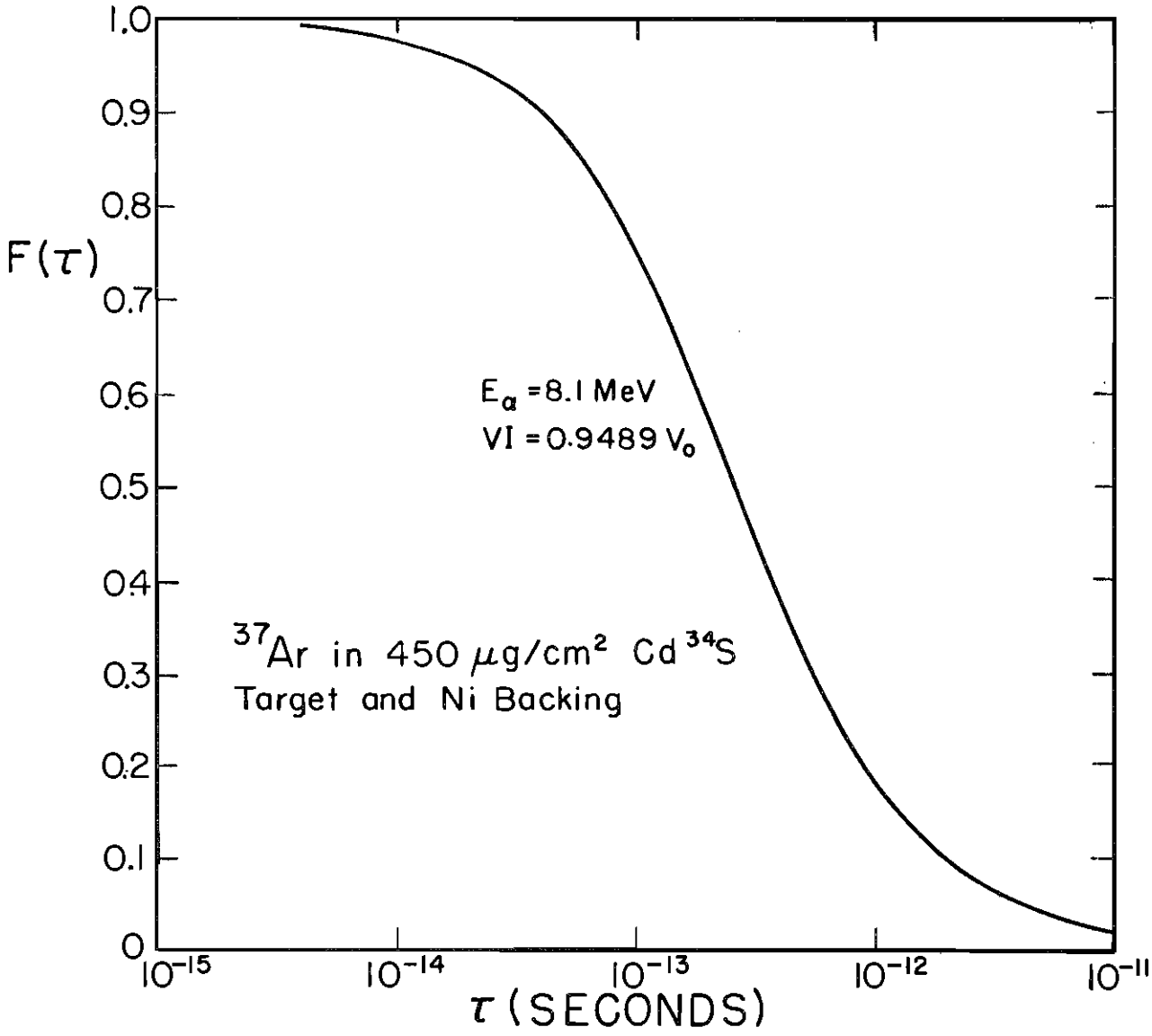
1.0
0.9
0.8
F(τ)
0.7
0.6
0.5
0.4
0.3
0.2
0.1
0
E_α = 8.1 MeV
VI = 0.9489 V_o
^{37}Ar in 450 μg/cm² Cd ^{34}S
Target and Ni Backing
10^{-15}
10^{-14}
10^{-13}
10^{-12}
10^{-11}
τ (SECONDS)

Figure 11. Full-energy-loss peaks of the 1.41-MeV γ ray corresponding to the $(1 \rightarrow 0)$ transition in ^{37}Ar. The state was populated by bombarding a 450 $\mu g/cm^2$ CdS target (enriched to 85.61% in ^{34}S) on a 1 μ Ni foil with 7.63-MeV α particles. The experimental Doppler shifts in keV are shown. The spectra were recorded with the detector at 0, 90, and 143°.

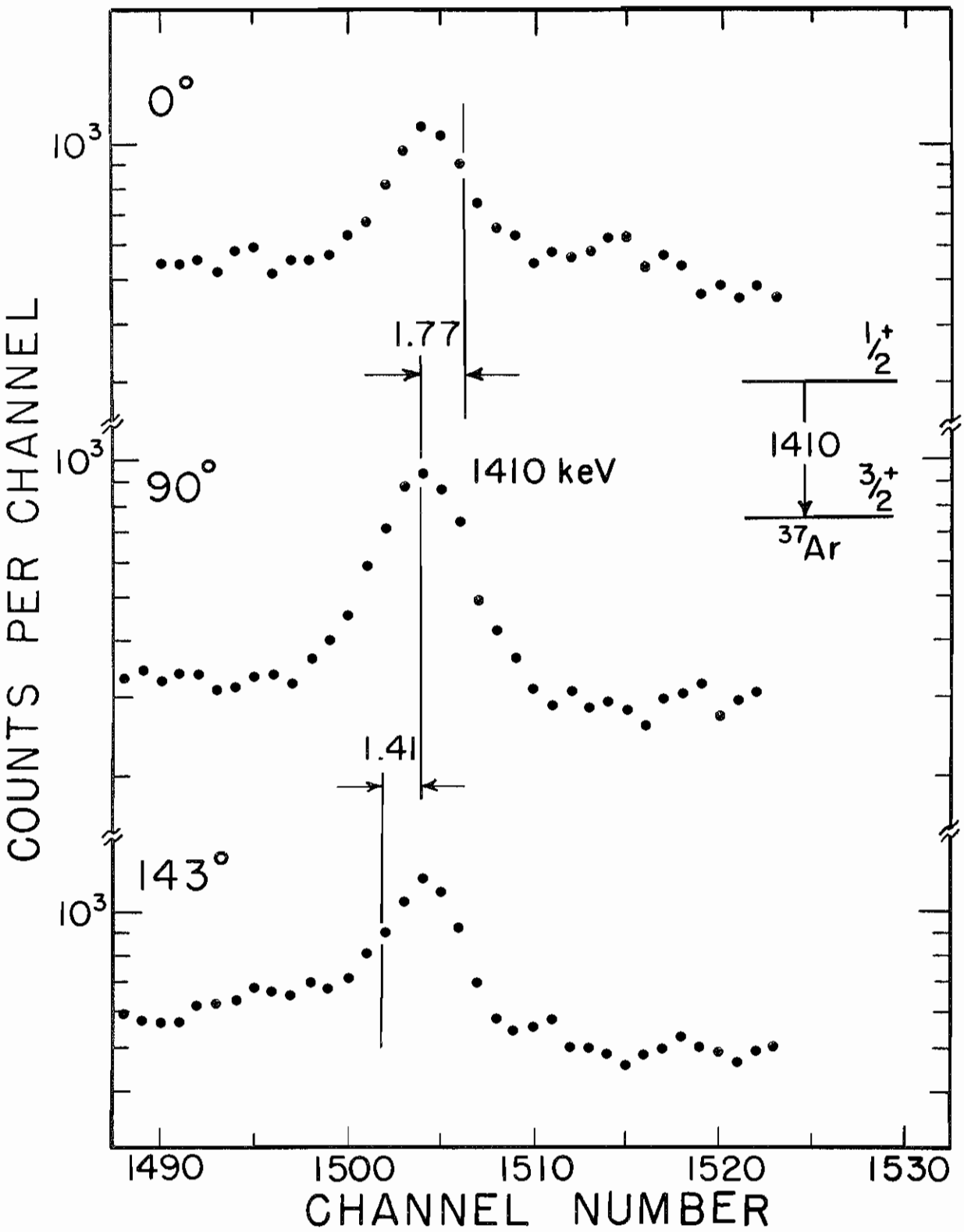
0°
90°
143°
10^3
10^3
10^3
1.77
1.41
1410 keV
$1^+/2$
1410
$3^+/2$
^{37}Ar
COUNTS PER CHANNEL
1490
1500
1510
1520
1530
CHANNEL NUMBER

Figure 12. Plot of centroid position in channels vs $\cos\theta$ for the 1.41-MeV γ ray. The solid line represents a least-squares fit of Eq. (27) to the data and corresponds to the indicated value of $F_{exp}(\tau)$. The dashed line corresponds to the expected full shift. The data in (a) were obtained at E_a = 7.63 MeV and those in (b) were obtained at E_a = 8.10 MeV.

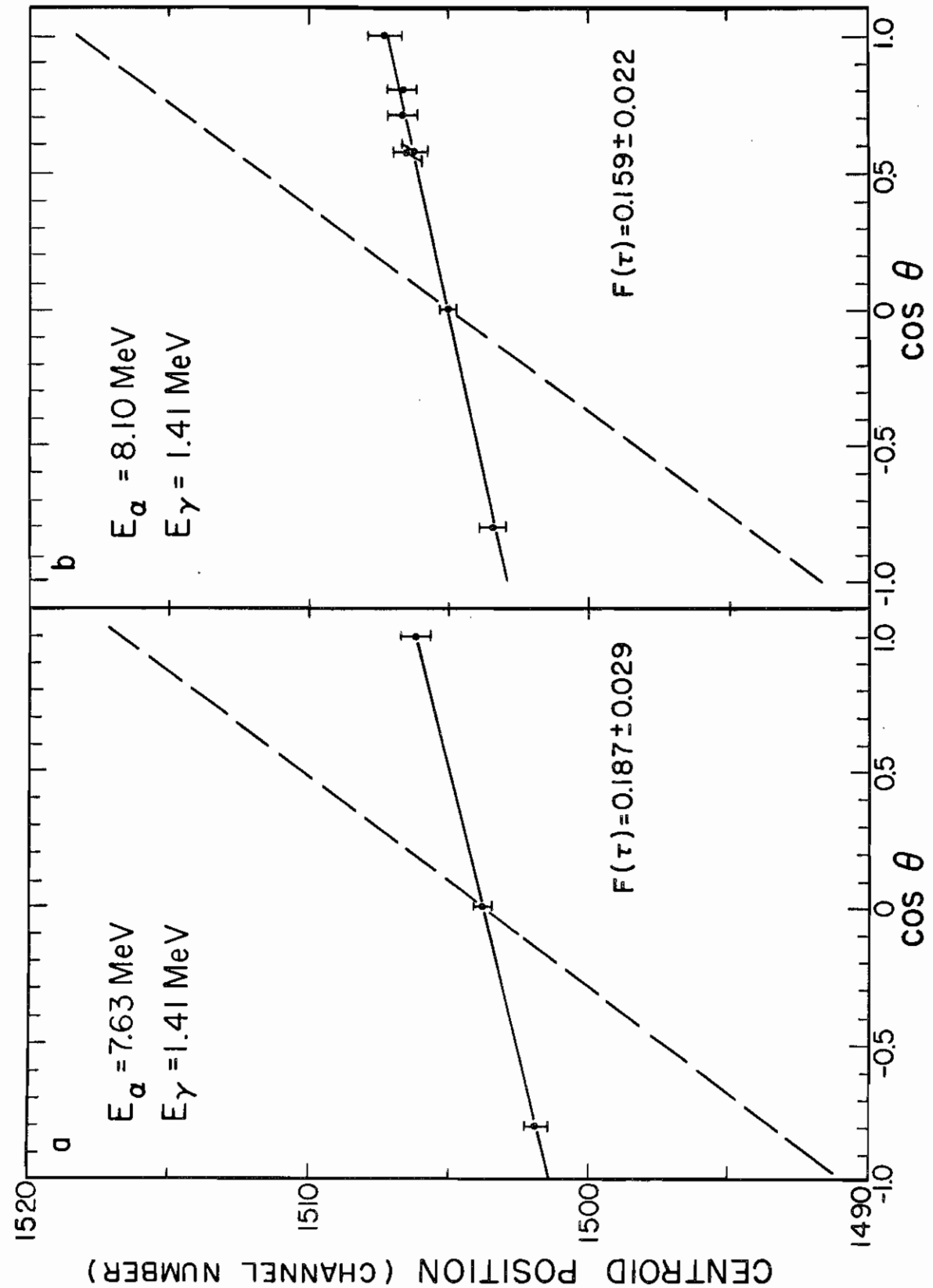
CENTROID POSITION (CHANNEL NUMBER)
1520
1510
1500
1490
a
E_α = 7.63 MeV
E_γ = 1.41 MeV
F(τ)=0.187±0.029
b
E_α = 8.10 MeV
E_γ = 1.41 MeV
F(τ)=0.159±0.022
-1.0
-0.5
0
0.5
1.0
cos θ

values of $F_{exp}(\tau)$ and τ.)

2.22 MeV Level

Although the 2.22-MeV level was studied at only one bombarding energy (8.10 MeV), two different sets of runs at this energy were recorded. No 2.217-MeV γ rays were observed at $E_\alpha = 7.63$ MeV (20 keV below the threshold for the production of this level). However a 2.232-MeV γ ray from the first excited state of ^{32}S was observed at bombarding energies of 7.63 and 8.10 MeV. Sample spectra recorded at $E_\alpha = 8.10$ MeV with the detector at 0, 90, and 143° are plotted (dots) in Fig. 13(a). The spectra plotted with X's were obtained by bombarding the natural CdS target with 8.10 MeV α particles. A straight-line background has been subtracted from these spectra. In order to analyze such spectra, a computer program CONTAM was written to subtract the ^{32}S peak from the total spectrum. Two different experimental line shapes were used to subtract out the ^{32}S peak: 1) the line shape obtained from the ^{32}S target at $E_\alpha = 8.10$ MeV and 2) the line shape obtained from the ^{34}S target at $E_\alpha = 7.63$ MeV. The differences between the total spectra and the line shapes of type 1 are shown in Fig. 13(b), and the Doppler shifts in keV are indicated. The program CONTAM first read in a 256 channel portion of a spectrum that contained the ^{32}S peak alone. A background under the peak was obtained (as described for the program SUNNY). This background was subtracted and

Figure 13. (a) The composite spectra (dots) show the full-energy-loss peaks of the 2.22- and 2.23-MeV γ rays. The 2.22-MeV γ ray corresponds to the $(3 \rightarrow 0)$ transition in ^{37}Ar, and the 2.23-MeV γ ray corresponds to the $(1 \rightarrow 0)$ transition in ^{32}S. The levels were populated by bombarding a 450 $\mu g/cm^2$ $Cd^{34}S$ target on a Ni backing with 8.10-MeV α particles. The X's show the full-energy-loss peaks of the 2.23-MeV γ ray recorded using a natural 180 $\mu g/cm^2$ CdS target on a Ni backing at E_α = 8.10 MeV. The amplitude and position of the 2.23-MeV γ ray have been varied to give a good visual fit to the same γ ray in the composite spectra. A linear background has been subtracted from both sets of spectra.

(b) The differences between the dots and the X's are shown, and the spectra show the shapes of the full-energy-loss peaks for the $(3 \rightarrow 0)$ transition in ^{37}Ar. The experimental Doppler shifts in keV are indicated.

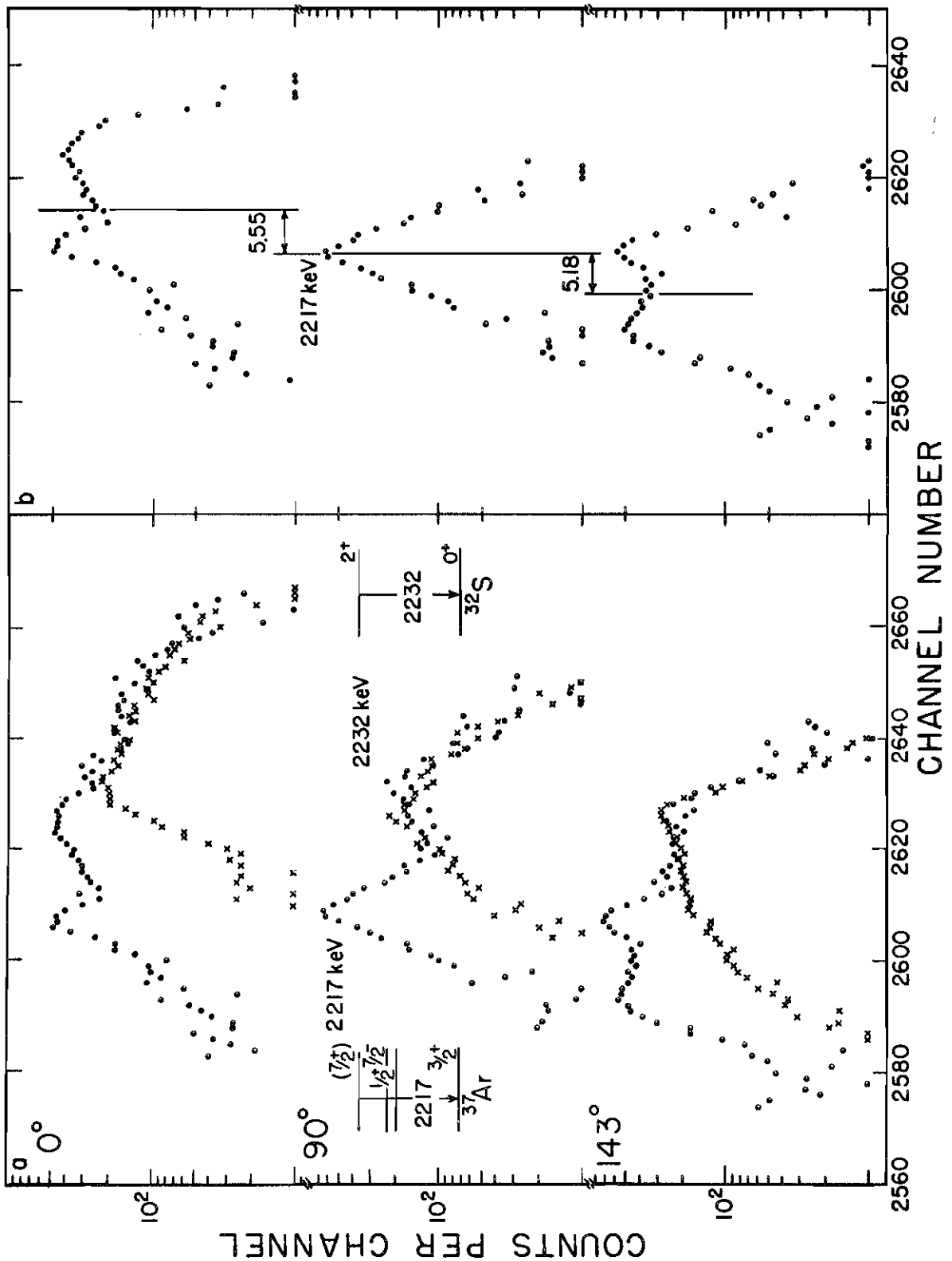
a
b
0°
90°
143°
2217 keV
2232 keV
5.55
5.18
2217 keV
2232
2⁺
0⁺
32S
(7/2⁺)
1/2⁺
7/2⁻
2217
3/2⁺
37Ar
COUNTS PER CHANNEL
CHANNEL NUMBER
10²
2560
2580
2600
2620
2640
2660

the results stored in the matrix YCON. The peak of interest was then read in, the background subtracted, and the results stored in the matrix YPEAK. YPEAK and YCON were then displayed on the scope simultaneously. The difference between the two peaks could also be observed by changing the position of a sense switch. The position and amplitude of YCON were adjusted until a good fit to the ^{32}S peak in the total spectrum was obtained. The difference peak could also be observed as the amplitude and position of YCON were varied. The centroid and area of the difference peak were then calculated and used to determine $F_{exp}(\tau)$. The value of $F_{exp}(\tau)$ (see Table VI) for this level (0.392) is the weighted average of four values of $F_{exp}(\tau)$. These four values were obtained from two sets of runs at E_a = 8.10 MeV and two different line shapes for the ^{32}S γ ray and agreed within the errors. The error (0.026) assigned to the weighted average is the largest of the four statistical errors. The lifetime determined from the above value of $F_{exp}(\tau)$ is 380 ± 50 fsec ($=10^{-15}$ sec). A plot of the centroid position vs $\cos\theta$ is shown in Fig. 14 for the (3 → 0) transition.

2.49-MeV Level

The 2.49-MeV level was studied at bombarding energies of 8.10 and 8.75 MeV. No 2.489-MeV γ rays were observed at E_a = 7.85MeV (110 keV below the threshold for this level). Two sets of runs at a bombarding energy of 8.10 MeV yield almost identical results for $F_{exp}(\tau)$.

Figure 14. Plot of the centroid position in channels vs $\cos\theta$ for the 2.22 → 0 transition in ^{37}Ar. The solid line represents a least-squares fit of Eq. (27) to the data and corresponds to the indicated value of $F_{exp}(\tau)$. The dashed line corresponds to the expected full shift. These results were obtained from the data recorded at E_a = 8.10 MeV.

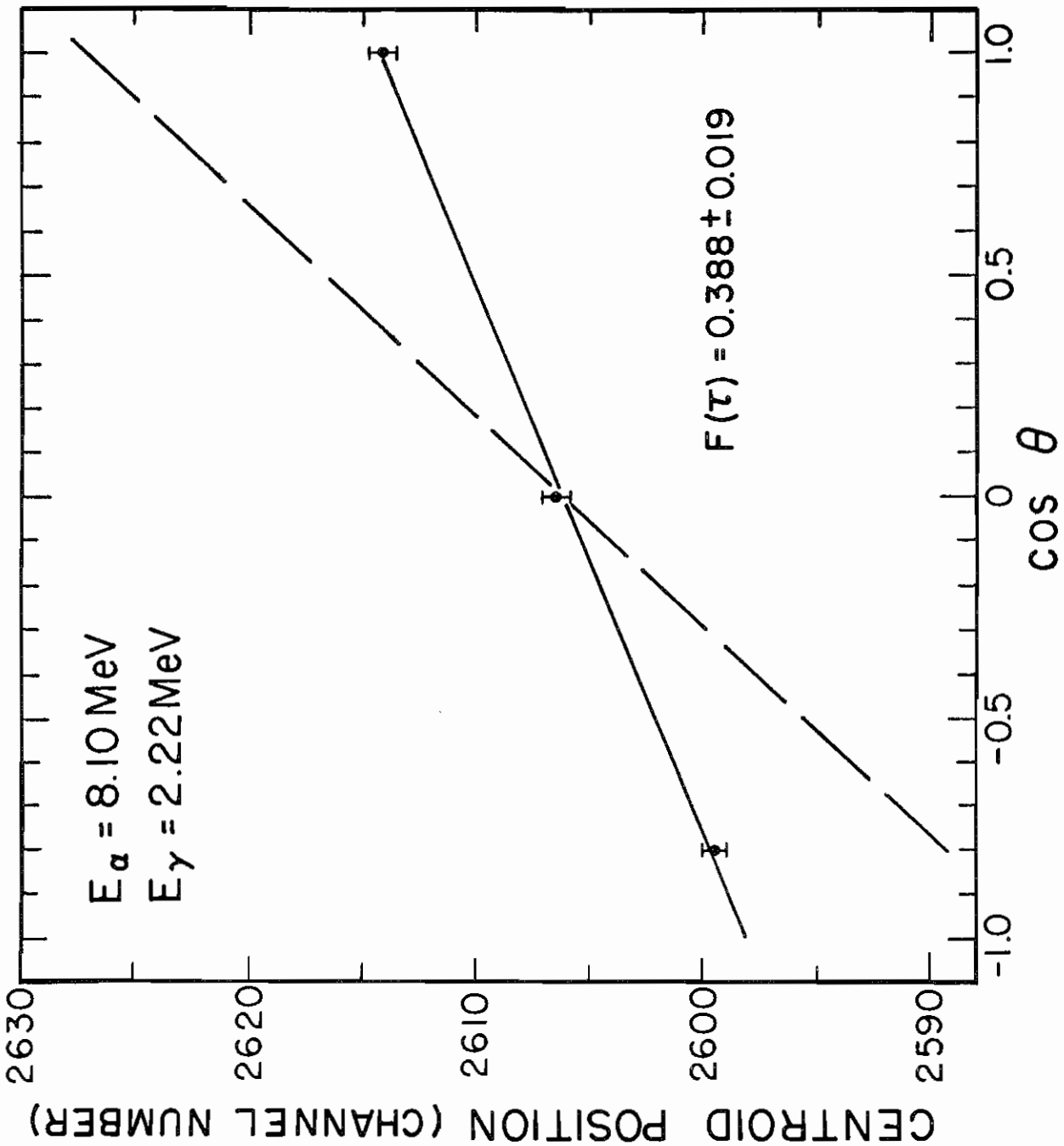
CENTROID POSITION (CHANNEL NUMBER)
2630
2620
2610
2600
2590
-1.0
-0.5
0
0.5
1.0
cos θ
F(τ) = 0.388±0.019
Eα = 8.10 MeV
Eγ = 2.22 MeV

The run at E_a = 8.75 MeV yields a slightly smaller value of $F_{exp}(\tau)$, (see Table VI), but within statistics it is in agreement with the other two runs. The weighted average of the lifetime measurements of this level is 775^{+105}_{-89} fsec. The centroid positions as a function of $\cos\theta$ are shown in Fig. 15 for two different bombarding energies. Sample spectra recorded at E_a = 8.10 MeV are shown in Fig. 16, and the Doppler shifts in keV are indicated.

2.80-MeV Level

The 2.80-MeV level was studied at only one bombarding energy (8.75 MeV). A plot of the centroid position vs $\cos\theta$ is shown in Fig. 17. The Doppler shift is seen to be almost maximum, and $F_{exp}(\tau) = 0.968 \pm 0.024$ which corresponds to a mean lifetime of 14 ± 11 fsec. Since the shift is almost the maximum possible, a more conservative statement about this result would be $\tau \leq 25$ fsec.

Table VI is a summary of the measured mean lifetimes of the levels of ^{37}Ar studied in this investigation. Columns one through three give the level number, the excitation energy, and the bombarding energy. The fourth column gives the value of $F_{exp}(\tau)$ determined for each experimental condition by the methods described previously. Column five gives the mean lifetime corresponding to each value of $F_{exp}(\tau)$, and column six gives the weighted averages of these lifetimes. The errors in column four and five are statistical, but in column six the total errors are given.

Figure 15. Plot of the centroid position in channels vs $\cos\theta$ for the $2.49 \rightarrow 0$ transition in ^{37}Ar. The solid line represents a least-squares fit of Eq. (27) to the data and corresponds to the indicated value of $F_{exp}(\tau)$. The dashed line corresponds to the expected full shift. These results for (a) and (b) were obtained from the data recorded at E_a = 8.10 and 8.75 MeV, respectively.

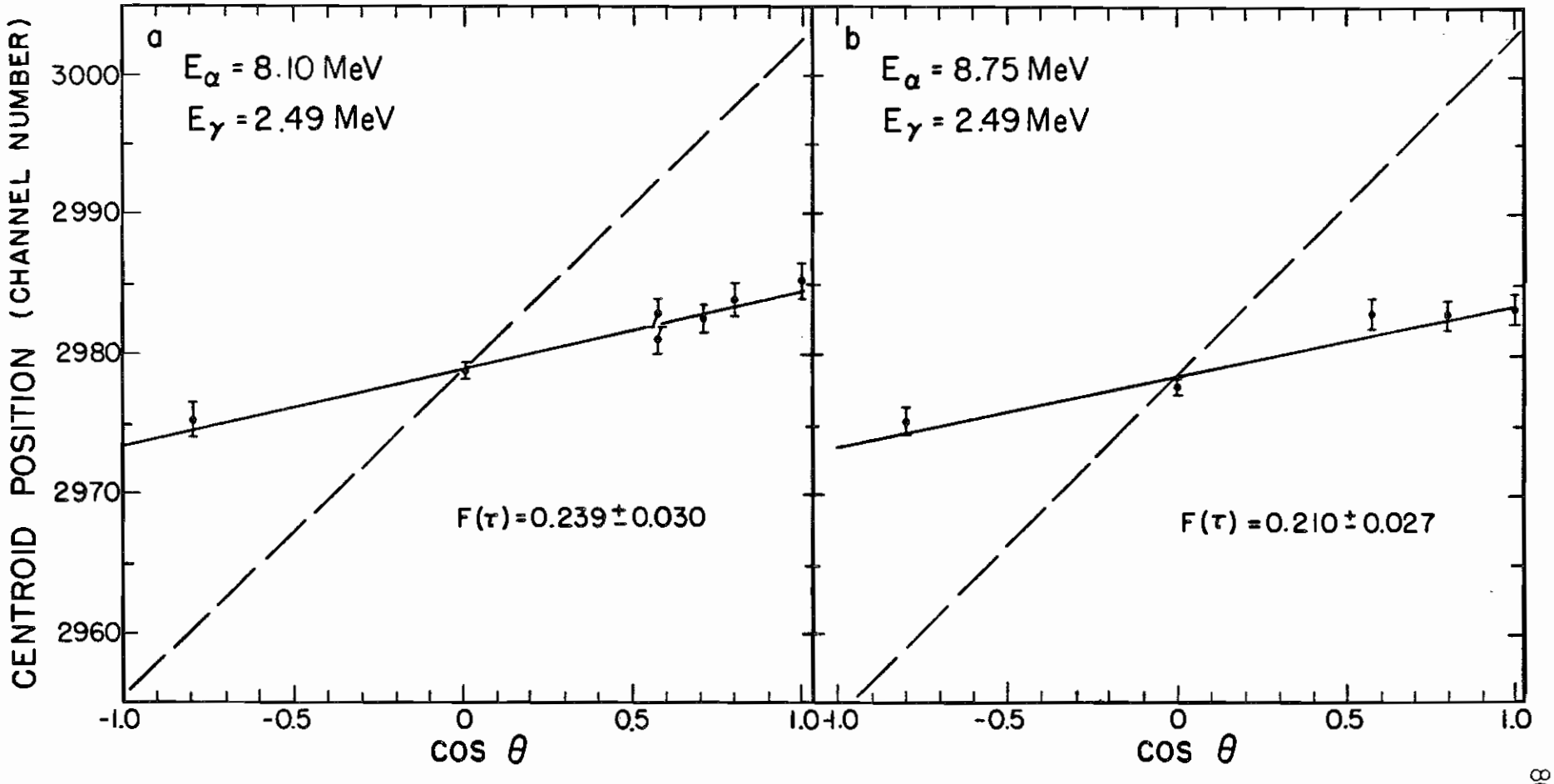
a
E_α = 8.10 MeV
E_γ = 2.49 MeV
F(τ) = 0.239 ± 0.030
b
E_α = 8.75 MeV
E_γ = 2.49 MeV
F(τ) = 0.210 ± 0.027
CENTROID POSITION (CHANNEL NUMBER)
3000
2990
2980
2970
2960
-1.0
-0.5
0
0.5
1.0
cos θ

Figure 16. Full-energy-loss peaks of the 2.49-MeV γ ray corresponding to the $(4 \rightarrow 0)$ transition in ^{37}Ar. The state was populated by bombarding a 450 $\mu g/cm^2$ target (enriched to 85.61% in ^{34}S) on a 1 μ Ni foil with 8.10 MeV α particles. The spectra were recorded with the detector at 0, 90, and 143°, and the experimental Doppler shifts in keV are indicated. The spectra have a dispersion of 0.7330 keV/channel.

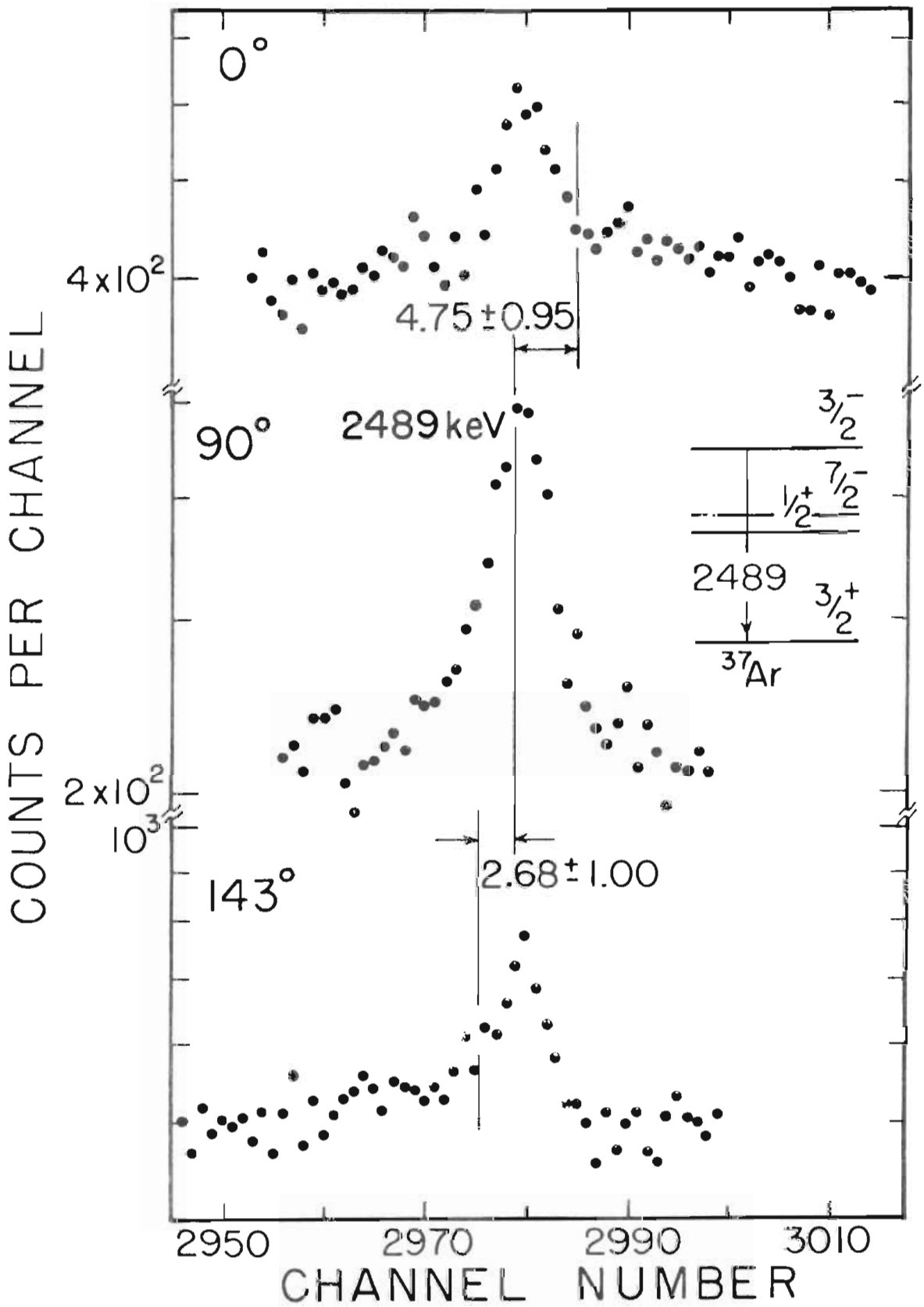
0°
4x10²
4.75±0.95
90°
2489 keV
3/2⁻
7/2⁻
1/2⁺
2489
3/2⁺
³⁷Ar
2x10²
10³
143°
2.68±1.00
COUNTS PER CHANNEL
2950
2970
2990
3010
CHANNEL NUMBER

Figure 17. Plot of the centroid position in channels vs $\cos\theta$ for the 2.80 → 0 transition in ^{37}Ar. The solid line represents a least-squares fit of Eq. (27) to the data and corresponds to the indicated value of $F_{exp}(\tau)$. The dashed line corresponds to the expected full shift. The results were obtained from the data recorded at E_α = 8.75 MeV.

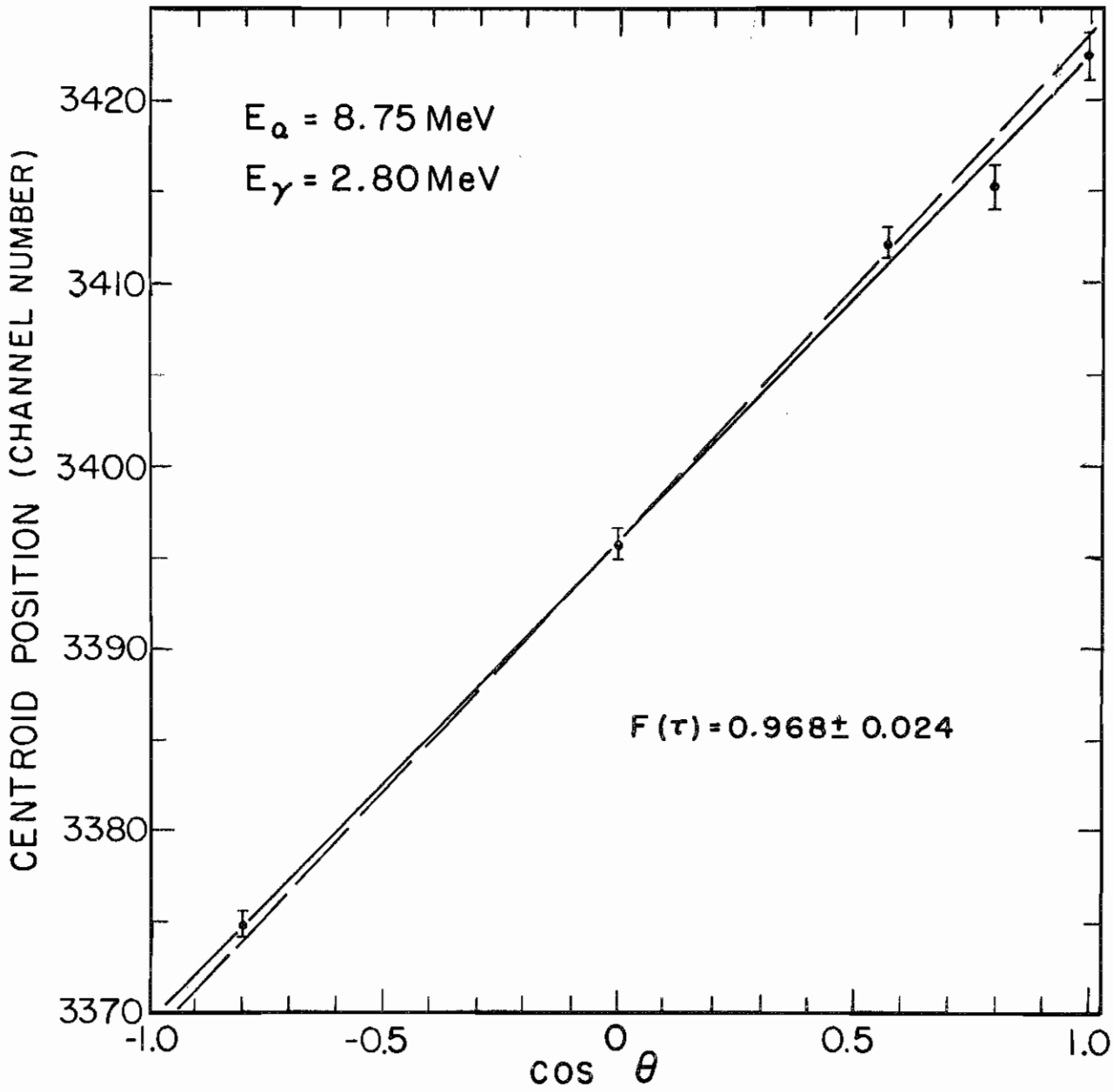
E_α = 8.75 MeV
E_γ = 2.80 MeV
F (τ) = 0.968± 0.024
CENTROID POSITION (CHANNEL NUMBER)
3420
3410
3400
3390
3380
3370
-1.0
-0.5
0
0.5
1.0
cos θ

Table VI

Mean Lifetimes of the Levels of ^{37}Ar.

Level number	E_x (MeV)	E_α (MeV)	$F(\tau)$	Mean lifetime [a] (fsec)	<Mean lifetime> [b] (fsec)
1	1.41	7.63	0.187 ± 0.029	$0.97^{+0.21}_{-0.16}$ psec	
		8.10 [c]	0.160 ± 0.034	$1.16^{+0.39}_{-0.21}$ psec	$1.08^{+0.17}_{-0.13}$ psec
		8.10 [d]	0.159 ± 0.022	$1.17^{+0.23}_{-0.16}$ psec	
3	2.22	8.10	0.392 ± 0.026 [e]	380 ± 38	380 ± 50
4	2.49	8.10 [c]	0.240 ± 0.034	730^{+150}_{-110}	
		8.10 [d]	0.239 ± 0.030	735^{+135}_{-100}	775^{+105}_{-89}
		8.75	0.210 ± 0.027	870^{+150}_{-110}	
5	2.80	8.75	0.968 ± 0.024	14 ± 10	14 ± 11 (< 25)

[a] Statistical errors.

[b] Total errors calculated as explained in the text.

[c] Run 1 at this energy.

[d] Run 2 at this energy.

[e] Average of four values, see text.

D. Synthesis of Results

The branching ratios, spins, multipole mixing ratios, and mean lifetimes of the five low-lying levels of ^{37}Ar determined in this investigation have been used to calculate the electromagnetic transition strenths in Weisskopf units. (54) The Weisskopf unit (W.u.) is an estimate of the single-particle transition strength between two levels assuming that for the initial state $J_i = L + 1/2$ and for the final state $J_f = 1/2$, where L is the lowest-order multipole allowed by the spins. The radial wave function is assumed to be constant throughout the nucleus, and the radius is assumed to be given by $R = r_o A^{1/3}$ where $r_o = 1.2$ F (see reference 54). The formulae used in calculating the Weisskopf estimates are from the article by Skorka et al. (55) Transition strengths that are much larger than any observed value allow certain possible spin values and mixing ratios to be excluded.

Transition strengths in W.u. have been calculated for the observed transitions in ^{37}Ar using the mixing ratios from Table V. The larger mixing ratio (4.54) for the ($2 \rightarrow 0$) transition is unlikely since it leads to an E3 transition strength >123 W.u. which is a factor of 20 larger than the average E3 strength of 6.4 W.u. given by Skorka et al. (55) for $A \leq 40$. The larger negative mixing ratio (-3.57) for the ($4 \rightarrow 0$) transition is also unlikely since it yields a M2 strength >40 W.u. which is over two orders of magnitude larger than the average M2 strength of 0.31 W.u. given by Skorka et al. (55) If negative parity is assumed for the third

excited state, the smaller mixing ratio (0.03) for the (3 → 0) transition yields a M2 strength > 174 W.u., and the larger mixing ratio (5.49) yields an E3 transition strength $>1.8 \times 10^5$ W.u. On the basis of these transition strengths, negative parity is ruled out and positive parity is assigned to this level. The larger mixing ratio for the (3 → 0) transition leads to a M3 transition strength $>6.5 \times 10^6$ W.u., and, therefore, this mixing ratio is ruled out.

Table VII gives the transition strengths in W.u. for the observed transitions in ^{37}Ar. The mixing ratios determined in this experiment are used where possible. A mixing ratio of zero is assumed for the (4 → 0) transition since M2 and E1 radiations are competing. Since the mixing ratio for the (1 → 0) transition could not be determined, transition strengths were calculated for both pure M1 and pure E2 radiations. A mixing ratio of zero (consistent with the experimental value of 0.03 ± 0.04) was assumed for the (3 → 0) transition. The mixing ratio for the (5 → 0) transition is also unknown, and transition strengths for pure M1 and pure E2 are calculated. The E3 strength for the (2 → 0) transition is in agreement with other E3 strengths in this mass region. (55)

The tentative spin and parity of $7/2^+$ determined for the 2.22-MeV level in this work is supported by the following evidence: Naude et al. (19) found that of their two tentative spin assignments (5/2 and 7/2), 7/2 was the more probable. Dieperink and Brussaard (10) also pointed out

Table VII

Electromagnetic Transition Strengths in ^{37}Ar.

Transition	J_i^π	J_f^π	δ	Multipole	$\lvert M\rvert^2$ (Weisskopf units)
$(1 \rightarrow 0)$	$1/2^+$	$3/2^+$	0^a	M1	0.01 ± 0.001
			∞^a	E2	18.5 ± 2.5
$(2 \rightarrow 0)$	$7/2^-$	$3/2^+$	0.09 ± 0.03	M2	0.07 ± 0.01
				E3	$1.2 \; {}^{+\,1.2}_{-\,0.7}$
$(3 \rightarrow 0)$	$(7/2^+)$	$3/2^+$	0^b	E2	5.5 ± 0.7
$(4 \rightarrow 0)$	$3/2^-$	$3/2^+$	0^b	E1	$7.3 \pm 0.9 \times 10^{-5}$
$(5 \rightarrow 0)$	$5/2^+$	$3/2^+$	0^a	M1	$0.10 \; {}^{+\,0.38}_{-\,0.05}$
			∞^a	E2	$47 \; {}^{+170}_{-\,21}$

[a] Assumed pure transitions.

[b] Assumed; consistent with the experimental value of $\delta = 0.03 \pm 0.04$.

that a J^{π} assignment of $7/2^{+}$ is most likely since the level is not observed in the (d,p) reaction and since the ^{37}K ground state ($J^{\pi} = 3/2^{+}$) (15) β decays to the 2.80-MeV ($5/2^{+}$) level of ^{37}Ar but not to the 2.22-MeV level. Dieperink and Brussaard (10) also predicted a $7/2^{+}$ level below the $5/2^{+}$ level (see Chapter VI), and the 2.22-MeV level is the only possible candidate.

Chapter V

COMPARISON WITH THEORY

In 1964 Glaudemans et al. (56) investigated the properties of nuclei between ^{29}Si and ^{40}Ca using an inert ^{28}Si core with the remaining particles interacting in the $2s_{1/2}$ and $1d_{3/2}$ orbits. The interaction matrix elements were taken as sums over two-particle matrix elements and were calculated by treating them as parameters to be fitted to reproduce the experimentally observed levels. In addition to the 15 two-particle matrix elements, the binding energies to the core of the $2s_{1/2}$ and $1d_{3/2}$ nucleons were included as parameters. By varying these 17 parameters until a best fit was obtained to 50 of the low-lying states of nuclei in this region, wave functions and additional energy levels were determined. The agreement with experimentally observed energy levels was, in general, good. The wave functions were subsequently used to calculate many properties of the nuclei in the A = 29-40 mass region. In a sequel to the 1964 paper, Glaudemans et al. (57) in 1966 used a surface delta interaction (SDI) (58) as an approximation to the two-body interaction for the nucleons outside the ^{28}Si core. This refinement of the above model decreased the number of

free parameters in the search without appreciably affecting the accuracy of the predicted energy levels. This decrease in the number of parameters, however, opened the way for additional calculations using a larger model space (e.g., the entire 2s-1d shell). Wildenthal et al. (59) made such an extension of the above model using a modified surface delta interaction (MSDI). (60) The shell-model basis was restricted to particles in the $1d_{5/2}$, $2s_{1/2}$, and $1d_{3/2}$ orbits with a closed ^{16}O core and with the additional restriction that the $1d_{5/2}$ orbit include, at most, two holes. For a given nuclear level the number of many-particle basis states was typically between 100 and 300 while, for the full 2s-1d shell, the number would have been between 1000 and 3000. The wave functions from this model were used in later papers (9, 61) to calculate magnetic dipole and electric quadrupole transition rates as well as moments and log ft values for even parity states in the A = 30-34 mass region. The general agreement between theory and experiment is good, and for ^{33}S the agreement is excellent. The success of this model in the region A = 30-34 suggests tests of similar models in the upper end of the 2s-1d shell.

Dieperink and Brussaard (10) have performed a shell-model calculation for A = 36-39 nuclei using the full 2s-1d shell configuration space. The residual shell model interaction was derived from the Tabakin interaction. (11) The low-lying positive parity energy levels of ^{37}Ar calculated using this approach are given in Table VIII along with the experimentally determined energies. The main components of the wave functions (squares

Table VIII

Calculated Energy Levels and Major Components of the Wave Functions of the Low-Lying Positive Parity States of ^{37}Ar [a]

Experimental E_x (MeV)	0.0	1.41	2.22	2.80
Calculated [b] E_x (MeV)	0.0	1.34	2.27	2.36
J^π	$3/2^+$	$1/2^+$	$7/2^+$	$5/2^+$
Components of the wave Function in % $d_{3/2}^{-3}$	76.3	10.4	78.9	25.2
$d_{3/2}^{-2}s_{1/2}^{-1}$	--	51.4	11.9	13.2
$d_{3/2}^{-1}s_{1/2}^{-2}$	5.5	--	0	10.2
$d_{5/2}^{-1}d_{3/2}^{-2}$	3.5	10.2	4.0	39.6
$d_{5/2}^{-1}s_{1/2}^{-1}d_{3/2}^{-1}$	--	12.5	3.6	--
$s_{1/2}^{-3}$	0	8.5	0	0
$d_{5/2}^{-2}d_{3/2}^{-1}$	10.2	--	--	4.3
$d_{5/2}^{-2}s_{1/2}^{-1}$	--	5.5	--	--

[a] Components < 3 % are indicated by dashes.
[b] Relative to the ground state.

Table IX

Comparison of Experimental and Calculated Lifetimes and Electromagnetic Transition Strengths.

	E_x (MeV)	1.41		2.22	2.80	
	Transition	(1 → 0)		(3 → 0)	(5 → 0)	
	Multipole	M1	E2	E2	M1	E2
EXPERIMENTAL	δ	0[a]	∞[a]	0[b]	0[a]	∞[a]
	$\lvert M\rvert^2_{(W.u.)}$	0.01 ± 0.001	18.5 ± 2.5	5.5 ± 0.7	$0.10^{+0.38}_{-0.05}$	47^{+170}_{-21}
	τ	$1.08^{+0.17}_{-0.13}$ psec		380 ± 50 fsec	14 ± 11 fsec	
CALCULATED[c]	$\lvert\delta\rvert$	0.32			0.07	
	$\lvert M\rvert^2_{(W.u.)}$	0.014	2.5		0.42	0.82
	τ	0.74 psec			3.6 fsec	
CALCULATED[d]	$\lvert\delta\rvert$	0.53		--	0.12	
	$\lvert M\rvert^2_{(W.u.)}$	0.018	9.2	5.0	0.43	2.8
	τ	0.48 psec		415 fsec	3.4 fsec	

[a] Assumed pure transitions.

[b] Consistent with the experimental mixing ratio of 0.03 ± 0.04.

[c] Calculated using Dieperink's wave functions.

[d] Calculated using Wildenthal's wave functions.

of the amptitude) for each level are also given in the table. At the time these calculations were performed there were no experimentally determined γ-ray transition strengths between the positive parity states of ^{37}Ar, and no calculated values were given. Dieperink (23) has since used the wave functions of Table VIII and bare nucleon charges and moments to calculate transition strengths for some positive parity states in ^{37}Ar. No calculation of the lifetime of the $7/2^+$ level was made because this level had not been located at the time of the calculation. Table IX gives a comparison of the experimentally observed electromagnetic transition strengths and mean lifetimes with the theoretical values for the low-lying positive parity states of ^{37}Ar. The agreement between theory and experiment for the lifetimes is generally good, but individual transition strengths cannot be compared (in all cases) since the mixing ratios were not determined experimentally. Wildenthal (24) has also calculated transition strengths in ^{37}Ar using the same model space as Dieperink. (23) The two-body matrix elements were the Kuo-Brown matrix elements. (25) In calculating transition strengths an effective charge of 0.5 was used for both the protons and neutrons, and bare nucleon magnetic moments were assumed. These calculations are also compared with the results of the present experiment in Table IX. The calculated branching ratio for the $(5 \rightarrow 1)$ transition (assuming pure E2) is 0.08% and is not shown in the table. The agreement between the theoretical and experimental lifetimes is good. Dieperink's (23) calculation of the lifetime of the first excited state agrees more closely

with experiment but is probably not as meaningful since effective charges were not used.

No transition strengths have been calculated for the negative parity states of ^{37}Ar. Erné (62) has calculated energy levels for nuclei between ^{33}S and ^{41}Ca using an inert ^{32}S core with one nucleon in the $1f_{7/2}$ shell and the remaining nucleons in the $1d_{3/2}$ shell. However, the wave functions determined from this calculation are not detailed enough for successful predictions of electromagnetic transition rates. Maripuu and Hokken (63) have performed shell-model calculations for the negative parity states in ^{35}Cl, ^{35}S, ^{37}Cl, ^{39}Ar, and ^{39}K assuming an inert ^{32}S core with one particle in the $1f_{7/2}$ or $2p_{3/2}$ shell and the remainder in the $1d_{3/2}$ shell. M1 and E2 transition strengths and other properties have been calculated from the wave functions, but the model has not been extended to ^{37}Ar. Engelbertink and Glaudemans (64) have performed shell-model calculations for positive and negative parity states in ^{38}Ar using a similar model space for the negative parity states. Calculations for the positive parity states were performed assuming ten particles in the $2s_{1/2}$ and $1d_{3/2}$ shells, but this model also has not been extended to ^{37}Ar.

Chapter VI

SUMMARY AND CONCLUSIONS

In the course of this investigation the five lowest-lying levels of ^{37}Ar have been studied. The mean lifetimes of four of the levels have been determined along with the modes of γ decay. Angular distributions for levels 1, 2, and 4 give spins in agreement with previous assignments. On the basis of the angular distribution and lifetime, a tentative spin and parity of $7/2^+$ has been assigned to the 2.22-MeV level. From the above measurements the electromagnetic transition strengths (matrix elements of electromagnetic operators) between the levels have been calculated and (where possible) compared with theoretical calculations. The agreement between theory and experiment is generally good. More theoretical calculations are needed especially for the negative parity states. A more thorough study of the 2.80-MeV level ($5/2^+$) is also needed since the low yield of this level precluded an analysis of the angular distribution. A more careful measurement of the mean life of the 1.61-MeV level ($7/2^-$) using the RDM would be helpful since the initial measurement of the lifetime of this level (18) was performed at only one target-to-stopper distance.

A study of the higher excited states would provide more information for comparison with theory. Higher bombarding energies would be necessary, and (n, γ) coincident measurements would probably be required because of the increased γ-ray background. Since the over-all counting rate is lower when a coincidence experiment is performed, a thicker target would be necessary.

The upper end of the 2s-1d shell still has not been studied as thoroughly as the lower end, but experimental information is being accumulated rapidly. Theoretical shell-model calculations including particles in the $1d_{5/2}$, $2s_{1/2}$, $1d_{3/2}$, $1f_{7/2}$, and $2p_{3/2}$ orbits would help in understanding the properties of all low-lying levels of nuclei near the upper end of the 2s-1d shell. However, the inclusion of these shell-model states would require enormous amounts of computer memory. Therefore, some compromise between accuracy and computer memory must be reached. An extension of the work by Maripuu and Hokken (63) and by Engelbertink and Glaudemans (64) to other nuclei in this mass region would probably be sufficient to fill some of the gaps in the theoretical treatment. Extensions of this type, however, will probably not be made until more experimental data in this mass region have been collected.

APPENDICES

Appendix A

ENERGY LOSS OF HEAVY IONS

A. Electronic

Lindhard et al. (27, 28) have derived the following equation for the electronic part (denoted by the subscript e) of the energy loss for ions with $v < v_0 Z_1^{2/3}$:

$$(d\epsilon/d\rho)_e = k\epsilon^{1/2} \quad . \tag{A1}$$

ϵ and ρ are defined by Eqs. (14) and (15) of the text, and

$$k = \mathcal{E}_e \frac{0.0793\, Z_1^{1/2} Z_2^{1/2} (A_1 + A_2)^{3/2}}{(Z_1^{2/3} + Z_2^{2/3})^{3/4} A_1^{3/2} A_2^{1/2}} \quad , \tag{A2}$$

where $\mathcal{E}_e$ is a constant between 1 and 2 and $\approx Z_1^{1/6}$. The values of k predicted by Eq. (A2) are in reasonable agreement with those determined experimentally. However, Duckworth and co-workers (50, 51) and Fastrup and Hvelplund (52, 53) have found that the experimental electronic stopping power shows a periodic variation (with Z_1) about the LSS value. Figure A1 shows experimental data for the electronic stopping power from Hvelplund and Fastrup (53) for atoms of different Z_1 stopping in carbon. The oscilla-

Figure A1. Plot from reference 53 of the theoretical and experimental values of the electronic specific energy loss $[(-dE/dx)_e]$ in carbon for moving ions of different Z. The points show the oscillations of the experimental values of $(-dE/dx)_e$ about the value predicted by Lindhard, Scharff, and Schiøtt (solid curve).

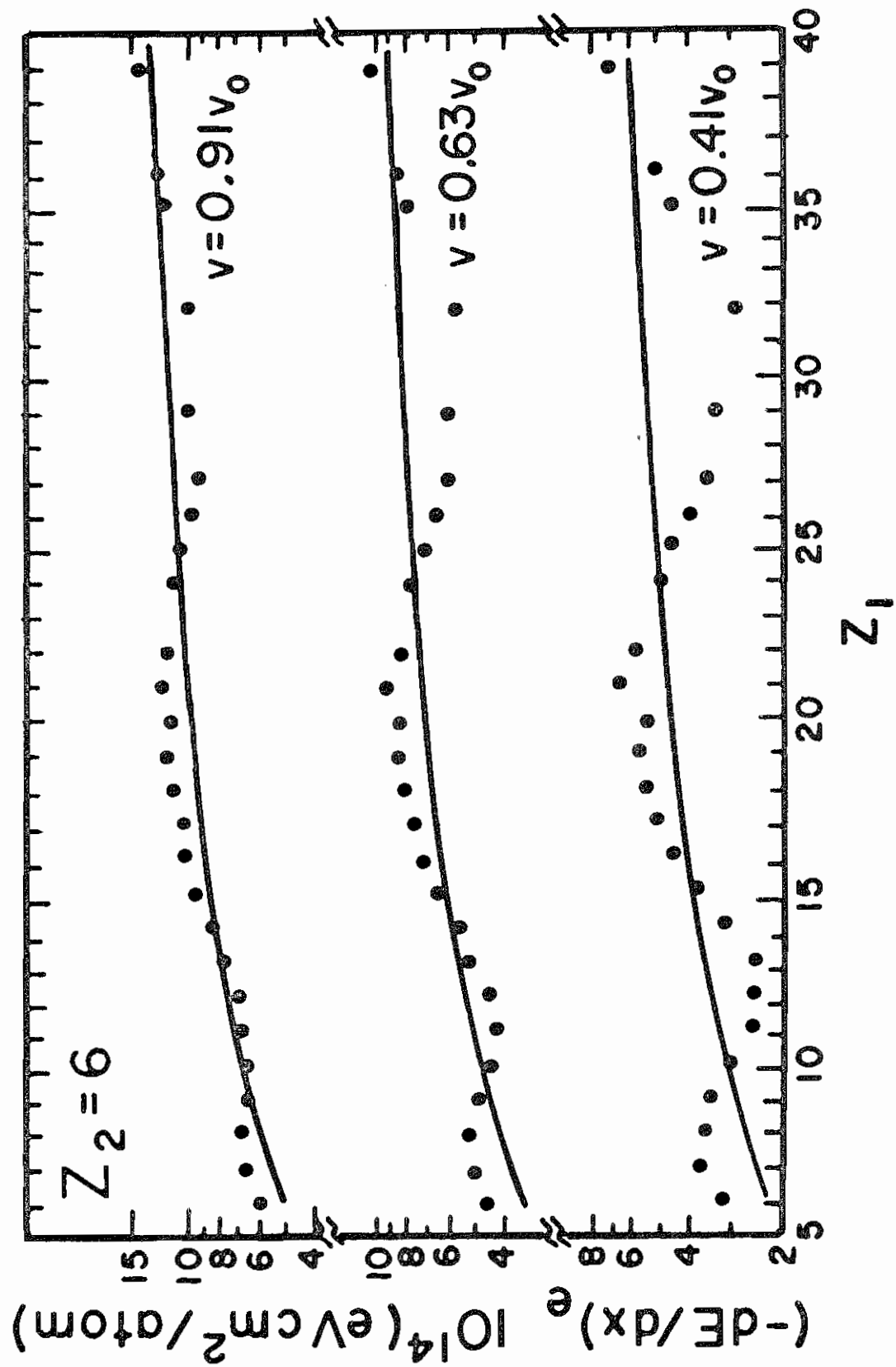
$Z_2=6$
$v=0.91v_o$
$v=0.63v_o$
$v=0.41v_o$
$(-dE/dx)_e$ 10^{14}(eV cm^2/atom)
Z_1
25
30
35
40
20
15
10
5
4
6
8
10
15

tions about the value predicted by LSS become greater with decreasing velocity and tend to decrease as Z_2 is increased. The positions of the maxima and minima, however, do not change with Z_2 and seem to depend upon atomic shell effects.

B. Nuclear

Lindhard et al. (27) have used a Thomas-Fermi type of potential to obtain a universal differential atomic or nuclear scattering cross section --

$$d\sigma(\delta) = \pi a^2 f(q)\, dq/q^2, \tag{A3}$$

where $q = \epsilon \sin(\delta/2)$ and δ is the deflection angle in the c.m. This equation can be used to derive an expression for the nuclear part (denoted by the subscript n) of the energy loss of heavy ions in matter:

$$(d\epsilon/d\rho)_n = \frac{1}{\epsilon}\int_0^{\epsilon} f(q)\, dq \quad . \tag{A4}$$

The function f(q) has been determined numerically by LSS and is given in Fig. A2(a). An analytical approximation to this function has been derived by Currie (35) and is given by

$$f(q) = \begin{cases} 1.43\, q^{0.35}, & q \leq 0.0085 \\ 0.25 + 0.18 \cdot \cos\left[\dfrac{1.966 + \log q}{1.6}\right] + \dfrac{0.0004}{q}, & 0.0085 < q \leq 0.14 \\ 0.25 + 0.185 \cdot \cos\left[\dfrac{1.966 + \log q}{1.37}\right], & 0.14 < q \leq 7.0 \\ 1/(2q), & q > 7.0 \end{cases} \tag{A5}$$

Figure A2. (a) Plot of the nuclear scattering cross section $f(q)$ in the center of mass vs q from reference 27.

(b) Plots of $(d\epsilon/d\rho)_e$ with $k = 0.15$ and $(d\epsilon/d\rho)_n$ vs $\epsilon^{1/2}$. For ^{37}Ar ions in Ni, $k = 0234$, while for ^{37}Ar ions in ^{34}S, $k = 0.172$.

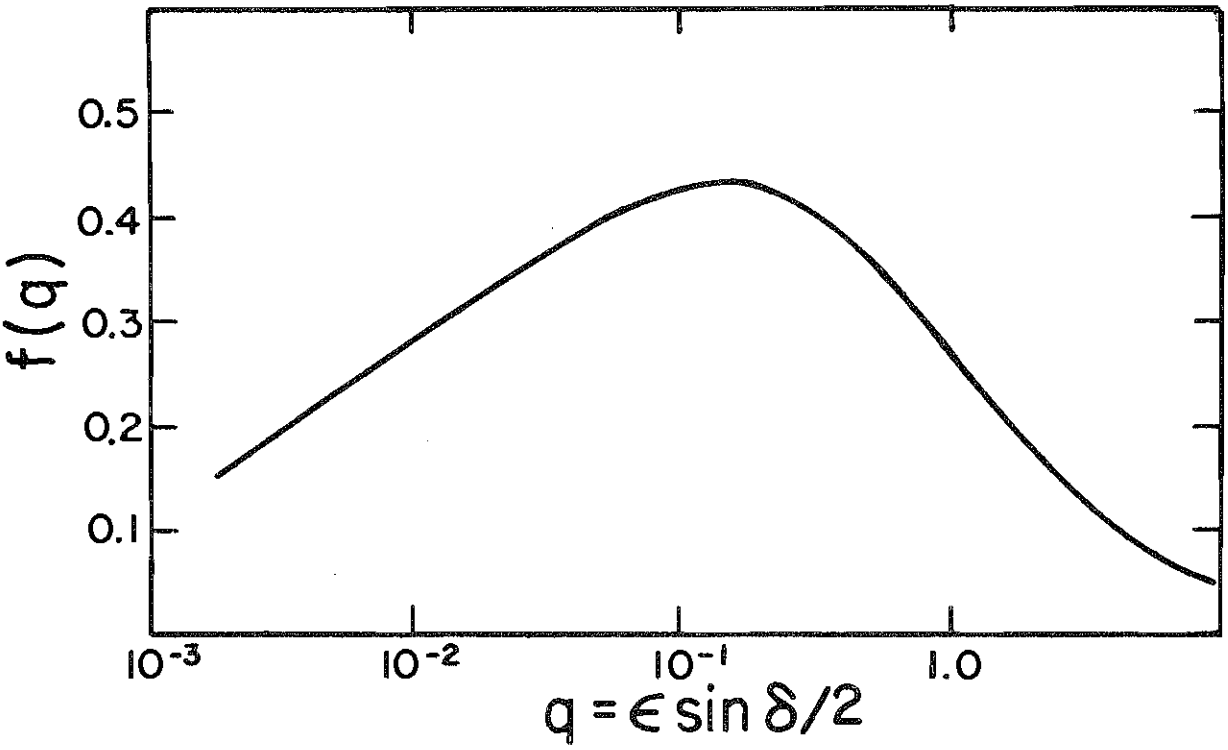
0.5
0.4
0.3
0.2
0.1
f(q)
10-3
10-2
10-1
1.0
q = ϵ sin δ/2

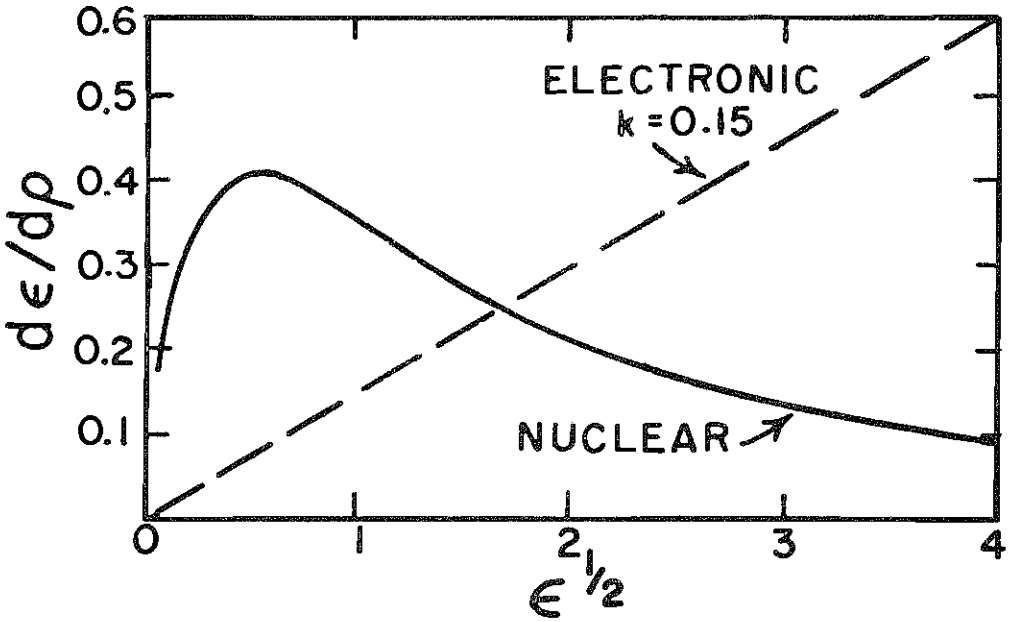
0.6
0.5
0.4
0.3
0.2
0.1
dϵ/dρ
ELECTRONIC
k = 0.15
NUCLEAR
0
1
2
3
4
ϵ 1/2

Several workers have given analytical expression for $(d\epsilon/d\rho)_n$. The one given by Currie (35) is

$$(d\epsilon/d\rho)_n = \begin{cases} 0.6111 \exp(-\epsilon^{1/2}/1.919)\left[1-\exp(-\epsilon^{1/2}/0.2406)\right], & \epsilon \leq 2.4 \\ (1/2\epsilon)\left\{0.31 + \ln\left[(0.6+\epsilon^2)/\epsilon\right]\right\}, & \epsilon > 2.4 \end{cases} \quad \text{(A6)}$$

The expression given by Warburton (65) for the nuclear part of the energy loss is

$$(d\epsilon/d\rho)_n = \begin{cases} 10.0^{(-0.984182 + 0.23497P + 0.09636P^2 - 0.03817P^3)}, \\ \qquad \text{where } P = 3.0 + \log \epsilon \qquad \epsilon \leq 4.0 \\ (1/2\epsilon)\left\{0.3 + \ln\left[(0.6+\epsilon^2)/\epsilon\right]\right\}, \qquad \epsilon > 4.0 \ . \end{cases} \quad \text{(A7)}$$

Figure A2(b) shows the electronic and nuclear parts of the energy loss in terms of universal variables. Both of these curves are from LSS. (27)

Appendix B

ENERGY LOSS APPROXIMATION DUE TO WARBURTON ET AL.

Warburton and co-workers (29-32) have developed an approximation to the rate of change of the z-component of the recoil velocity which makes the evaluation of $F(\tau)$ straightforward. A derivation of this expression is given in this Appendix along with a discussion of the validity of the approximation. Expressions for $F(\tau)$ using this approximation are also presented.

A general identity for $(-dE/dx)$ is

$$(-dE/dx) = -M_1 (dv/dt) \quad , \tag{B1}$$

and, therefore, $-M_1 (dv_z/dt)$ can be expressed as

$$-M_1 (dv_z/dt) = -M_1 (dv/dt)(dv_z/dv) = (-dE/dx)(dv_z/dv). \tag{B2}$$

Since the energy loss is composed of two parts: electronic and nuclear,

$$-M_1 (dv_z/dt) = (dv_z/dv) \left[(-dE/dx)_e + (-dE/dx)_n\right] \quad . \tag{B3}$$

Using the LSS (27) expression for $(d\epsilon/d\rho)_e$, the electronic energy loss can

be expressed as

$$(-dE/dx)_e = K_e(v/v_o) \quad , \tag{B4}$$

where

$$K_e = 11.53 \ \frac{Z_2 Z_1^{7/6}}{A_2(Z_1^{2/3} + Z_2^{2/3})^{3/2}} \quad . \tag{B5}$$

Equation (B3) thus becomes

$$-M_1 (dv_z/dt) = (dv_z/dv) \left[K_e(v/v_o) + (-dE/dx)_n \right] \quad . \tag{B6}$$

The relation $v_z = v \overline{\cos \phi(t)}$ (where $\phi(t)$ is the nuclear scattering angle) gives

$$dv_z/dv = \overline{\cos \phi(t)} + v \ \frac{d\left[\overline{\cos \phi(t)}\right]}{dv} \quad . \tag{B7}$$

If the left hand side of Eq. (B6) is separated into two parts consisting of an electronic part approximated by $K_e(v_z/v_o)$ and a nuclear part $-M_1(dv_z/dt)_n$, then

$$-M_1(dv_z/dt)_n + K_e(v_z/v_o) = (dv_z/dv) \left[K_e(v/v_o) + (-dE/dx)_n \right] \quad . \tag{B8}$$

Equation (B8) defines the quantity $-M_1(dv_z/dt)_n$ which in the absence of nuclear scattering is just $(-dE/dx)_n$. When nuclear scattering is included, $-M_1(dv_z/dt)_n$ includes the difference between $K_e(v/v_o)$ and $K_e(v_z/v_o)$ as well as the direct effects of nuclear scattering.

Solving for $-M_1(dv_z/dt)_n$ gives

$$-M_1(dv_z/dt)_n = (dv_z/dv)(-dE/dx)_n + \left[(dv_z/dv) K_e(v/v_o) - K_e(v_z/v_o) \right] \quad , \tag{B9}$$

and using Eq. (B7) gives

$$-M_1(dv_z/dt)_n = (-dE/dx)_n \left[\overline{\cos\phi(t)} + v\frac{d[\overline{\cos\phi(t)}]}{dv}\right] + v\frac{d[\overline{\cos\phi(t)}]}{dv} K_e(v/v_o). \quad \text{(B10)}$$

In order to calculate this quantity explicitly, $\overline{\cos\phi(t)}$ can be evaluated using Blaugrund's theory (33) (see Appendix C), however, the expression is not analytic but requires numerical integration.

Warburton et al. (32) have found that a good approximation to $-M_1(dv_z/dt)_n$ is $K_n(v_z/v_o)^{-1}$ where K_n is evaluated from range-energy data if possible. Usually range-energy data are not available, and Warburton et al. (32) point out that K_n can be evaluated from the LSS value of $(-dE/dx)_n$ at $v_z = v_o$. At $t=0, \overline{\cos\phi(0)} = 1$ if the recoiling nuclei are moving along the z-axis, therefore,

$$-M_1(dv_z/dt)_n = (-dE/dx)_n + \left.\frac{vd[\overline{\cos\phi(t)}]}{dv}\right|_{t=0} \left[(-dE/dx)_n + K_e(v/v_o)\right] . \quad \text{(B11)}$$

For most reactions $v(0) \approx v_o$, thus the above approximation is equivalent to setting $\left.\frac{d[\cos\phi(t)]}{dv}\right|_{t=0}$ to zero. This approximation is best when $A_2/A_1 < 1$ and when A_2 and A_1 are both small. However, for $A_2/A_1 > 1$ the approximation is not valid and the nuclear stopping is underestimated. Therefore, Warburton's method gives longer lifetimes by 5-20% depending upon A_1 and A_2. Thus if Warburton's method is to be used (i.e., $-M_1(dv_z/dt)_n = K_n(v_z/v_o)^{-1}$), then the value of $-M_1(dv_z/dt)_n$ must be increased at t=0 by approximately the second term on the right of Eq. (B11).

Warburton's approximation does give a rather simple analytic

expression for $F(\tau)$. For only one type of stopping material the expression for $F(\tau)$ can be calculated from Eq. (13) of the text and is

$$F(\tau) = \frac{x\gamma_i^x}{(1+\gamma_i^2)^{x/2}} \int_o^1 V^2 (\gamma_i^{-2} + V^2)^{x/2-1} \, dV \,, \qquad \text{(B12)}$$

where $x = a/\tau$, $a = M_1 v_o / K_e \rho$, $\gamma_i^2 = (K_e/K_n) \left[\bar{v}(0)/v_o\right]^2$, ρ = density of the stopping material, and $V \equiv v_z(t)/v(0)$. In general, however, the recoiling nucleus is created in some target of finite thickness, and recoils a distance D_i before entering the backing which is essentially infinitely thick. If the velocity at which the nucleus crosses from one material to the other is v_c, then

$$F(\tau) = \frac{1}{A_1^{x_1/2}} \left[\frac{x_2 C_1^{x_1/2}}{C_2^{x_2/2}} \int_o^{V_c} V^2 B_2^{x_2/2-1} \, dV + x_1 \int_{V_c}^1 V^2 B_1^{x_1/2-1} \, dV \right], \qquad \text{(B13)}$$

where $V_c = v_c/v(0)$, $A_j = (1 + \gamma_{ij}^{-2})$, $B_j = (V^2 + \gamma_{ij}^{-2})$, and $C_j = (V_c^2 + \gamma_{ij}^{-2})$. The subscript 1 refers to the target and 2 refers to the backing. A computer program DSAM2 has been written which calculates $F(\tau)$ from Eq. (B13) by evaluating the integrals numerically. Since the excited nucleus may be produced at any point in the target, the target is divided into ten layers of equal thickness, and $F_i(\tau)$ is calculated for each layer. The average $F(\tau)$ is calculated assuming that the yield is uniform across the target. The velocity at the crossing v_c is calculated by comparing the range $R_z(t')$ calculated from

$$R_z(t') = \int_0^{t'} v_z(t)\, dt \qquad \text{(B14)}$$

to D_i at each step in the integral over the time.

The $F(\tau)$ curves calculated from Blaugrund's (33) method can be approximately reproduced by DSAM2 if an increased value of K_n is used. For ^{37}Ar ions in a 450 $\mu g/cm^2$ $Cd^{34}S$ target on a Ni backing the effective value of K_n was found to be $\sim$ twice the value of K_n determined using the prescription given by Warburton et al. (32)

Appendix C

BLAUGRUND'S EXPRESSIONS FOR SPECIFIC ENERGY LOSS

Considering both electronic and nuclear energy loss processes, Blaugrund (33) has derived equations from which the velocity v(t) of an ion in a scattering material can be calculated. In practice, the most useful aspect of Blaugrund's work, however, is the derivation of the average value of the cosine of the nuclear scattering angle.

Using the universal variables introduced by Lindhard et al., (27) Blaugrund found it convenient to define the following dimensionless quantities: A variable $\mathcal{V} = v/v_o$ corresponding to the velocity of the recoiling nucleus and the parameter $\mathcal{U}$ defined by the relation $\epsilon = \frac{1}{2}\mathcal{U}\mathcal{V}^2$. From this definition

$$\mathcal{U} = \frac{1.63 \times 10^3 \, A_1 \, A_2}{Z_1 \, Z_2 \, Z^{1/2} (A_1 + A_2)} \quad , \tag{C1}$$

where $Z = (Z_1^{2/3} + Z_2^{2/3})$. An additional variable Θ was introduced such that $d\rho/d\Theta = \mathcal{V}$. Thus it can be shown that $\Theta = t/T$ where t is the time and

$$T = \frac{\hbar}{e^2} \frac{(A_1 + A_2)^2}{4\pi a^2 N A_1 A_2} , \qquad (C2)$$

where e is the charge on the electron and a and N are defined in the text. In terms of these variables a convenient expression for calculating ϵ is given by

$$\epsilon = 10.2 \frac{\mathcal{M}}{A_1} \frac{E}{mc^2} , \qquad (C3)$$

where m is the mass of the electron.

Working in dimensionless variables, one obtains the following expressions for Θ as a function of ϵ:

$$(d\epsilon/d\rho) = \mathcal{M} d\mathcal{V}/d\Theta , \qquad (C4)$$

or

$$d\Theta = \mathcal{M} d\mathcal{V}/(d\epsilon/d\rho) = (1/2\,\mathcal{M})^{1/2} \frac{d\epsilon}{\epsilon^{1/2}(d\epsilon/d\rho)} . \qquad (C5)$$

Noting that $(d\epsilon/d\rho)$ is a positive number while (dE/dx) is negative, one obtains the following expression for Θ:

$$\Theta = t/T = (1/2\,\mathcal{M})^{1/2} \int_{\epsilon}^{\epsilon_o} \frac{d\epsilon}{\epsilon^{1/2}(d\epsilon/d\rho)} , \qquad (C6)$$

where $(d\epsilon/d\rho) = (d\epsilon/d\rho)_n + (d\epsilon/d\rho)_e$ and ϵ_o is the value of ϵ at t = 0.

Blaugrund (33) has used Lewis' (34) extension of the multiple-scattering theory of Goudsmit and Saunderson (66) to derive an expression for $\overline{\cos \phi(t)}$ where $\phi(t)$ is the nuclear scattering angle. Portions of this derivation are presented here.

For an originally parallel beam of ions the angular distribution function at a distance x is given by Lewis (34) as

$$F(\phi, x) = \frac{1}{4\pi} \sum_{\ell=0}^{\infty} (2\ell+1)\, P_\ell(\cos\phi) \exp\left(-\int_0^x K_{\ell\phi}\, dx\right), \qquad \text{(C7)}$$

where

$$K_{\ell\phi} = N \int \left[1 - P_\ell(\cos\phi)\right] d\sigma(\phi) \qquad \text{(C8)}$$

In these equations the recoiling particle is assumed to be << lighter than the atoms of the stopping material and no distinction is made between the c.m. and laboratory angles. The $P_\ell(\cos\phi)$ are the unnormalized Legendre polynomials and $d\sigma(\phi)$ is the differential cross section for scattering as a function of the laboratory angle. It follows that

$$\overline{\cos\phi(t)} = \int_0^{2\pi} F(\phi, x) \cos\phi(t)\, d\phi = \exp\left(-\int_0^x K_{1\phi}\, dx\right), \qquad \text{(C9)}$$

and in general

$$\overline{P_\ell(\cos\phi)} = \exp\left(-\int_0^x K_{\ell\phi}\, dx\right). \qquad \text{(C10)}$$

The relationship between the c.m. and laboratory angles (δ and ϕ, respectively) is

$$\tan\phi = \frac{\sin\delta}{r + \cos\delta}, \qquad \text{(C11)}$$

where $r \equiv A_1/A_2$. Using Eq. (C11), Blaugrund expands $\cos\phi(t)$ in a series of Legendre polynomials $P_\ell(\cos\phi)$ and as a function of r. Thus from Eqs. (C8) and (C9), one can obtain an expression for $\overline{\cos\phi(t)}$ in terms of integrals over sums of Legendre polynomials (see Eqs. (10a) and (10b) of reference 33). The differential scattering cross section, $d\sigma(\delta)$, derived by

LSS (see Appendix A) can then be used to calculate $\overline{\cos\phi(t)}$.

To derive a simplified expression for $\overline{\cos\phi(t)}$, Blaugrund made use of the approximation

$$\overline{P_\ell(\cos\delta)} \approx \overline{(\cos\delta)}^\ell \quad , \tag{C12}$$

where

$$\overline{P_\ell(\cos\delta)} = \exp\left(-\int_0^x K_{\ell\phi}\, dx\right) , \tag{C13}$$

and

$$K_{\ell\phi} = N\int_0^\epsilon \left[1 - P_\ell(\cos\delta)\right]\, d\sigma(\delta) \ . \tag{C14}$$

Equations (C13), (C14), and (A3) are used to calculate $\overline{\cos\delta}$ as follows:

$$\overline{\cos\delta} = \exp\left[-N\int_0^x dx \int_0^\epsilon (1-\cos\delta)\,\pi a^2 f(q)\, dq/q^2\right] \ , \tag{C15}$$

and

$$\overline{\cos\delta} = \exp\left[-2\pi a^2 N\int_0^x \frac{(d\epsilon/d\rho)_n}{\epsilon}\, dx\right], \tag{C16}$$

where $(d\epsilon/d\rho)_n$ is given by Eq. (A4). Using the expression for ρ, Eq. (C16) becomes

$$\overline{\cos\delta} = \exp\left[-\frac{1}{2} I (1+r)^2/r\right] \ , \tag{C17}$$

where

$$I = \int_\epsilon^{\epsilon_0} \frac{(d\epsilon/d\rho)_n\, d\epsilon}{\epsilon\,(d\epsilon/d\rho)} \ . \tag{C18}$$

Using the above arguments, Blaugrund derives the following expressions for $\overline{\cos\phi(t)}$:

$$\overline{\cos\phi(t)} = \exp\left[-\frac{1}{2} G(r)\, I\, A_2/A_1\right] \ , \tag{C19}$$

where

$$G(r) = \begin{cases} 1 + 2/3\, r - 7/15\, r^2 + 8 \sum_{n=3}^{\infty} \dfrac{(-r)^n}{(2n+1)(2n-1)(2n-3)} , & r < 1 \\ 2/3 + 8/15 \cdot 1/r - 8 \sum_{n=3}^{\infty} \dfrac{(-1/r)^{n-1}}{(2n+1)(2n-1)(2n-3)} , & r > 1 \end{cases} \quad . \tag{C20}$$

G(r) is a function of ϵ if the approximation in Eq. (C12) is not used, but the dependence upon ϵ is very slight.

If there is more than one type of atom in the stopping material, let $\mathcal{M}$, Z_2, A_2, etc. refer to the heaviest of these atoms and let $\mathcal{M}_i$, Z_{2i}, A_{2i}, etc. refer to the i^{th} type of lighter atom. Then Eq. (C6) becomes

$$\Theta = (\tfrac{1}{2}\mathcal{M})^{1/2} \int_{\epsilon}^{\epsilon_o} \frac{d\epsilon}{\epsilon^{1/2} \left[(d\epsilon/d\rho) + \sum_i C_i \, (d\epsilon/d\rho)_i \right]} , \tag{C21}$$

where Θ and ϵ refer to the heaviest stopping atom,

$$C_i = \frac{N_i \, Z_{2i} \, a_i \, (A_1 + A_2)}{N \, Z_2 \, a \, (A_1 + A_{2i})} , \tag{C22}$$

and $(d\epsilon/d\rho)_i$ is the total specific energy loss at the energy $(\mathcal{M}_i/\mathcal{M})\epsilon$. Similarly, $\overline{\cos \phi(t)}$ can be calculated by modifying the expression for I such that

$$I = \int_{\epsilon}^{\epsilon_o} \frac{(d\epsilon/d\rho)_n + \Sigma_i \, C_i \, (A_{2i}/A_2)(G_i/G)(d\epsilon/d\rho)_{ni}}{\epsilon \left[(d\epsilon/d\rho) + \sum_i \, C_i \, (d\epsilon/d\rho)_i \right]} \, d\epsilon \quad . \tag{C23}$$

Appendix D

DESCRIPTION OF FTAU

A. General

The approximation $v_z(t) = v(t)\,\overline{\cos\phi(t)}$ can be used to express Eq. (13) of the text as

$$F(\tau) = \frac{1}{v(0)\tau}\int_0^\infty v(t)\,\overline{\cos\phi(t)}\,\exp(-t/\tau)\,dt \quad . \tag{D1}$$

In doing the integral in Eq. (D1) it is convenient either to have equal steps in t or to have the values of t correspond to the roots of some polynomials (such as Legendre polynomials). From Eq. (C21), however, it is seen that this involves an iterative search for ϵ corresponding to each value of t. Thus it is convenient to convert the integral in Eq. (D1) to an integral over ϵ using Eq. (C21). Thus

$$F(\tau) = \frac{T(\frac{1}{2}\mu)^{1/2}}{v(0)\,\tau}\int_0^{\epsilon_0} \exp\left[-t(\epsilon)/\tau\right]\, v(t)\,\frac{\overline{\cos\phi(\epsilon)}\quad\cdot\quad d\epsilon}{\epsilon^{1/2}\left[(d\epsilon/d\rho)+\sum_i C_i(d\epsilon/d\rho)_i\right]}\,, \tag{D2}$$

where t can now be evaluated directly at each value of ϵ. Since ϵ varies over a large range, it is convenient to convert the integral in Eq. (D2) to

one over $y = \ln \epsilon$. This is convenient because y can now be varied in equal steps, and Simpson's rule can be used to evaluate the integral. Equation (D2) becomes

$$F(\tau) = \frac{T(\frac{1}{2}\mu)^{1/2}}{v(0)\tau} \int_{-\infty}^{y(0)} \exp\left[t(y)/\tau\right] \; v(y) \frac{\cos\phi(y) \cdot \epsilon \cdot d\epsilon}{\epsilon^{1/2}\left[(d\epsilon/d\rho) + \sum_i C_i (d\epsilon/d\rho)_i\right]} \cdot \tag{D3}$$

The lower limit can be taken to be ~ -6.0 in practice when evaluating the integral.

B. FTAU

The program FTAU evaluates Eq. (D3) using numerical integration. The finite target thickness is treated in the same manner as described in Appendix B. A simplified flow chart of the program is given at the end of this Appendix along with a listing of the program. The program uses the following input parameters:

TITLE -- a 64 character description of the data

A(1) -- atomic mass of the recoiling particle

Z(1) -- atomic number of recoiling particle

NE -- the number of elements in the target

NEB -- the number of elements in the backing

RHO -- the density of the target

RHOB -- the density of the backing

THICK -- the target thickness in $\mu g/cm^2$

NLAY -- the number of layers into which the target is to be divided

L(I) -- the matrix of the number of atoms of each type per molecule in the target

LB(I) -- same as L(I) except for the backing

A(2)- A(4) -- the atomic masses of the atoms of the target with A(2) being the heaviest

AB(2)- AB(4) -- the atomic masses of the atoms of the backing with AB(2) being the heaviest

Z(2)- Z(4) -- the atomic numbers of the atoms of the target

ZB(2)- ZB(4) -- the atomic numbers of the atoms of the backing

FET -- the number by which the LSS value of k is to be multiplied for the target

FEB -- same as FET except for the backing

VI -- the initial recoil velocity in units of $v_o = 2.19 \times 10^8$ cm/sec.

The integral in Eq. (D3) is divided into 401 parts. The size of the initial step in the target is determined in the following manner: A first step in the time is taken as 0.004 psec. Equation (C21) is then used to calculate $(\epsilon_o - \epsilon)$ = DENT assuming that the integrand is constant. This step in ϵ is then converted to a step in y = DIST. DIST is the step size then for the remainder of the target or for 401 steps, whichever is first. This procedure ensures that the first step in the time will be $\approx$ 0.004 psec which is

the shortest lifetime used in the program. When the recoiling nucleus enters the backing the same procedure is used to calculate a new DIST such that the initial time step is ≈ 0.004 psec. These calculations are performed in lines 185-191 of the program (see the listing). The number of steps was decided upon empirically once the method of calculating DIST was chosen. Using this method the final energy of the nucleus is $\sim$1 keV or less when the initial energy is $\sim$1 MeV.

A function subprogram FCT(E) has been written to evaluate the integrand of Eq. (C23). The nuclear part of the energy loss is evaluated using Eq. (A7), and the electronic part is calculated from Eq. (A1) and (A2). The constants FET and FEB are used to multiply the value of k in order to take into account the oscillations in the electronic stopping (see Appendix A). This function subprogram has another entry point TIME(E) which is used to evaluate the integrand of Eq. (C21).

The time that the nucleus crosses into the backing is determined by calculating the range R_z [RZ(J) in the program] along the z-axis at each step in y. This range is compared with the target thickness for that layer of the target (DTH); if $R_z >$ DTH, the parameters of the backing material are used in the calculations, and a new DIST is calculated. The range calculations are carried out in lines 209-213 of the program.

Simpson's rule is used to evaluate the integral in Eq. (D3). The integral is divided into two parts (target and backing) and each part is evaluated separately since the step sizes are different. The following

variables are used in evaluating the integral:

GRAND -- the integrand of Eq. (D3) for the target

GRAL -- the integrand of Eq. (D3) for the backing

FTAU(M, K) -- the value of $F(\tau)$ for the K^{th} value of τ and the M^{th} layer of the target.

This evaluation is carried out in lines 258 through 284 using the IBM Scientific Subroutine Package (67) program DQSF. A given value of y corresponds directly to a value of v, ϵ, and $(d\epsilon/d\rho)$. However, in order to calculate t and $\overline{\cos \phi(t)}$, the integrals in Eq. (C21) and (C23) must be evaluated. If the subscript J is used to label the steps in y and varies from 1 to 401, then the evaluation of these integrals can be performed by calculating running sums. The integrals are divided into a sum of two parts such that

$$I_J = I_J(\epsilon) = I_1 + \int_{\epsilon(J+1)}^{\epsilon(J)} \frac{(d\epsilon/d\rho)_n + \sum_i C_i (A_{2i}/A_2)(G_i/G)(d\epsilon/d\rho)ni}{\epsilon\left[(d\epsilon/d\rho) + \sum_i C_i (d\epsilon/d\rho)_i\right]} \qquad (D4)$$

where Eq. (C23) has been used as an example and I_1 is the integral from $\epsilon_o = \epsilon(1)$ to $\epsilon(J)$. Each integral is evaluated using the IBM Scientific Subroutine Package (67) program DQG4. DQG4 performs the integration by Gaussian Quadrature (68) using four points, and the values of the integrand at each point are calculated from FCT(E) and TIME(E). The integral is exact for a polynomial up to degree seven. The evaluation of these integrals is performed in the DO LOOP starting with line 196. At

the boundary between the backing and the target, both $\overline{\cos \phi (t)}$ and t are calculated in such a manner that they are continuous.

The following variable names are used by the program:

COSP = $\overline{\cos \phi (t)}$

VCOS = v $\overline{\cos \phi (t)}$

TIMS = t in psec

FUN1 = v $\overline{\cos \phi (t)}$/ $\left\{\epsilon^{1/2} \left[\underline{(d\epsilon/d\rho)} + \sum_i C_i \underline{(d\epsilon/d\rho)_i}\right]\right\}$.

The above parameters are computed only for the thickest layer of the target (M = 1) since for each succeeding layer the previous values can be used and new values must be calculated only for the backing.

To speed up the calculation large matrices are used to store parameters that will be used over again. For example, all of the above parameters are stored in 401-point vectors. These are not functions of τ and are useful for computing $F(\tau)$ for all τ for a given target layer. The range is calculated only once and is stored in a 401-point vector. For the first layer of the target (M=1) the distance in the target is the greatest. For each succeeding layer DTH can be compared to values of RZ(J) already calculated and the value of J at the crossing = NCROS determined. The values of t and $\overline{\cos \phi (t)}$ do not need to be recomputed for the time the nucleus is in the target but only for the time it is in the backing. The values of $F(\tau)$ are stored in a 10X56 matrix where there are 56 values of τ and the average $F(\tau)$ is computed for each τ after the entire matrix is computed.

A slower method using less memory would be to calculate the

average value of $F(\tau)$ for the ten layers for each value of τ. This would mean that the values of t, $\overline{\cos\phi(t)}$, etc., for the target would have to be recomputed for each value of τ as well as for each layer instead of only for each layer.

Further comments on the program are available in the listing and the sequence in which the calculations are performed is given in the flow chart. An $F(\tau)$ vs τ curve is presented in Figure D1 for ^{37}Ar recoiling in a 450 $\mu g/cm^2$ $Cd^{34}S$ target on a Ni backing. $F(\tau)$ for each of the ten layers is shown and for the first five layers is seen to be the same since the ^{37}Ar nuclei stop in the target. Figure 10 is an average of these curves.

The following variables are used as flags by the program in making logical decisions:

NTHRU = 0 → This is the first layer of the target, therefore, the thickest.

= 1 → The values of v, ϵ, $\overline{\cos\phi(t)}$, etc., for the target have already been calculated.

NLP2 = 0 → Recalculate μ, k, etc., for the backing since this is the first time the particle has been in the backing.

= 1 → The backing parameters have already been calculated.

NRFLG = 0 → Calculate the range in the target.

= 1 → Do not calculate the range.

Figure D1. Plot of $F(\tau)$ vs τ in seconds for ^{37}Ar ions recoiling in a 450 $\mu g/cm^2$ $Cd^{34}S$ target on a Ni backing. NLAY is the target layer number corresponding to each curve where the thickest target layer is 1. Curves 1-5 are seen to be identical since the recoiling ions stop in the target. The curve shown in Fig. 10 is the average of these 10 curves.

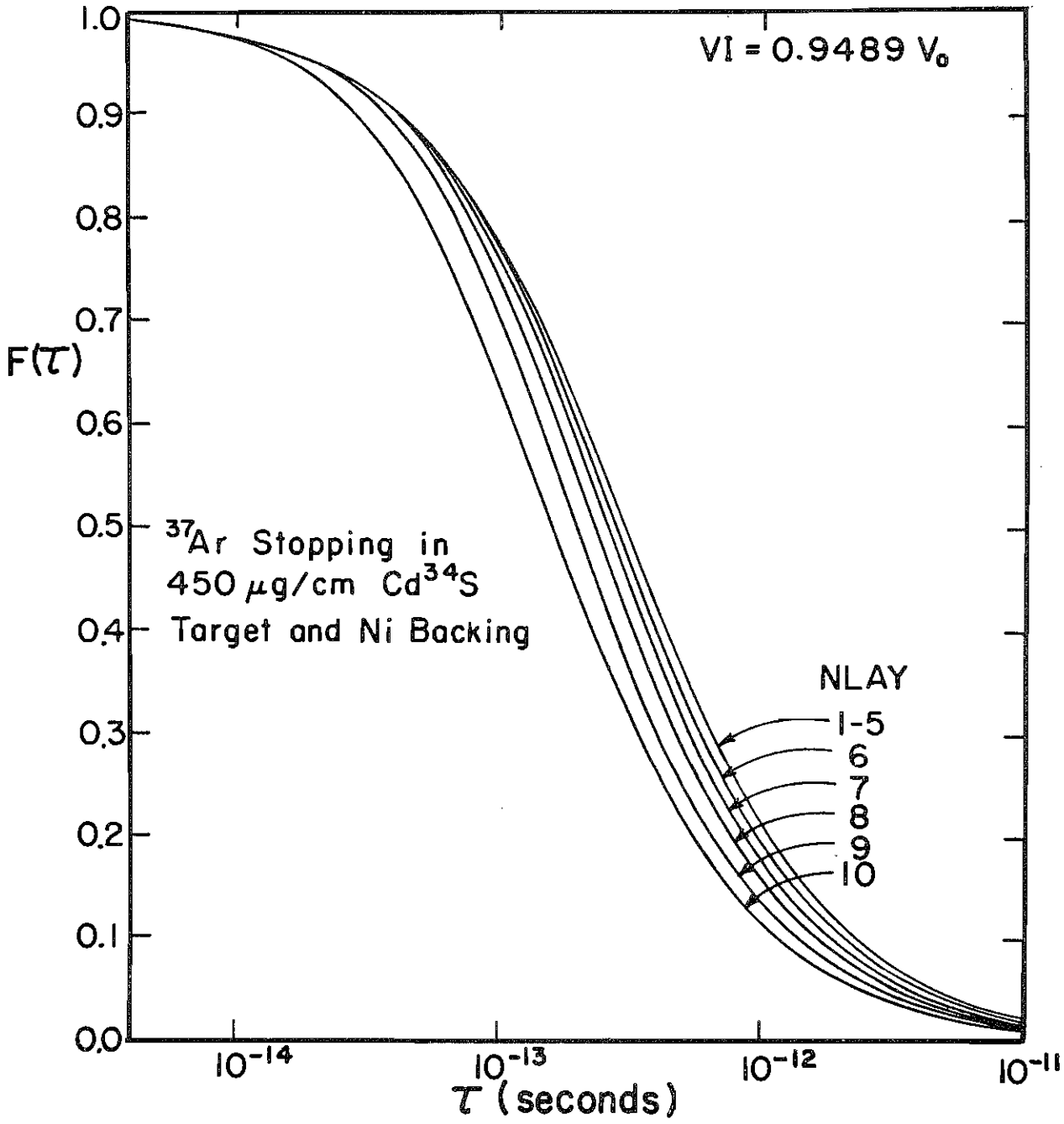
VI = 0.9489 V₀
F(τ)
1.0
0.9
0.8
0.7
0.6
0.5
0.4
0.3
0.2
0.1
0.0
³⁷Ar Stopping in
450 μg/cm Cd³⁴S
Target and Ni Backing
NLAY
1-5
6
7
8
9
10
10⁻¹⁴
10⁻¹³
10⁻¹²
10⁻¹¹
τ (seconds)

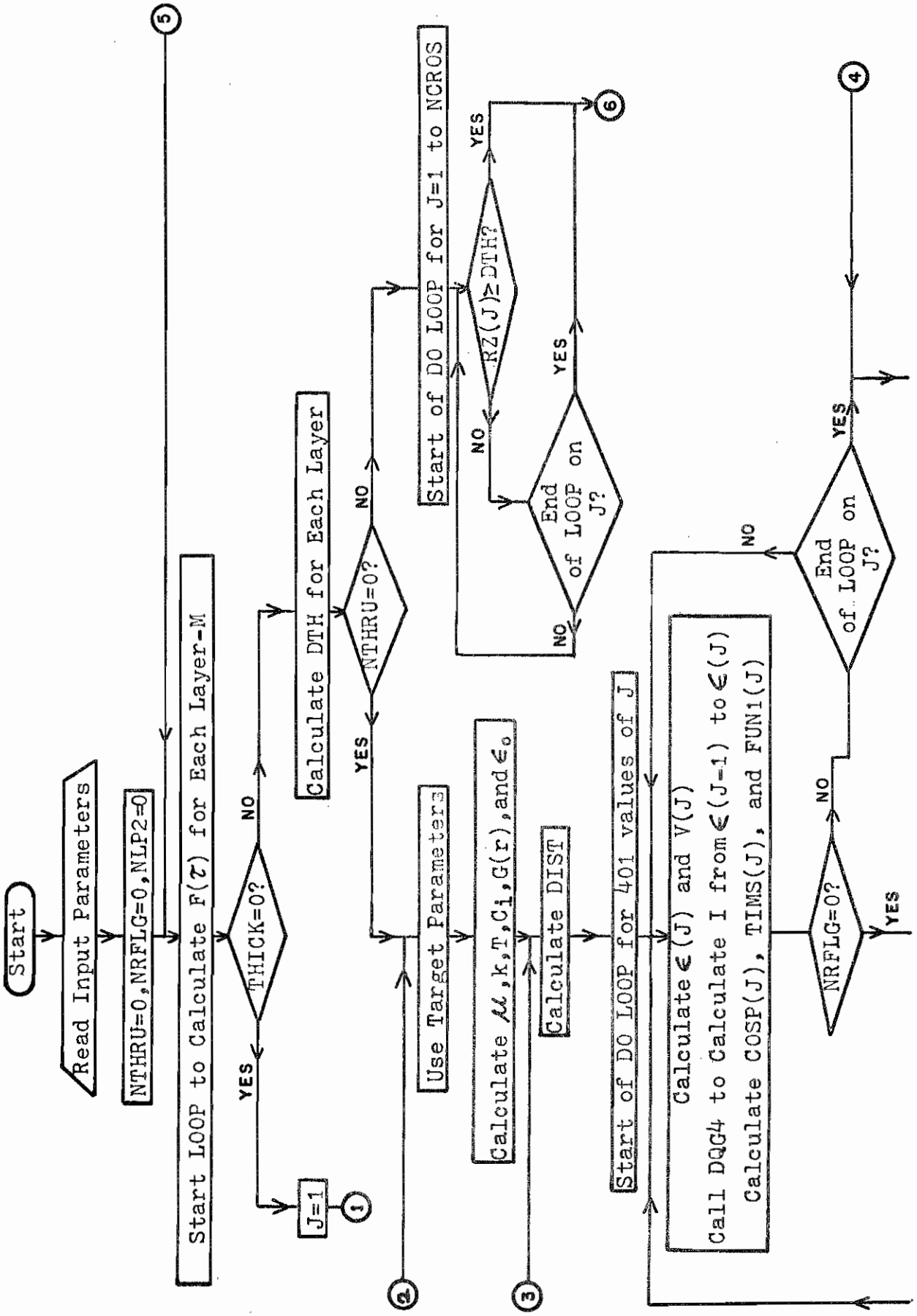
Start
Read Input Parameters
NTHRU=0, NRFLG=0, NLP2=0
Start LOOP to Calculate F(τ) for Each Layer-M
THICK=0?
NO
YES
J=1
1
Calculate DTH for Each Layer
NTHRU=0?
NO
YES
2
Use Target Parameters
Calculate μ, k, T, Ci, G(r), and ∈o
3
Calculate DIST
Start of DO LOOP for J=1 to NCROS
RZ(J)≥DTH?
YES
NO
End of LOOP on J?
YES
NO
6
Start of DO LOOP for 401 values of J
Calculate ∈(J) and V(J)
Call DQG4 to Calculate I from ∈(J-1) to ∈(J)
Calculate COSP(J), TIMS(J), and FUN1(J)
End of LOOP on J?
NO
YES
4
NRFLG=0?
NO
YES
5

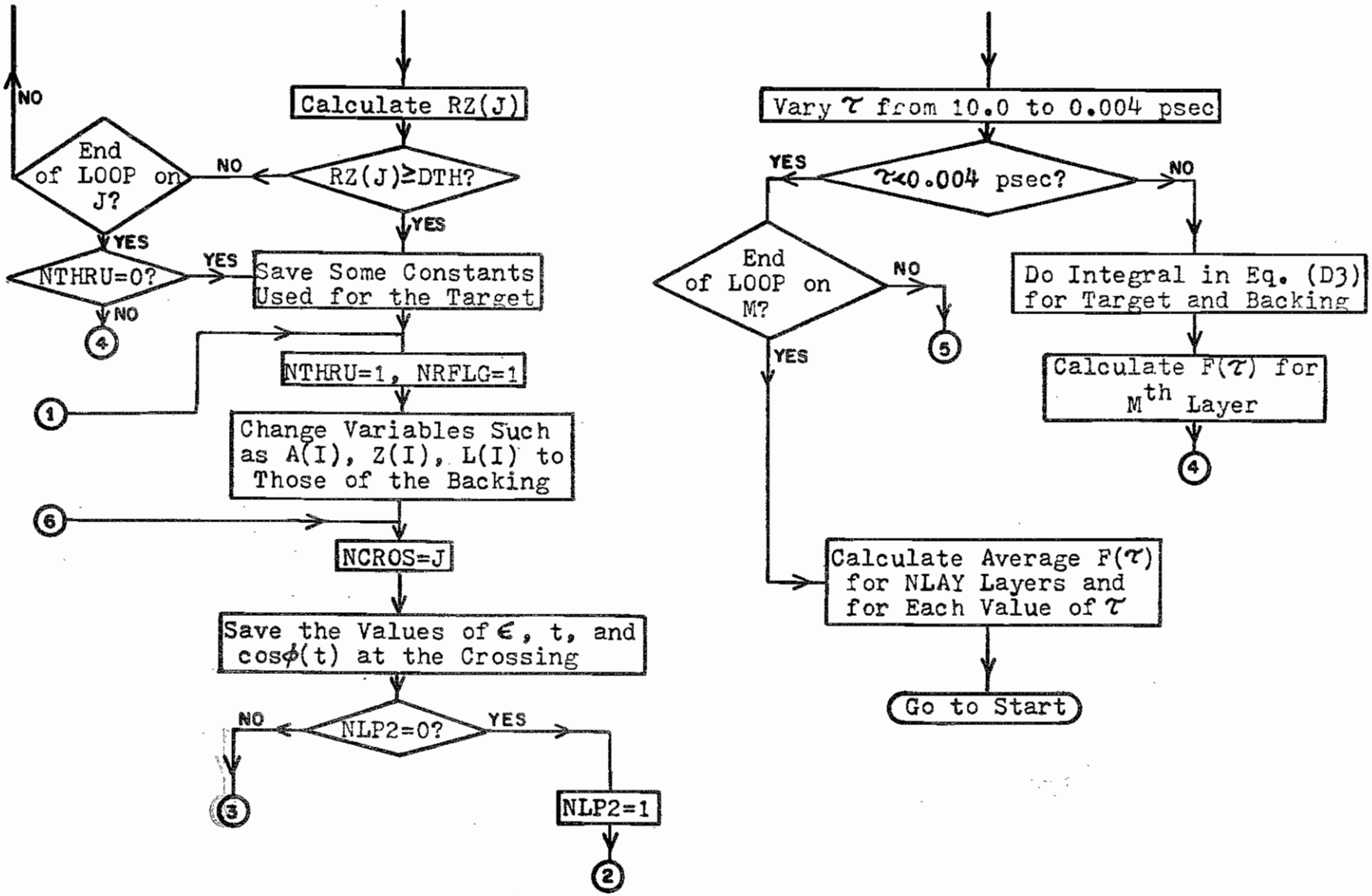

Flow Chart of FTAU

```
C
C     XXXXXXXXXXXXXXXXXXXXXXXXXXXXXXXXXXXXXXXXXXXXXXXXXXXXXXXXXXXXXXXXXXX
C     XXXXXXXXXXXXXXXXXXXXXXXXXXXXXXXXXXXXXXXXXXXXXXXXXXXXXXXXXXXXXXXXXXX
C     XXXXXXXXXXXXXXXXXXXXXXXX              XXXXXXXXXXXXXXXXXXXXXXXXXXXXXX
C     XXXXXXXXXXXXXXXXXXXXXXXX              XXXXXXXXXXXXXXXXXXXXXXXXXXXXXX
C     XXXXXXXXXXXXXXXXXXXXXXXX     FTAU     XXXXXXXXXXXXXXXXXXXXXXXXXXXXXX
C     XXXXXXXXXXXXXXXXXXXXXXXX              XXXXXXXXXXXXXXXXXXXXXXXXXXXXXX
C     XXXXXXXXXXXXXXXXXXXXXXXX              XXXXXXXXXXXXXXXXXXXXXXXXXXXXXX
C     XXXXXXXXXXXXXXXXXXXXXXXXXXXXXXXXXXXXXXXXXXXXXXXXXXXXXXXXXXXXXXXXXXX
C     XXXXXXXXXXXXXXXXXXXXXXXXXXXXXXXXXXXXXXXXXXXXXXXXXXXXXXXXXXXXXXXXXXX
C
C  A PROGRAM TO CALCULATE F(TAU) BASED ON THE ARTICLE BY BLAUGRUND IN
C  NUCLEAR PHYSICS,88,501(1966).  A(1) IS THE AMU OF THE RECOILING ION.
C  A(2),A(3),AND A(4) ARE THE AMU'S OF THE COMPONENTS OF THE STOPPING
C  MATERIAL(TARGET).  NE IS THE NUMBER OF ELEMENTS IN THE TARGET, AND
C  L(2),L(3), AND L(4) ARE THE NUMBER OF ATOMS OF THE ITH TYPE.  AB(2),
C  AB(3), AND AB(4) ARE THE AMU'S OF THE COMPONENTS OF THE BACKING.  NEB
C  IS THE NUMBER OF ELEMENTS IN THE BACKING, AND LB(I) IS THE NUMBER OF
C  ATOMS OF THE ITH TYPE.  THE ENERGY IN KEV=EKEV=CM*V**2.  ALL VELOCI-
C  TIES ARE IN UNITS OF VO=2.19*10.0**8 CM/SEC.  THICK=TARGET THICKNESS
C  IN MHG/CM**2.  ALL TIME IS MEASURED IN UNITS OF PSEC.  AA IS THE AMU
C  OF THE STOPPING MATERIAL. A(2) AND AB(2) MUST BE THE HEAVIEST ATOMS
C  IN THE TARGET AND THE BACKING,RESPECTIVELY.
C  THIS PROGRAM USES THE FOLLOWING SUBROUTINES FROM THE IBM SCIENTIFIC
C  SUBROUTINE PACKAGE-- DQG4 AND DQSF.
C  DQG4 IS A DOUBLE PRECISION SUBROUTINE WHICH PERFORMS NUMERICAL
C  INTEGRATION USING FOUR POINT GAUSSIAN QUADRATURE.
C  DQSF IS A DOUBLE PRECISION SUBROUTINE WHICH PERFORMS NUMERICAL
C  INTEGRATION USING SIMPSON'S RULE.
C
C
      IMPLICIT REAL*8(A-H,P-Z)
      COMMON C,A,G,XKE,AMAS,NE,NEE
      DIMENSION C(5),A(5),G(5),XKE(5),AMAS(5)
      DIMENSION Z(5),L(5),ZSUM(5),R(5),RMAS(5),TITLE(20),ASUM(5)
      DIMENSION EL(405),V(405),RZ(405),FUN1(405),EKEV(405),TIMS(405),
     1COSP(405),GRAND(405),GRAL(405),AREA(405),VCOS(405)
      DIMENSION AB(5),ZB(5),LB(5),FAVG(60),TAU(60),FTAU(10,60)
      EXTERNAL FCT,TIME
      DATA STOP/4HSTOP/
C     FORMAT STATEMENTS NUMBERED 1,2,50 THRU 100,91
    1 FORMAT(4I5,F10.5,F10.5,I5,F10.5)
    2 FORMAT(8F10.5)
   50 FORMAT(1H1)
   51 FORMAT(5H CM= ,F12.6,5X,6H FAC= ,F12.8,5X,8H CONST= ,F12.5)
   52 FORMAT(1H )
   53 FORMAT(4X,12H PROJECTILES,16X,18H   TARGET MATERIAL)
   54 FORMAT(2X,5H A(1),5X,5H Z(1),8X,5H A(2),5X,5H Z(2),5X,5H A(3),5X,5
     1H Z(3),5X,5H A(4),5X,5H Z(4),4X,10H RHO(G/CC),2X,3H FE,6H THICK,5X
     2,5H NLAY)
   55 FORMAT(4(F10.2,F10.5),F10.4,4X,F7.3,F10.4,I5)
   56 FORMAT(3X,5H ASUM,5X,5H ZSUM,5X,5H R(I),7X,5H AMAS,5X,4H XKE)
   57 FORMAT(3F10.5,F12.5,F10.5)
   58 FORMAT(3H C(,I2,4H) = ,F10.5)
   59 FORMAT(2X,5H C(2),5X,5H G(3),5X,5H G(4))
   60 FORMAT(3F10.5)
   61 FORMAT(5H AA= ,F12.4,3X,4H T= ,F12.5,3X,7H ELEL= ,F12.6)
   62 FORMAT(10F12.6)
   63 FORMAT(19H BACKING PARAMETERS)
   64 FORMAT(1X,6H AB(1),4X,6H ZB(1),7X,6H AB(2),4X,6H ZB(2),4X,6H AB(3)
     1,4X,6H ZB(3),4X,6H AB(4),4X,6H ZB(4),3X,11H RHOB(G/CC),2X,3H FE)
   65 FORMAT(20H CROSSING PARAMETERS)
   66 FORMAT(4H M= ,I3,4H V= ,F8.5,7H TIMS= ,F10.6,7H COSP= ,F8.5,8H EZE
     1RO= ,F10.4,5X,5H RZ= ,F10.5,8H NCROS= ,I4)
   67 FORMAT(3X,4H TAU,3X,26H FTAU(L=1) TO FTAU(L=NLAY),14H ----FTAU(AVG
     1))
   68 FORMAT(F10.5,3X,11F10.4)
   91 FORMAT(16A4)
C  READ DATA IN AND SET UP HEADINGS
    6 READ(1,91) (TITLE(I),I=1,16)
      IF(TITLE(1).EQ.STOP) GO TO 999
      WRITE(3,50)
      WRITE(3,91) (TITLE(I),I=1,16)
      READ(1,1) NE,(L(I),I=2,4),RHO,THICK,NLAY,FET
      READ(1,1)NEB,(LB(I),I=2,4),RHOB,FEB
      NEE=NE+1
      NEP=NEB+1
      A(3)=0.0
      Z(3)=0.0
      A(4)=0.0
      Z(4)=0.0
      AB(3)=0.0
      AB(4)=0.0
      ZB(3)=0.0
      ZB(4)=0.0
      READ(1,2) (A(I),I=1,NEE),(Z(I),I=1,NEE)
      READ(1,2)(AB(I),I=2,NEP),(ZB(I),I=2,NEP)
      READ(1,2)VI
      WRITE(3,62)VI
      CM=24.812*A(1)
      EZERO=CM*VI**2
      CONST=88.53*5.2917*1.60206/(4.803**2)
      FAC=1.05443/(6.0249*(4.803*5.2917*0.8853)**2*4.0*3.14159)
      WRITE(3,51) CM,FAC,CONST
      WRITE(3,52)
      WRITE(3,53)
      WRITE(3,54)
      WRITE(3,55) A(1),Z(1),A(2),Z(2),A(3),Z(3),A(4),Z(4),RHO,FET,THICK,
     1NLAY
      WRITE(3,52)
      NSTEP1=401
      V0=2.1897
      TCONST=0.0
      N1=1
C  COSP IS THE AVERAGE VALUE OF COS(PHI) DEFINED BY BLAUGRUND
      COSP(1)=1.0
      TIMS(1)=0.0
      V(1)=VI
      VCOS(1) = VI
      RZ(1)=0.0
      Y=0.0
      TIM=0.0
      NTHRU=0
      NRFLG=0
      NCROS=0
      NLP2=0
      NSTRT=2
      TARN=NLAY
      DELT=THICK/TARN
      DO 101 M=1,NLAY
      IF(THICK.NE.0.0) GO TO 41
      J=1
      GO TO 42
   41 SUB=(2.0*DFLOAT(M)-1.0)/2.0
      DTH=THICK-SUB*DELT
```

```
      IF(NTHRU.EQ.0)GO TO 23                                            FTAU 126
      DO 32 J=1,NCROS                                                   FTAU 127
      DIF=OTH-RZ(J)                                                     FTAU 128
      IF(DIF)31,31,32                                                   FTAU 129
   32 CONTINUE                                                          FTAU 130
   31 GO TO 22                                                          FTAU 131
C  COMPUTE PARAMETERS FOR THE TARGET THE FIRST TIME THROUGH THE LOOP.   FTAU 132
C  NEXT TIME THROUGH COMPUTE THEM FOR THE BACKING.                      FTAU 133
  222 NLP2=1                                                            FTAU 134
   23 AA=0.0                                                            FTAU 135
      WRITE(3,56)                                                       FTAU 136
      DO 4 I=2,NEE                                                      FTAU 137
      ASUM(I)=A(1)+A(I)                                                 FTAU 138
      ZSUM(I)=Z(1)**(2./3.)+Z(I)**(2./3.)                               FTAU 139
      R(I)=A(1)/A(I)                                                    FTAU 140
      AMAS(I)=1630.0*A(1)*A(I)/(Z(1)*Z(I)*ZSUM(I)**0.5*(ASUM(I)))      FTAU 141
      XKE(I)=0.0793*Z(1)**(1./6.)*(Z(1)*Z(I))**0.5*ASUM(I)**1.5/(ZSUM(I) FTAU 142
     1**0.75*A(1)**1.5*A(I)**0.5)                                       FTAU 143
      XKE(I)=XKE(I)*FET                                                 FTAU 144
      AA=AA+L(I)*A(I)                                                   FTAU 145
      WRITE(3,57) ASUM(I),ZSUM(I),R(I),AMAS(I),XKE(I)                   FTAU 146
    4 CONTINUE                                                          FTAU 147
C   T IS  THE SAME AS BLAUGRUND'S T                                     FTAU 148
      T=FAC*ASUM(2)**2*AA*ZSUM(2)/(A(1)*A(2)*RHO*DFLOAT(L(2)))         FTAU 149
      TCONS=T*(AMAS(2)/2.0)**0.5                                        FTAU 150
      IF(NE-1) 6,7,8                                                    FTAU 151
C    COMPUTE C(I)                                                       FTAU 152
    8 DO 5 I=3,NEE                                                      FTAU 153
      C(I)=L(I)*Z(I)*ZSUM(2)**0.5*ASUM(2)/(L(2)*Z(2)*ZSUM(I)**0.5*ASUM(I FTAU 154
     1))                                                                FTAU 155
      WRITE(3,58) I,C(I)                                                FTAU 156
    5 CONTINUE                                                          FTAU 157
C  COMPUTE G(R)=G(I)                                                    FTAU 158
    7 DO 9 I=2,NEE                                                      FTAU 159
      SUM=0.0                                                           FTAU 160
      IF(R(I)-1.0) 14,10,10                                             FTAU 161
C     R LESS THAN 1                                                     FTAU 162
   14 DO 15 J=3,10                                                      FTAU 163
      X=J                                                               FTAU 164
      SUM=SUM+8.0*(-R(I))**J/((2.0*X+1.)*(2.0*X-1.)*(2.0*X-3.))        FTAU 165
   15 CONTINUE                                                          FTAU 166
      G(I)=1.0+(2./3.)*R(I)-(7./15.)*R(I)**2+SUM                        FTAU 167
      GO TO 9                                                           FTAU 168
C  R GREATER THAN 1                                                     FTAU 169
   10 DO 16 J=3,10                                                      FTAU 170
      X=J                                                               FTAU 171
      SUM= SUM-(8.0*(-1.0/R(I))**(J-1))/((2.0*X+1.)*(2.0*X-1.)*(2.0*X-3. FTAU 172
     1))                                                                FTAU 173
   16 CONTINUE                                                          FTAU 174
      G(I)=(2./3.)+(8./15.)/R(I)+SUM                                    FTAU 175
    9 CONTINUE                                                          FTAU 176
      WRITE(3,59)                                                       FTAU 177
      WRITE(3,60) (G(I),I=2,NEE)                                        FTAU 178
C                                                                       FTAU 179
      ELEL=A(2)/(Z(1)*(Z(2)*ZSUM(2)**0.5*ASUM(2))                       FTAU 180
      WRITE(3,61) AA,T,ELEL                                             FTAU 181
C  ELZ IS BLAUGRUND'S EPSILON(ZERO)                                     FTAU 182
  105 ELZ=CONST*ELEL*EZERO                                              FTAU 183
C  EL IS THE MATRIX OF EPSILONS                                         FTAU 184
      EL(N1)=ELZ                                                        FTAU 185
      YOEPZ=DLOG(ELZ)                                                   FTAU 186
C  DENT IS THE DELTA EL FOR TIME=0.004 PSEC AND THE INTEGRAND OF EQ. 5A FTAU 187
C   EVALUATED AT ELZ                                                    FTAU 188
      DENT=0.004/(TCONS*TIME(EL2))                                      FTAU 189
C  DIST= STEP SIZE FOR YOEP                                             FTAU 190
      DIST=YOEPZ-DLOG(ELZ-DENT)                                         FTAU 191
      FUN1(N1)=V(N1)*COSP(N1)*TIME(EL(N1))                              FTAU 192
C  START LOOP TO EVALUATE QUANTITIES AT 401 POINTS                      FTAU 193
C  QUANTITIES EVALUATED--EL,ENERGY,V,INTEGRAL OF EQ 15A(Y),COSP,TIMS(TIME), FTAU 194
C  FUN1,RZ=RANGE ALONG BEAM DIRECTION                                   FTAU 195
 1000 DO 20 J=NSTRT,NSTEP1                                              FTAU 196
      YOEP=YOEPZ-DIST                                                   FTAU 197
      EL(J)=DEXP(YOEP)                                                  FTAU 198
      EKEV(J)=EL(J)/(CONST*ELEL)                                        FTAU 199
      V(J)=(EKEV(J)/CM)**0.5                                            FTAU 200
      CALL DQG4(EL(J),EL(J-1),FCT,GRL)                                  FTAU 201
      T=Y+GRL                                                           FTAU 202
      COSP(J)=COSP(N1)*DEXP(-Y*G(2)/(2.0*R(2)))                         FTAU 203
      CALL DQG4(EL(J),EL(J-1),TIME,TIMM)                                FTAU 204
      TIM=TIMM+TIM                                                      FTAU 205
      TIMS(J)=TIMS(N1)+TIM*TCONS                                        FTAU 206
      FUN1(J)=V(J)*COSP(J)*TIME(EL(J))                                  FTAU 207
      IF(NRFLG.EQ.1) GO TO 200                                          FTAU 208
      VCOS(J)=V(J)*COSP(J)                                              FTAU 209
      VSUM=0.5*(VCOS(J)+VCOS(J-1))                                      FTAU 210
      RZ(J)=RZ(J-1)+100.0*VO*RHO*VSUM*(TIMS(J)-TIMS(J-1))               FTAU 211
C  JUMP OUT OF LOOP IF RZ GREATER THAN THICKNESS OF TARGET FOR GIVEN LAYER FTAU 212
      IF(RZ(J).GE.OTH) GO TO 122                                        FTAU 213
  200 TOEPZ=YOEP                                                        FTAU 214
   20 CONTINUE                                                          FTAU 215
      IF(NTHRU.EQ.1) GO TO 24                                           FTAU 216
C  SAVE SOME VALUES OF PARAMETERS USED IN THE TARGET                    FTAU 217
  122 ELELT=ELEL                                                        FTAU 218
      DISTT=DIST                                                        FTAU 219
      TCONST=TCONS                                                      FTAU 220
C  CHANGE VARIABLES TO THOSE OF BACKING                                 FTAU 221
   42 NTHRU=1                                                           FTAU 222
      FET=FE8                                                           FTAU 223
      RHO=RHO8                                                          FTAU 224
      NRFLG=1                                                           FTAU 225
      WRITE(3,52)                                                       FTAU 226
      WRITE(3,63)                                                       FTAU 227
      WRITE(3,64)                                                       FTAU 228
      DO 40 I=2,4                                                       FTAU 229
      L(I)=LB(I)                                                        FTAU 230
      A(I)=AB(I)                                                        FTAU 231
   40 Z(I)=ZB(I)                                                        FTAU 232
      WRITE(3,55) A(1),Z(1),A(2),Z(2),A(3),Z(3),A(4),Z(4),RHO8,FET      FTAU 233
      WRITE(3,65)                                                       FTAU 234
      NE=NE8                                                            FTAU 235
      NEE=NEP                                                           FTAU 236
C  NCROS=VALUE OF J WHEN THE ION ENTERS THE BACKING                     FTAU 237
   22 IF(J.EQ.2) J=1                                                    FTAU 238
      NCROS=J                                                           FTAU 239
      NSTRT=NCROS+2                                                     FTAU 240
      IF(THICK.EQ.0.0) GO TO 43                                         FTAU 241
      EZERO=EL(NCROS)/(CONST*ELELT)                                     FTAU 242
   43 N1=NCROS+1                                                        FTAU 243
      V(N1)=V(J)                                                        FTAU 244
      TIMS(N1)=TIMS(J)                                                  FTAU 245
      COSP(N1)=COSP(J)                                                  FTAU 246
      TIM=0.0                                                           FTAU 247
      Y=0.0                                                             FTAU 248
      WRITE(3,66) M,V(N1),TIMS(N1),COSP(N1),EZERO,RZ(NCROS),NCROS       FTAU 249
      IF(NCROS.EQ.NSTEP1) GO TO 24                                      FTAU 250
C  GO BACK AND CALCULATE BACKING PARAMETERS AT STATMENT 222             FTAU 251
      IF(NLP2.EQ.0) GO TO 222                                           FTAU 252
      GO TO 105                                                         FTAU 253
```

```
C   VARY TAU FROM 10.0 TO 0.004 PSEC
  24  K=0
      XI=1.0
      TAU(1)=10.0
 117  K=K+1
      IF(TAU(K).LT.0.004) GO TO 101
C   EVALUATE INTEGRAND FOR TARGET AND DO INTEGRAL TO CALCULATE F(TAU)
      DO 25 I=1,NCROS
      IF((TIMS(I)/TAU(K)).GE.30.0) GO TO 47
      NSPAC=I
  25  GRAND(I)=EL(I)*FUN1(I)*DEXP(-TIMS(I)/TAU(K))
      IF(NCROS.GE.3) GO TO 47
      AREA(NCROS)=0.0
      GO TO 48
  47  CALL GQSF(DISTT,GRAND,AREA,NSPAC)
  48  FT1=AREA(NSPAC)*TCONST
C  EVALUATE INTEGRAND FOR BACKING AND DO INTEGRAL TO CALCULATE F(TAU)
      NPT2=NSTEP1-N1+1
      DO 26 I=N1,NSTEP1
      IF((TIMS(I)/TAU(K)).GE.30.0) GO TO 301
  26  GRAL(I-NCROS)= EL(I)*FUN1(I)*DEXP(-TIMS(I)/TAU(K))
      GO TO 302
 301  NPT2=1-N1
 302  IF(NPT2.LE.2) GO TO 225
      CALL GQSF(DIST,GRAL,AREA,NPT2)
      GO TO 226
 225  AREA(NPT2)=0.0
 226  FT2=AREA(NPT2)*TCONS
C  COMPUTE F(TAU) FOR GIVEN LIFETIME AND TARGET LAYER
      FTAU(M,K)=(FT1+FT2)/(VI*TAU(K))
 120  IF(TAU(K)-5.0*XI-0.000001) 147,147,119
 119  TAU(K+1)=TAU(K)-XI
      GO TO 117
 147  IF(TAU(K)-2.0*XI-0.000001) 141,141,140
 140  TAU(K+1)=TAU(K)-0.5*XI
      GO TO 117
 141  IF(TAU(K)-XI-0.000001)139,139,118
 118  TAU(K+1)=TAU(K)-0.2*XI
      GO TO 117
 139  XI=0.1*XI
      GO TO 120
 101  CONTINUE
 111  KMAX=K-1
      WRITE(3,50)
      WRITE(3,67)
C   COMPUTE AVERAGE VALUE OF F(TAU) FOR NLAY LAYERS
      DO 152 K=1,KMAX
      FTU=0.0
      DO 151 M=1,NLAY
 151  FTU=FTU+FTAU(M,K)
      FAVG(K)=FTU/FLOAT(NLAY)
      WRITE(3,68) TAU(K),(FTAU(M,K),M=1,NLAY),FAVG(K)
 152  CONTINUE
      GO TO 6
 999  STOP
      END
```

```
C   XXXXXXXXXXXXXXXXXXXXXXXXXXXXXXXXXXXXXXXXXXXXXXXXXXXXXXXXXXXXXXXXXXXXXXX
C   XXXXXXXXXXXXXXX      FCT(E) OR TIME(E)      XXXXXXXXXXXXXXXXXXXXX
C   XXXXXXXXXXXXXXXXXXXXXXXXXXXXXXXXXXXXXXXXXXXXXXXXXXXXXXXXXXXXXXXXXXXXXXX
C A FUNCTION SUBPROGRAM TO CALCULATE THE INTEGRAND IN EQ.15A(FCT) OR IN
C  EQ. 5A(TIME) OF BLAUGRUND'S PAPER
C
      FUNCTION FCT(E)
      IMPLICIT REAL*8(A-H,P-Z)

      COMMON C,A,G,XKE,AMAS,NE,NEE
      DIMENSION C(5),A(5),G(5),XKE(5),AMAS(5)
    1 NSKP=0
      GO TO 22
      ENTRY TIME(E)
      NSKP=1
   22 XE=XKE(2)*E**0.5
      E1=E
      IF(E-4.0) 11,11,12
   11 P=3.0*DLOG10(E)
      XN=10.0**(-0.984182+0.23497*P+0.09636*P**2-0.03817*P**3)
      XNPRM=XN
      GO TO 13
   12 XN=(0.30+DLOG((0.6+E**2)/E))/(2.0*E)
      XNPRM=XN
   13 IF(NE-1)14,14,15
   15 DO 19 I=3,NEE
      E=E*AMAS(I)/AMAS(2)
      XE=XE+C(I)*XKE(I)*E**0.5
      IF(E-4.0) 16,16,17
   16 P=3.0*DLOG10(E)
      XNS=10.0**(-0.984182+0.23497*P+0.09636*P**2-0.03817*P**3)
      GO TO 18
   17 XNS=(0.30+DLOG((0.6+E**2)/E))/(2.0*E)
   18 XN=XN+C(I)*XNS
      IF(NSKP.EQ.1) GO TO 19
      XNPRM=XNPRM+C(I)*A(I)*G(1)*XNS/(A(2)*G(2))
   19 CONTINUE
      E=E1
   14 IF(NSKP.EQ.1) GO TO 21
      FCT=XNPRM/(E*(XE+XN))
      RETURN
   21 TIME=1.0/((XE+XN)*E**0.5)
      RETURN
      END
C
C
C
C
C    XXXXXXXXXXXXXXXXXX    SAMPLE DATA    XXXXXXXXXXXXXXXXX
C
C
AR37 IN CO34S TARGET AND NI BACKING
  2    1    1    0  4.88        450.0      10     1.20
  1    1              8.90        1.20
36.9869  112.41     33.9679      18.0      48.0      16.0
58.71      28.0
0.9489
```

Appendix E

PUBLISHED WORKS

Reprinted from THE PHYSICAL REVIEW, Vol. 188, No. 4, 1806-1812, 20 December 1969
Printed in U. S. A.

Mean Lifetimes and Branching Ratios of Low-Lying Levels in ^{33}S†

C. E. RAGAN, III,* C. E. MOSS,‡ R. V. POORE, AND N. R. ROBERSON
Duke University and Triangle Universities Nuclear Laboratory, Durham, North Carolina 27706
AND
G. E. MITCHELL AND D. R. TILLEY
North Carolina State University, Raleigh, North Carolina 27607 and Triangle Universities Nuclear Laboratory, Durham, North Carolina 27706

(Received 20 August 1969)

The mean lifetimes of the levels of ^{33}S below 3.3-MeV excitation energy have been measured by the Doppler shift attenuation method. The ^{30}Si$(\alpha, n)^{33}$S reaction was used to populate these states. SiO_2 targets (enriched to 95% in ^{30}Si) evaporated onto Ni backings were bombarded with α-particles ranging in energy 5.5–9.0 MeV. γ-ray spectra were recorded with a 20-cc Ge(Li) detector at 0°, 90°, and 510° to the beam. The following mean lifetimes were found: τ(0.842-MeV level) = 1.66±0.34 psec, τ(1.968) = 182±22 fsec, τ(2.313) = 183±25 fsec, τ(2.869) < 15 fsec, τ(2.937) > 4 psec, τ(2.970) = 82±12 fsec, τ(3.221) < 65 fsec. The branching ratios of the 2.970-MeV level were determined to be (90±5)% to the ground state and (10±5)% to the second excited state.

I. INTRODUCTION

THE low-lying levels of ^{33}S have been the subject of a number of investigations; the available information up to 1967 is summarized by Endt and Van der Leun.[1] The energy levels have been located primarily by the ^{32}S$(d, p\gamma)^{33}$S and ^{32}S$(n, \gamma)^{33}$S reactions.[2–4] However, relatively little is known about the absolute strengths of the γ-ray transitions. Recently, certain collective aspects of ^{33}S have been studied via the ^{31}P$(^3$He, $p)^{33}$S reaction,[5] and Dubois[6] has used the ^{34}S$(^3$He, $\alpha)^{33}$S reaction to study the lowest $T=\frac{3}{2}$ states as well as some of the low-lying $T=\frac{1}{2}$ states.

Theoretical calculations have been carried out by Bishop,[7] Glaudemans *et al.*,[8] and Glaudemans, Wildenthal, and McGrory.[9] The calculations for the $(2s_{1/2}, 1d_{3/2})$ shell performed by Glaudemans, Wildenthal, and McGrory[9] using a surface δ interaction give good agreement with experiment. Wiechers and Brussaard[10] have calculated the $M1$-transition probability for the 0.842→0 transition in ^{33}S using the wave functions of Glaudemans *et al.*[8]

The present paper[11] describes a study of the low-lying levels of ^{33}S up to an excitation energy of 3.3 MeV. The mean lifetimes of the first seven excited states of ^{33}S were measured using the Doppler-shift attenuation method (DSAM). States of interest were populated by the ^{30}Si$(\alpha, n)^{33}$S reaction. The γ-ray decay modes of the 2.97-MeV state were determined, and limits on the branching of other states were obtained.

II. PROCEDURE

A. General

The Triangle Universities Nuclear Laboratory FN tandem Van de Graaff accelerator was used to accelerate

† Work supported in part by the U.S. Atomic Energy Commission.
* National Defense Education Act Fellow.
‡ Present address: University of Colorado, Boulder, Colo.
[1] P. M. Endt and C. Van der Leun, Nucl. Phys. A105, 1 (1967).
[2] J. A. Becker, L. F. Chase, Jr., D. B. Fossan, and R. E. McDonald, Phys. Rev. 146, 761 (1966).
[3] J. M. O'Dell, R. W. Krone, and F. W. Prosser, Jr., Nucl. Phys. 82, 574 (1966).
[4] G. Van Middelkoop and H. Gruppelaar, Nucl. Phys. 80, 321 (1966).
[5] R. S. Cox, R. W. West, and R. J. Ascuitto, Phys. Rev. 175, 1419 (1968).
[6] J. Dubois, Nucl. Phys. A117, 533 (1968).
[7] G. R. Bishop, Nucl. Phys. 14, 376 (1959).
[8] P. W. M. Glaudemans, G. Wiechers, and P. J. Brussaard, Nucl. Phys. 56, 529 (1964); 56, 548 (1964).
[9] P. W. M. Glaudemans, B. H. Wildenthal, and J. B. McGrory, Phys. Letters 21, 427 (1966).
[10] G. Wiechers and P. J. Brussaard, Nucl. Phys. 73, 604 (1965).
[11] A preliminary version of this work was presented at a recent American Physical Society meeting: N. R. Roberson, C. E. Ragan, III, C. E. Moss, R. V. Poore, G. P. Lamaze, G. E. Mitchell, and D. R. Tilley, Bull. Am. Phys. Soc. 14, 629 (1969).

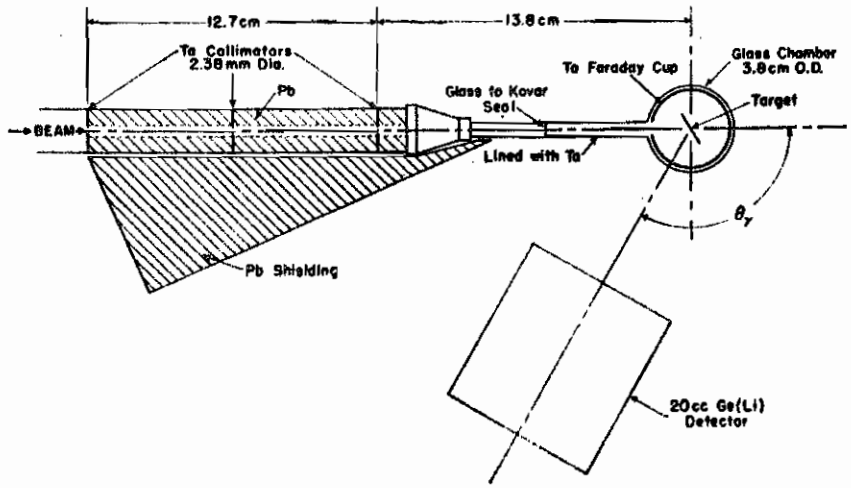

FIG. 1. Schematic drawing of the scattering chamber showing the beam path to the target, the collimating system, and the lead used to shield the 20-cc Ge(Li) detector.

α particles to energies ranging from 5.5–9.0 MeV. In Fig. 1a schematic drawing of the experimental setup is shown. A series of three Ta collimators served to define the beam. Each collimator was followed by a coaxial lead tube for shielding purposes. The stainless-steel beam pipe immediately before the collimators was lined with Ta sheet.

The target chamber (a glass cylinder approximately 13.5 cm high×3.8 cm diam) was connected to the beam pipe by a Ta-lined glass tube. The chamber was also lined with Ta which served as a Faraday cup. A vacuum of 5×10^{-7} Torr was maintained in the target chamber by a Vac-Ion pump connected to the top of the chamber.

The γ rays were detected with a 20-cc Ge(Li) detector placed ~8 cm from the target. The resolution of the detector was ~4.5 keV [full width half-maximum (FWHM)] for 1.33-MeV γ rays. Spectra were recorded with a 2048-channel analog-to-digital converter in conjuction with a DDP-224 on-line computer. After a spectrum was recorded at each angle it was stored on magnetic tape for later analysis.

B. Experimental Procedure

Targets were prepared by evaporating SiO_2 (enriched to 95% in ^{30}Si) from a Ta boat onto 1.5-μ Ni foils. The thickness of the SiO_2 targets ranged 15–150 μg/cm^2. The target thickness was estimated by noting the thin film interference pattern formed on a glass slide during evaporation. Another estimate of the target thickness was obtained by measuring the energy lost by α particles in the SiO_2 target. This value was converted into a target thickness by use of the energy-loss data of Whaling.[12] (The energy loss was determined by measuring the energy difference between α particles which had been elastically scattered at 135° from the Ni foil and those which had been scattered from the Ni foil after passing through the target.) The results of the two methods of measurement agree to within 10%.

The particular form of the DSAM used follows closely that described by Warburton, Olness, and Poletti.[13] The heavy-ion recoils were produced by using the endothermic reaction ^{30}Si$(\alpha, n)^{33}$S with a Q value of −3.504 MeV. These recoils were confined to a narrow cone about the beam axis by using an α-particle energy slightly above the threshold energy. Beam energies 0.5–1.0 MeV above threshold produced half-angles of the heavy-ion recoils of the order of 10°. The velocities of the ^{33}S recoils, v/v_0, ranged from 0.88–1.11, where $v_0=c/137$.

For most of the transitions studied, data were acquired at several different bombarding energies and with several different target thicknesses. The γ rays were detected at 0°, 90°, and 150° to the beam axis in order to obtain several values of the experimental Doppler shift ΔE_γ and thus several values of $F(\tau)$ for each experimental condition. (Data were accumulated at each angle for several hours at a time, and then the runs at each angle were combined.) The energy calibration of the detector was based on the γ rays from ^{56}Co.

In most of the spectra small baseline or gain shifts were noted. These shifts were monitored by recording γ rays of known energy from radioactive sources at the same time as γ rays from the reaction. In most cases, the energy of the "source" γ ray was chosen to be very close to the energy of the "reaction" γ rays; thus, any observed shifts could be corrected by treating them as baseline shifts. The source γ rays were chosen to be lower in energy than the reaction γ rays in order to minimize background contributions to the γ rays of interest. The primary sources used were ^{137}Cs, ^{60}Co, and ^{88}Y. The 2.937-MeV γ ray from the fifth excited state of ^{33}S, which was determined to be a long-lived state in many preliminary runs, was also used to monitor the stability of the system.

[12] W. Whaling, in *Handbuch der Physik*, edited by S. Flügge (Springer-Verlag, Berlin, 1958), Vol. 34, p. 193.

[13] E. K. Warburton, J. W. Olness, and A. R. Poletti, Phys. Rev. 160, 938 (1967).

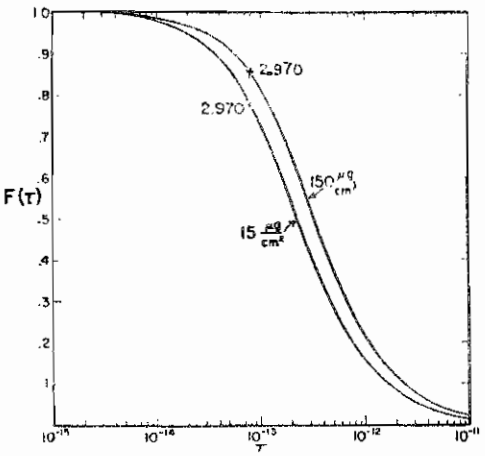

FIG. 2. Theoretical curves of $F(\tau)$ versus τ in seconds for two different target thicknesses. The upper curve is for a 150-μg/cm^2 SiO_2 target evaporated onto a Ni backing, and the lower curve is for a 15-μg/cm^2 SiO_2 target on a Ni backing. The two experimental values of $F(\tau)$ for the 2.97-MeV state are shown, and the lifetimes are seen to agree rather well. α_B and α_T are the characteristic slowing down times for ^{33}S ions in Ni and SiO_2, respectively.

In order to determine the branching ratios, spectra were recorded with the detector at 60° using a bombarding energy of 8.75 MeV and a target thickness of 150 μg/cm^2. The efficiency of the Ge(Li) detector was determined by using the known energies and intensities[14] of the γ rays from a ^{56}Co source placed ~8 cm from the detector.

C. DSAM

The DSAM has become a widely used method of measuring lifetimes of nuclear levels. The details of the method outlined here follow closely those given by Warburton, Olness, and Poletti.[13] The experimental Doppler-shift attenuation factor $F_{\exp}(\tau)$ is given by

$$F_{\exp}(\tau)=\Delta E_\gamma/E_{\gamma 0}\beta(0)(\cos\theta_1-\cos\theta_2), \quad (1)$$

where ΔE_γ is the experimentally observed shift between the two detector angles θ_1 and θ_2, $E_{\gamma 0}$ is the unshifted γ-ray energy, and $\beta(0)=v(0)/c$, where $v(0)=v_z(0)$ is the initial recoil velocity of the excited nucleus. The initial recoil velocity of ^{33}S along the beam direction $v_z(0)$ can be calculated from the center-of-mass velocity $v_{\text{c.m.}}$. Since the outgoing neutrons in the ^{30}Si$(\alpha, n)^{33}$S reaction have some ditribution in the c.m. system, the value of $v_z(0)$ has some upper and lower limit. These limits can be computed from

$$\langle v_z(0)\rangle=v_{\text{c.m.}}[1+\gamma^{-1}\langle\cos\theta_{\text{c.m.}}\rangle], \quad (2)$$

where $\theta_{\text{c.m.}}$ is the c.m. angle of the outgoing ^{33}S nucleus, and γ^{-1} is the ratio of the speed of the outgoing ^{33}S nucleus in the c.m. to the speed of the c.m. in the laboratory system. Following Warburton *et al.*,[13] $\langle\cos\theta_{\text{c.m.}}\rangle$ was set equal to 0 ± 0.33. Thus, Eq. (2) becomes

$$\langle v_z(0)\rangle\simeq v_{\text{c.m.}}(1\pm0.33\gamma^{-1}). \quad (3)$$

For an ensemble of N nuclei with lifetime τ recoiling into a backing there are a certain number dN which decay in time dt, i.e.,

$$dN/dt=-N/t. \quad (4)$$

If the velocity as a function of time is known, then this expression can be converted to an expression for $dN(V)/dV$, where $V\equiv v_z(t)/v(0)$. The general theory for the stopping of heavy ions in different backings has been given by Lindhard, Scharff, and Schiøtt (LSS).[15] Their expression for the energy loss can be approximated[13] by

$$-M_1(dv_z/dt)=K_e(v_z/v_0)+K_n(v_z/v_0)^{-1}, \quad (5)$$

where M_1 is the mass of the recoiling nucleus and K_e and K_n are constants determined from the LSS value and experimental data. Using Eq. (5) the expression for $dN(V)/dV$ becomes

$$dN(V)/dV=[N_0/(\gamma_i^{-2}+1)^{x/2}\times[xV(\gamma_i^{-2}+V^2)^{x/2-1}+\gamma_i^{-x}\delta(V)], \quad (6)$$

where $x=\alpha/\tau$, $\alpha=M_1v_0/K_e\rho\gamma_i^2=(K_e/K_n)[v(0)/v_0]^2$, and ρ is the density of the backing.

TABLE I. γ-ray branching ratios for the low-lying levels of ^{33}S.

Level	E_i (MeV)	E_f (MeV)	Branching ratios Ref. 1	Present
2	1.968	0	100	100
		0.842	<0.5	<1.5
3	2.313	0	35	34±5
		0.842	65	66±5
		1.968	<3	<6
4	2.869	0	100	100
		0.842	<3	<3
		1.968	<3	<3
		2.313	...	<4
5	2.937	0	50	...
		0.842	<2	<2
		1.968	50	...
		2.313	...	<2
6	2.970	0	...	90±5
		0.842	...	<3
		1.968	...	10±5
		2.313	...	<2
7	3.221	0	40	38±5
		0.842	60	62±5
		1.968	...	<2
		2.313	...	<5
		2.869	...	<7
		2.937	...	<2
		2.970	...	<2

[14] J. B. Marion, Nucl. Data A4, 301 (1968).

[15] J. Lindhard, M. Scharff, and H. E. Schiøtt, Kgl. Danske Videnskab. Selskab, Mat.-Fys. Medd. 33, No. 14 (1963).

TABLE II. Mean lifetimes of the levels of ^{33}S.

Level number	E_x (MeV)	E_p (MeV)	Target thickness (μg/cm^2)	$F(\tau)$[a]	Mean lifetime[a] (fsec)	(Mean lifetime)[b] (fsec)
1	0.842	5.60	15	0.095±0.013	$1.60_{-0.31}^{+0.29}$psec	1.66±0.34 psec
			150	0.111±0.031	$2.07_{-0.47}^{+0.88}$psec	
2	1.968	7.20	150	0.671±0.012	182±8	182±22
3	2.313	7.20	150	0.651±0.028	196±18	
		8.08	15	0.566±0.046	180±28	183±25
		8.08	150	0.700±0.037	164±22	
4	2.869	8.08	15	1.019±0.019	<10	
		8.08	150	0.999±0.013	<10	<15
		8.75	150	1.004±0.022	<14	
5	2.937	8.08	150	0.00±0.038	>4.7 psec	>4 psec
6	2.970	8.08	15	0.778±0.018	80±7	
		8.08	150	0.858±0.007	79±4	82±12
		8.75	150	0.831±0.023	91±7	
7	3.221	8.75	150	0.944±0.050	<60	<65

[a] Statistical errors.

[b] Total errors calculated as explained in the text.

The quantity $F(\tau)$, in terms of $dN(V)/dV$, is given by

$$F(\tau)=\int_0^1 V\frac{dN(V)}{dV}dV\Big/\int_0^1\frac{dN(V)}{dV}dV. \quad (7)$$

Using Eqs. (6) and (7) gives

$$F(\tau)=\frac{x\gamma_i^x}{(1+\gamma_i^2)^{x/2}}\int_0^1 V^2(\gamma_i^{-2}+V^2)^{x/2-1}dV. \quad (8)$$

If the recoiling ions are stopping in two different media and v_c is the velocity at which the ions cross from one media to the other, then

$$F(\tau)=\frac{1}{A_1^{x1/2}}\left[\frac{x_2C_1^{x1/2}}{C_2^{x2/2}}\int_0^{V_c}V^2B_2^{x2/2-1}dV+x_2\int_{V_c}^1 V^2B_1^{x1/2-1}dV\right], \quad (9)$$

where $V_c=v_c/v_c(0)$, $A_j=(1+\gamma_{ij}^{-2})$, $B_j=(V^2+\gamma_{ij}^{-2})$, and $C_j=(V_c^2+\gamma_{ij}^{-2})$. The subscript 1 refers to the target and 2 refers to the backing.

Since an ensemble of nuclei recoiling into a backing have a certain velocity distribution, the emitted γ rays have a certain energy distribution, and this gives rise to a particular line shape for the detected γ rays. The theoretical line shape can be determined by folding the response function of the γ-ray detector into the distribution given by Eq. (6). If the response function of the detector is Gaussian, then the theoretical distribution is given by

$$(dN/dV)_{\rm th}=C_n\int_0^1[dN(U)/dU]\times\exp[-(U-V)^2/\sigma^2]dU, \quad (10)$$

where the normalization C_n and σ are determined from the experimental distribution. The theoretical distribution given in Eq. (10) is fitted to the experimental distribution by normalizing the two distributions at the unshifted energy $E_{\gamma 0}$ and then varying x and γ_i^2 in discrete steps. The best fit is determined from the minimum value of χ^2.

D. Analysis

The centroids of the peaks of interest in each spectrum were determined by a computer program which calculated the first moment and its statistical uncertainty after subtracting background. The background was approximated by least-squares fitting an exponential to the portions of the spectrum near the peaks. The Doppler shifts were then computed and corrected for any baseline shifts by observing the shifts of the "source" γ rays. The experimental Doppler shift attenuation factor $F_{\rm exp}(\tau)$ was then computed from Eq. (1).

In order to extract the lifetime from the experimental value of $F_{\rm exp}(\tau)$, Eq. (8) was used to evaluate $F(\tau)$ as a function of the lifetime. The value of K_e, the electronic stopping parameter, was obtained for ^{33}S ions recoiling in Ni by increasing the LSS value of $(-dE/dx)_{\rm electronic}$ at $v_z=v_0$ by 15%. Evidence presented by several investigators[16–19] indicates that for $Z=16$ ions in any backing the value of K_e is ~15% larger than the LSS value. The value of K_n, the nuclear-stopping parameter, was obtained directly from the LSS theory by using the value of $(-dE/dx)_{\rm nuclear}$ at $v_z=v_0$.

[16] J. H. Omrod and H. E. Duckworth, Can. J. Phys. 41, 1424 (1963).
[17] J. H. Omrod, J. R. MacDonald, and H. E. Duckworth, Can. J. Phys. 43, 275 (1965).
[18] B. Fastrup, P. Hvelplund, and C. A. Sautter, Kgl. Danske Videnskab. Selskab, Mat.-Fys. Medd. 35, No. 10 (1966).
[19] P. Hvelplund and B. Fastrup, Phys. Rev. 165, 408 (1968).

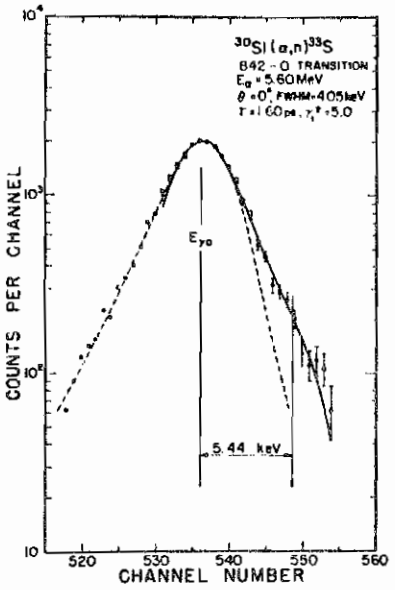

FIG. 3. 0.842-MeV γ ray from the ^{33}S 0.842→0 transition observed at 0°. The state was populated by bombarding a 15-μg/cm^2 SiO_2 target evaporated onto a Ni backing with 5.60-MeV α particles. The spectrum has a dispersion of 0.435 keV/channel. Background has been subtracted. The solid curve is a theoretical fit to the line shape and was obtained as explained in the text. The dashed curve is the line shape observed with the detector at 90°. The parameters of the theoretical fit are given in the figure.

The target thickness was taken into account explicitly in calculating the theoretical value of $F(\tau)$. The target was divided into 10 layers, and $F_i(\tau)$ was calculated for each layer i by using Eqs. (8) and (9). The velocity of the ion as it crossed into the backing V_c was calculated for each layer of the target using an expression for the distance along the beam direction as a function of V. The cross section for the reaction was assumed to be uniform throughout the target, and the average value of $F(\tau)$ was calculated from the 10 values of $F_i(\tau)$ for values of τ ranging 10^{-15}–10^{-11} sec. Figure 2 shows $F(\tau)$ plotted against τ for two different target thicknesses. The experimental values of $F(\tau)$ for the 2.970-MeV state are shown for two target thicknesses, and the lifetimes are seen to agree rather well. The characteristic slowing down times for ^{33}S ions in Ni and SiO_2 (α_B and α_T) are also indicated.

Most of the γ rays studied in this work exhibited line shapes as well as shifts. Information on the stopping parameters of the backing as well as the lifetime can be extracted from a line-shape analysis. However, for all but one of the γ rays the shoulder caused by the Doppler shift is on the low-energy side of the peak. This introduces difficulties in folding in the detector response function since the Ge(Li) detector exhibited a pronounced low-energy tail. The response function is not Gaussian, and the line shape is degraded by the tailing. The 0.842-MeV γ ray had a shoulder on the high-energy side, and a line-shape analysis was carried out.

In calculating the statistical error in $F(\tau)$ and τ the statistical uncertainty in the position of each centroid was doubled, and this uncertainty was then used in determining a statistical error in $F(\tau)$ and τ. The total error was then calculated by assuming the following errors in addition to the statistical errors: a 15% error in the electronic stopping parameter (K_e) of the target and the backing, a 20% error in the nuclear stopping parameter (K_n) of the target and the backing, a 10% error in the target thickness, and a variation in the initial recoil velocity of ~5% determined from Eq. (3). These assumptions provide error estimates that are rather conservative.

III. RESULTS

A. Branching Ratios

Branching ratios were determined by using the spectra recorded with the detector at 60° since this is the nearest angle measured to 55°, the zero of $P_2(\cos\theta)$. A limit on the branching of a given state was obtained by summing the region of the spectrum at which the γ ray was expected. This sum plus two standard deviations was used to set a limit on the branch. The branching ratios of the first seven excited states of ^{33}S are given in Table I. The 0.969-MeV γ ray resulting from the transition 2.937→1.968 was broadened by a contaminant γ ray, and the branching of the 2.937-MeV state could not be determined. Assuming that the branching is 50% to the ground state and 50% to the second excited state,[1] a limit of $<2\%$ is obtained for the 2.937→2.313 transition. The information obtained on the branching of the 2.970-MeV state is new. The branching ratios for the 3.221- and 2.313-MeV states are in good agreement with the previous work, and limits on all possible branches of the 3.221-MeV state have been obtained.

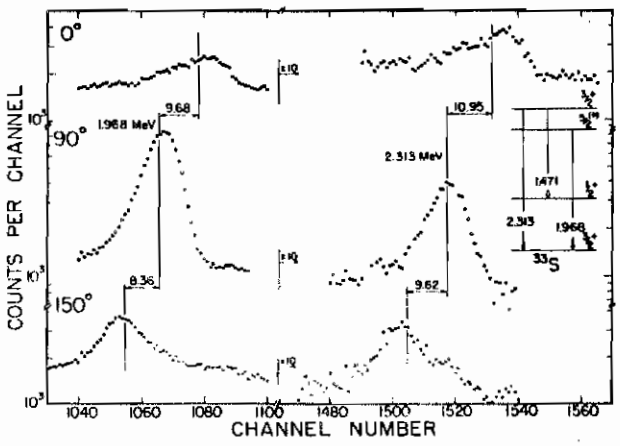

FIG. 4. Full-energy loss peaks of the 1.968- and the 2.313-MeV γ rays corresponding to the 1.968→0 and 2.313→0 transitions, respectively. The levels were populated by bombarding a 150-μg/cm^2 SiO_2 target evaporated onto a Ni backing with 7.20-MeV α particles. Spectra were recorded with the detector at 0°, 90°, and 150°. The experimental shifts in keV are shown. These spectra have a dispersion of 0.768 keV/channel.

TABLE III. Electromagnetic transition strengths in ^{33}S.

E_x (MeV)	E_γ (MeV)	J_i^π	J_f^π	δ Reference 2	δ Reference 3	δ	Multipole	$\lvert M \rvert^2$ (Weisskopf units)
0.842	0.842	$\frac{1}{2}+$	$\frac{3}{2}+$			$\pm 0.18^a$	$M1$	3.1×10^{-2}
							$E2$	6.0
1.968	1.968	$\frac{5}{2}+$	$\frac{3}{2}+$	$0.38<\delta<1.04$	0.79 ± 0.26	0.79	$M1$	1.4×10^{-2}
							$E2$	9.3
2.313	2.313	$\frac{3}{2}+$	$\frac{3}{2}+$			0^b	$M1$	4.9×10^{-3}
						∞^b	$E2$	3.7
2.313	1.471	$\frac{3}{2}+$	$\frac{1}{2}+$	$0.13<\delta<1.33$		0.47[c]	$M1$	2.9×10^{-2}
				$-8.1<\delta<-0.73$			$E2$	11.9
2.937	2.937	$\frac{7}{2}-$	$\frac{3}{2}+$	0.09 ± 0.27	0.48 ± 0.09	0^b	$M2$	$10^{-3}\lvert M \rvert^2<(2.5)^d$
				$2.1<\delta<\infty$	1.64 ± 0.45	∞^b	$E3$	$0.7<\lvert M \rvert^2<(2\times10^3)^d$
2.937	0.969	$\frac{7}{2}-$	$\frac{5}{2}+$	0.0 ± 0.01	0.08 ± 0.09	0^b	$E1$	$5\times10^{-6}<\lvert M \rvert^2<(10^{-4})^d$
3.221	3.221	$\frac{5}{2}-$	$\frac{3}{2}+$			0^b	$E1$	$>1.7\times10^{-4}$
3.221	2.379	$\frac{5}{2}-$	$\frac{1}{2}+$			0^b	$E1$	$>6.5\times10^{-4}$

[a] Calculated from τ and $B(E2\uparrow)$.
[b] Assumed.
[c] Assumed near midpoint of the range of arctanδ.
[d] Upper limit on τ of 10^{-9} sec from Ref. 2.

B. Lifetimes

Table II is a summary of the measured values $F(\tau)$ and τ. Columns 1–4 list the level number, the excitation energy, the bombarding energy, and the target thickness. Columns 5 and 6 list the weighted averages of $F(\tau)$ and τ based on shifts between different combinations of angles for each experimental condition. Column 7 gives the weighted averages of the lifetimes given in column 6. In columns 5 and 6 the errors are statistical, but in column 7 the total error is given. In setting limits on lifetimes the values of $F(\tau)$ used were obtained by adding or subtracting the total error on $F(\tau)$ to the value of $F(\tau)$ shown in Table II.

0.842-MeV Level

As mentioned previously the 0.842-MeV γ ray shown in Fig. 3 was the only one on which a line-shape analysis was carried out. The solid curve is the best fit to the 0° data minus the background using the method described in Sec. II C. Because of the low-energy tail, the theoretical distribution was fitted only to the points from $E_{\gamma 0}-0.5$ (FWHM) to the last data point shown. The dashed line shown in Fig. 3 is the line shape observed with the detector at 90°. The maximum shift in this case was only 5.44 keV, and the shoulder is so small that this shape was used only to check the previous values of the stopping parameters. The minimum value of χ^2 was obtained with the stopping parameters of Sec. II D; the lifetime of 1.60 psec is consistent with the value of 1.66 ± 0.34 psec obtained from the shift measurement.

1.968- and 2.313-MeV Levels

Sample spectra obtained in the investigation of these two levels are shown in Fig. 4. These spectra were obtained with the detector at 0°, 90°, and 150° with a beam energy of 7.20 MeV and a target thickness of 150 μg/cm^2. The γ rays are the ground-state branches of these two levels. Neither of the γ rays are shifted by the maximum amount, as can be seen by comparing the observed shift shown in the figure to the maximum shift [which is just the denominator of Eq. (1)]. Both of the states have a value of $F(\tau)\approx0.66$, which implies nearly equal lifetimes. The lifetime of the 1.968-MeV level is 182 ± 22 fsec, while the lifetime of the 2.313-MeV level is 183 ± 25 fsec.

Triplet at 2.9 MeV

Sample spectra of the ground state branches of the triplet at approximately 2.9 MeV are shown in Fig. 5. These spectra were recorded under the same conditions as those of Fig. 4, except for an increase of the beam energy to 8.08 MeV. The lifetimes of the 2.869- and the 2.970-MeV levels were determined to be less than 15 and 82 ± 12 fsec, respectively. As mentioned previously the 2.937-MeV state is long lived and the ground-state branch of this level was used to correct the spectra in Fig. 5 for baseline shifts. In setting a lower limit of 4 psec on the lifetime of the 2.937-MeV level an error of 1.0 channel was assumed for the error in the experimental Doppler shift. This corresponds to a $F(\tau)$ of 0.0 ± 0.04.

3.221-MeV Level

This level was populated by bombarding the target with 8.75-MeV α particles. Only the thick target (150 μg/cm^2) yield was high enough for a lifetime analysis. The value of $F(\tau)$ is sufficiently close to one that only an upper limit of 65 fsec can be set on the lifetime. The value of $F(\tau)$ quoted in Table II (0.944) corresponds to a lifetime of 34 fsec.

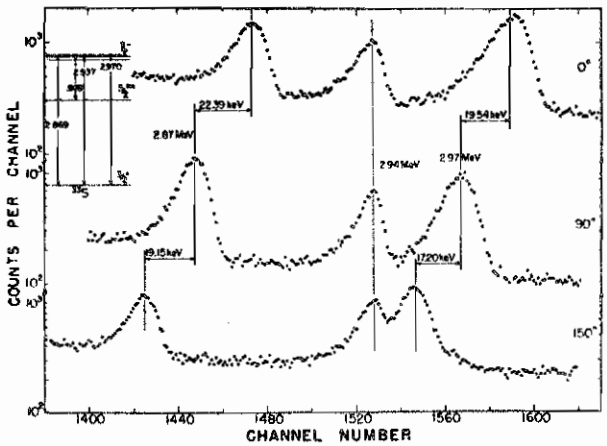

FIG. 5. Full-energy loss peaks of the ground-state branches of the triplet at approximately 2.9 MeV. The levels were populated by bombarding a 150-μg/cm^2 SiO_2 barget evaporated onto a Ni backing with 8.08-MeV α particles. Spectra were recorded with the detector at 0°, 90°, and 150°. The experimental shifts in keV are indicated. These spectra have a dispersion of 0.854 keV/channel.

IV. DISCUSSION

The calculated values of the electromagnetic transition strengths in Weisskopf units[20] (W.u.) are given in Table III for the levels of ^{33}S below 3.3 MeV with known spins. The values of the measured mixing ratios[2,3] are given in columns 5 and 6, while the values used to calculated the transition strengths are shown in column 7. The branching ratios used to calculate the transition strengths are those given in Ref. 1. For the decays from the 2.937-MeV level, only pure transitions were assumed since only upper and lower limits of the lifetime are known. The value of the mixing ratio $|\delta| = 0.18$ for the first excited state at 0.842 MeV was obtained from the value of $B(E2\uparrow)$ from Coulomb excitation measurements[21] and from the lifetime determined by this experiment. This yields an $M1$ strength of 3.1×10^{-2} W.u. and an $E2$ strength of 6.0 W.u.

Wiechers and Brussaard[10] have calculated $M1$-transition probabilities in the $(2s_{1/2}, 1d_{3/2})$ shell using the wave functions of Glaudemans *et al.*[8] For the 0.842-MeV transition in ^{33}S these authors give values of $\Gamma(M1)$ of 0.023 and 0.013 meV, where the two values are calculated using single-particle and effective nucleon g factors, respectively. The transition strengths are then 1.9×10^{-3}, and 1.0×10^{-3} W.u. and are smaller than the experimental value of 3.1×10^{-2} by approximately a factor of 10. This difference is of the same order of magnitude as that observed for the 1.28-MeV level in ^{29}Si and the 1.26-MeV level in ^{31}P.

The two levels of ^{33}S at 2.869 and 2.970 MeV do not have spin assignments. On the basis of the present lifetime measurements, the spins and parities $\frac{1}{2}\pm$, $\frac{3}{2}\pm$, $\frac{5}{2}\pm$, and $\frac{7}{2}^+$ are allowed.

As was pointed out by Becker *et al.*,[2] the decay of the 2.937-MeV level ($J^\pi=\frac{7}{2}^-$) via $E3/M2$ radiation to the ground state and $E1$ radiation to the 1.968 level is unusual. The lower limit of 4 psec set on the lifetime by this experiment indicates that either the recoil-distance[22] or electronic timing method would be suitable for an accurate lifetime measurement. Knowledge of the transition strengths for this level should provide a sensitive test for theoretical calculations as well as allow one to determine whether a large inhibition of the $E1$ or an enhancement of the $E3/M2$ is resonsible for this unusual competition.

Following a preliminary report of this work,[11] we became aware of a similar study[23] of the levels of ^{33}S.

ACKNOWLEDGMENTS

The authors would like to thank Dr. E. K. Warburton for the use of his energy-loss programs and his line-shape analysis program, and thanks are extended to Dr. J. W. Olness for a helpful discussion on the use of the line-shape-analysis program. We are obliged to Dr. A. W. Waltner for the use of some of the radioactive sources and to G. P. Lamaze for his assistance in collecting the experimental data.

[20] D. H. Wilkinson, in *Nuclear Spectroscopy*, edited by F. Ajenberg-Selove (Academic Press Inc., New York, 1960), Part B, p. 862 ff.

[21] I. Kh. Lemberg, in *Reactions Between Complex Nuclei*, edited by A. Zucker, F. T. Howard, and E. C. Halbert (Wiley-Interscience, Inc., New York, 1960), p. 112.

[22] K. W. Jones, A. Z. Schwarzschild, E. K. Warburton, and D. B. Fossan, Phys. Rev. 178, 1773 (1969).

[23] J. E. Cummings and D. J. Donahue (to be published).

PHYSICAL REVIEW C VOLUME 1, NUMBER 6 JUNE 1970

Mean Lifetimes of Low-Lying Levels of ^{34}S†

C. E. Ragan, III, R. V. Poore, and N. R. Roberson
Duke University, Durham, North Carolina 27706 and Triangle Universities Nuclear Laboratory, Durham, North Carolina 27706

and

G. E. Mitchell and D. R. Tilley
North Carolina State University, Raleigh, North Carolina 27606 and Triangle Universities Nuclear Laboratory, Durham, North Carolina 27706

(Received 16 February 1970)

The mean lifetimes of the levels of ^{34}S below 5.0-MeV excitation energy have been measured by the Doppler-shift attenuation method. The ^{31}P$(\alpha, p)^{34}$S reaction was used to populate these states. GaP targets evaporated onto 1-μ Ni foils were bombarded with α particles ranging in energy from 5.0 to 7.3 MeV. γ rays were detected with a 30-cc Ge(Li) detector at 0, 90, and 143° to the beam axis. The following mean lifetimes were found: τ(2.13-MeV level) = 400 ± 32 fsec, τ(3.30) = 175 ± 25 fsec, τ(3.92) > 1.39 psec, τ(4.07) < 24 fsec, τ(4.11) = 110 ± 10 fsec, τ(4.62) = 135 ± 17 fsec, τ(4.69) = 131 ± 13 fsec, τ(4.88) = (57 ± 22 fsec), τ(4.89) = (52 ± 14 fsec).

I. INTRODUCTION

Extensive shell-model calculations[1-3] have provided wave functions of the low-lying energy levels for many s-d-shell nuclei. Sensitive tests of these wave functions have been comparisons between the calculated and measured values of the lifetimes of the nuclear levels. Recent results[4-6] for $A = 31, 33$, and 38 give an indication of the good agreement to be expected. Clearly, more experimental results are needed throughout the s-d shell.

The present paper[7] describes the measurement of the mean lifetimes of the first nine excited states of ^{34}S. The levels of interest were populated using the ^{31}P$(\alpha, p)^{34}$S reaction, and the lifetimes were measured using the Doppler-shift attenuation method (DSAM). This investigation is a sequel to an earlier measurement[8] of the lifetimes of ^{33}S using the ^{30}Si$(\alpha, n)^{33}$S reaction.

II. EXPERIMENTAL PROCEDURE

The experiment was performed with a ^{4}He^{++} beam from the Triangle Universities Nuclear Laboratory FN Van de Graaff accelerator. The collimating system and scattering chamber have been described in detail elsewhere.[8] The γ rays from the reaction were detected with a 30-cc Ge(Li) detector placed ~8 cm from the target. The resolution of the detector was 2.6 keV (full width at half maximum) for 1.33 MeV γ rays. The spectra were recorded with a 2048-channel analog-to-digital converter (ADC) in conjunction with a DDP-224 on-line computer.[9]

Targets were prepared by evaporating GaP from a Ta boat onto 1 μ Ni foils. Target thicknesses were determined by measuring the energy lost by α particles in the GaP targets.[8] The effective target thickness (with the target oriented at 60° to the beam) was 300 μg/cm^2.

The ^{31}P$(\alpha, p)^{34}$S reaction is endothermic for the excited states of ^{34}S ($Q_0 = +0.632$ MeV), thus the recoils can be confined to a narrow cone about the beam axis by using a bombarding energy not far above the threshold energy. This allows DSA measurements to be made by observing only γ-ray singles spectra.

The experimental Doppler-shift attenuation factor $F_{\exp}(\tau)$ is defined as the ratio of the experimentally observed shift to the expected full shift. The full shift can be obtained in two ways: (1) by measuring the shift of nuclei recoiling into a vacuum, or (2) by calculating it from the reaction kinematics. The latter procedure was used here. The experimentally observed shifts were determined as explained in the next section. If the angular distribution is assumed to be isotropic in the c.m. then the average recoil velocity of the excited nuclei is just the c.m. recoil velocity. A spread in this velocity can be estimated by assuming[10] that $\langle \cos \theta_{c.m.} \rangle = 0 \pm 0.33$. For the present study (with beam energies ranging from 5.0–7.3 MeV) the spread in the recoil velocity is 8 to 13%, depending on the excited state and the beam energy. These velocity spreads correspond to half-angles of the ^{34}S recoils of 15 to 23°.

In calculating the recoil velocities, the target thickness was taken into account by subtracting from the incident beam energy one half of the target thickness in keV. Since the target was 100–120

keV thick, this correction was 50–60 keV and was small compared to the spread in the velocity due to angular distribution effects.

The γ rays were detected at 0, 90, and 143° to the beam axis in order to obtain several values of the experimental Doppler shifts ΔE_γ for each set of experimental conditions. The energy and efficiency calibrations of the detector were based on the known energies and intensities[11] of the γ rays from ^{56}Co. A calibration spectrum was usually recorded every 8 to 10 h to check for long term drifts in the electronics. Electronic drifts from one run to the next were monitored by using unshifted γ rays originating from the reaction, from a ^{56}Co source, and from the ^{40}K and ThC″ contained in the concrete walls of the laboratory.

III. ANALYSIS

The centroids of the peaks in each spectrum were determined by subtracting an exponential background from the regions below the peaks and then calculating the centroid of the remainder. These centroids were then used to determine values of $F_{exp}(\tau)$. The uncertainty in $F_{exp}(\tau)$ was calculated by doubling the statistical uncertainty in the position of each centroid. The total error in the mean lifetime was then calculated by assuming the following errors in addition to the statistical errors: a 15% error in the electronic stopping of the target and the backing, a 10% error in the target thickness, and a 10% error in the initial recoil velocity.

In a preliminary report of this work, $F(\tau)$ was calculated as a function of τ using the approximations of Warburton, Olness, and Poletti.[10] All of the lifetimes quoted in this paper, however, were obtained by computing $F(\tau)$ using the formalism given by Blaugrund[12] (see Appendix). The two methods of computing the mean lifetimes give results that agree within the experimental errors. However, the values of τ using Blaugrund's theory are consistently lower than those obtained using the method of Warburton. For example, Blaurund's theory yields a value of $\tau = 131 \pm 13$ fsec for the sixth excited state of ^{34}S, while Warburton's method yields $\tau = 153 \pm 14$ fsec.

IV. RESULTS

The available information on the low-lying levels of ^{34}S is summarized in Fig. 1. The branching ratios for the levels below 5.0 MeV are the results of a previous experiment at this laboratory.[13] The branching ratios for the two levels above 5.0 MeV are the results of the work of a group at Heidelberg.[14] The branching ratios for the β^+ de-

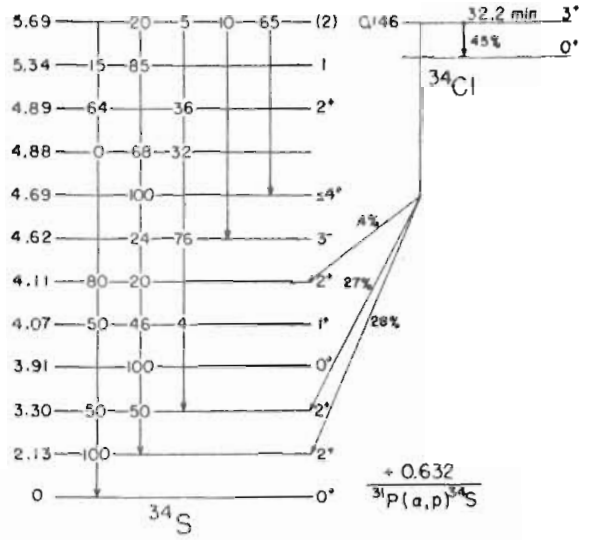

FIG. 1. The low-lying levels of ^{34}S. The spins and branching ratios of levels below 5.0 MeV are from a recent summary (Ref. 13). The spins and branching ratios of the levels at 5.34 and 5.69 MeV are from Ref. 14. The branching ratios for the decay of the 146-keV level of ^{34}Cl are from Ref. 15. (Note: The energy axis is not drawn to scale.)

cay of the 146-keV level in ^{34}Cl to the first, second, and fifth excited states of ^{34}S are from Endt and Van der Leun.[15] The threshold for the production of this 146-keV level in ^{34}Cl is 6.52 MeV. It was not populated when studying the first and second excited states of ^{34}S.

No γ rays from a given state were observed unless the α-particle bombarding energy was ~1.7 MeV above the threshold energy for that state. An estimate of the "effective threshold" for this reaction is, therefore, 1.5 to 1.6 MeV above the true threshold. The γ-ray singles spectra were recorded at bombarding energies of 5.0, 6.6, 7.0, and 7.3 MeV.

In studying a particular level, care was taken to keep the beam energy below the effective threshold for any higher states which had a branch through the state of interest. If a γ-ray branch corresponding to a transition from a higher state to the state of interest was observed in the spectrum, then the observed $F_{exp}(\tau)$ was either corrected[16] for the branch, or the level was not studied at that beam energy or higher beam energies. The only uncertainty is the possibility that some state above 5.69-MeV excitation energy might have a resonance near threshold causing the effective threshold to be less than about 1 MeV.

Table I is a summary of the measured lifetimes. Columns one through four list the level number, the excitation energy, the bombarding energy, and the transition. The letters S and D in column four

indicate that the single- or double-escape peak was used to determine $F_{exp}(\tau)$. The fifth and sixth columns list the weighted averages of $F_{exp}(\tau)$ and the lifetimes based on shifts between three angles for each experimental condition. The last column lists the weighted averages of the lifetimes. The errors given in columns five and six are statistical, while the total error is given in the last column.

2.13- and 3.30-MeV Levels

The 2.13- and 3.30-MeV levels were the only ones populated at a beam energy of 5.0 MeV. At this energy approximately 6% of the counts in the 2.13-MeV peak are due to the branching from the second excited state. The half-angle of the recoils for the first excited state is 23°. This is the largest recoil angle used in this experiment.

Sample spectra obtained in the investigation of the 2.13-MeV state are shown in Fig. 2. The spectra are the sums of several runs at each angle. The 90° line shape is broadened because of the finite angular spread of the recoiling nuclei with respect to the beam axis. The value of $F_{exp}(\tau)$ for this state has been corrected[16] for the feeding from the second excited state to give an $F_{exp}(\tau)$ of 0.363 ± 0.007. This corresponds to a mean lifetime of 400 ± 32 fsec. The value of $F_{exp}(\tau)$ for the

TABLE I. Mean lifetimes of the levels of ^{34}S.

Level number	E_x	E_α	Transition	$F(\tau)$	τ^a (fsec)	$\langle\tau\rangle^b$ (fsec)
1	2127	5.0	(1 → 0)	0.352 ± 0.006	420 ± 10	400 ± 32[c]
			(1 → 0)	0.363 ± 0.007[c]	400 ± 11	
2	3303	5.0	(2 → 0)	0.596 ± 0.035	175 ± 21	175 ± 25
3	3915	6.6	(3 → 1)	0.071 ± 0.023	$2.85^{+1.45}_{-0.70}$ psec	
		7.0	(3 → 1)	0.129 ± 0.041	$1.55^{+0.75}_{-0.41}$ psec	(1.89 ± 0.50)
		7.3	(3 → 1)	0.084 ± 0.048	$2.41^{+3.58}_{-0.81}$ psec	>1.39 psec
		7.3	(3 → 1)	0.031 ± 0.096	$7.0^{+\infty}_{-5.4}$ psec	
4	4074	6.6	(4 → 1)	0.980 ± 0.059	9 ± 25	
		6.6	(4 → 0)D	0.978 ± 0.024	10 ± 11	
		6.6	(4 → 0)S	0.963 ± 0.049	17 ± 20	
		6.6	(4 → 0)	0.984 ± 0.018	7 ± 8	<24
		7.0	(4 → 1)	0.935 ± 0.028	30 ± 11	
		7.3	(4 → 1)	0.972 ± 0.045	13 ± 20	
5	4114	6.6	(5 → 0)D	0.741 ± 0.021	111 ± 11	
		6.6	(5 → 0)S	0.746 ± 0.039	109 ± 18	110 ± 10
		6.6	(5 → 0)	0.743 ± 0.016	110 ± 8	
6	4623	6.6	(6 → 2)	0.718 ± 0.094	123 ± 46	
		7.0	(6 → 1)	0.695 ± 0.077	135 ± 41	
		7.3	(6 → 2)	0.719 ± 0.041	123 ± 21	135 ± 17
		7.3	(6 → 2)	0.704 ± 0.048	130 ± 24	
		7.3	(6 → 1)	0.636 ± 0.045	170 ± 28	
7	4688	7.0	(7 → 1)D	0.689 ± 0.046	139 ± 24	131 ± 13
		7.0	(7 → 1)	0.708 ± 0.010	130 ± 6	
8	4875	7.0	(8 → 2)	0.856 ± 0.102	63 ± 43	
		7.3	(8 → 2)	0.868 ± 0.112	58 ± 48	(57 ± 22)
		7.3	(8 → 2)	0.877 ± 0.064	55 ± 27	
9	4889	7.0	(9 → 2)	0.839 ± 0.077	70 ± 32	
		7.3	(9 → 2)	0.907 ± 0.068	42 ± 29	(52 ± 14)
		7.3	(9 → 2)	0.886 ± 0.041	50 ± 17	

[a]Statistical errors only.
[b]Total errors.
[c]Corrected for branching from 3303-keV level.

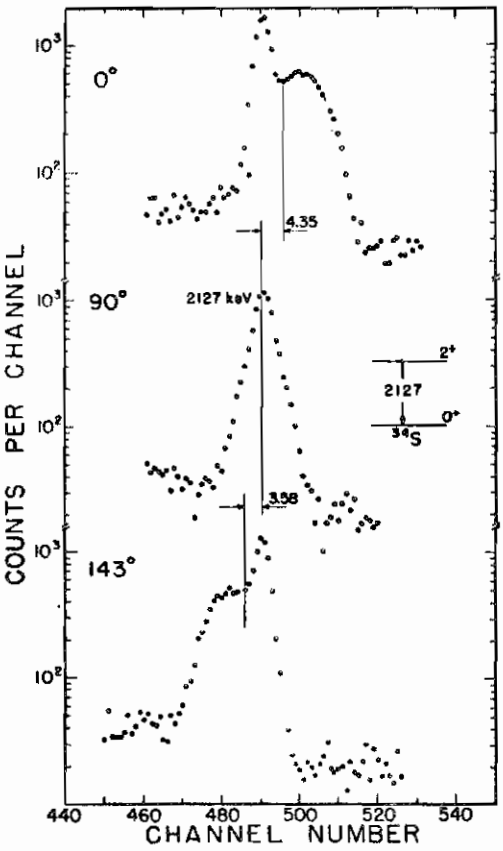

FIG. 2. The full-energy-loss peak of the 2127-keV γ ray corresponding to the $(1 \rightarrow 0)$ transition in ^{34}S. The state was populated by bombarding a 300-μg/cm^2 GaP target on a Ni backing with 5.0-MeV α particles. The spectrum has a dispersion of 0.790 keV/channel. Spectra were recorded with the detector at 0, 90, and 143°. The experimental shifts of the centroids in keV are shown.

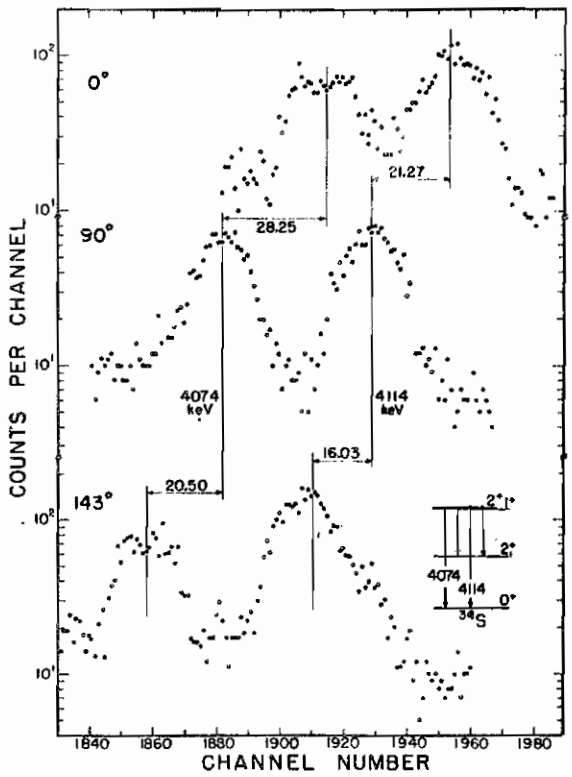

FIG. 3. The full-energy-loss peaks of the 4074- and 4114-keV γ rays corresponding to the $(4 \rightarrow 0)$ and $(5 \rightarrow 0)$ transitions in ^{34}S, respectively. The levels were populated at a bombarding energy of 6.6 MeV. Spectra were recorded with the detector at 0, 90, and 143°. The experimental shifts of the centroids in keV are indicated. The spectra have a dispersion of 0.860 keV/channel.

second excited state is 0.596 ± 0.035. This corresponds to a mean lifetime of 175 ± 25 fsec. The second excited state was not studied at 6.6 MeV, because this energy is above the threshold for the production of the 146-keV level in ^{34}Cl which β^+ decays to the 3.30-MeV state.

3.91-MeV Level

The third excited state has a lifetime longer than any other low-lying level of ^{34}S. The values of $F_{\exp}(\tau)$ are small, and in some cases the uncertainty in $F_{\exp}(\tau)$ is larger than the measured value. The large uncertainties and the small values of $F_{\exp}(\tau)$ lead to a large uncertainty in the lifetime. The weighted average of the four experimental determinations of the mean lifetime is 1.89 ± 0.50 psec. However, a more conservative statement about this result is $\tau > 1.39$ psec.

Doublet at 4.1 MeV

Sample spectra of the ground-state branches of the 4.07- and the 4.11-MeV levels are shown in Fig. 3. These spectra were recorded at $E_\alpha = 6.6$ MeV with the detector at 0, 90, and 143°. The lower member of the doublet was shifted by almost the maximum amount and has $F_{\exp}(\tau) \approx 1$. At 0 and 143° there is some evidence that the angular distribution is not isotropic about 90° in the c.m. Both branches of this state were studied at three beam energies, and Table I shows the consistency of the results. The weighted average of the lifetime of this level was increased by two standard deviations, yielding an upper limit of 24 fsec for the mean lifetime of this level.

The level at 4.11 MeV was studied only at $E_\alpha = 6.6$ MeV. At this energy the feeding by the 0.4% branch from the β^+ decay of the 146-keV level in ^{34}Cl is negligible, while at higher energies the effects of this branch becomes noticeable. Analysis of the photopeak and both escape peaks gives approximately the same value of $F_{\exp}(\tau)$ (0.743) for

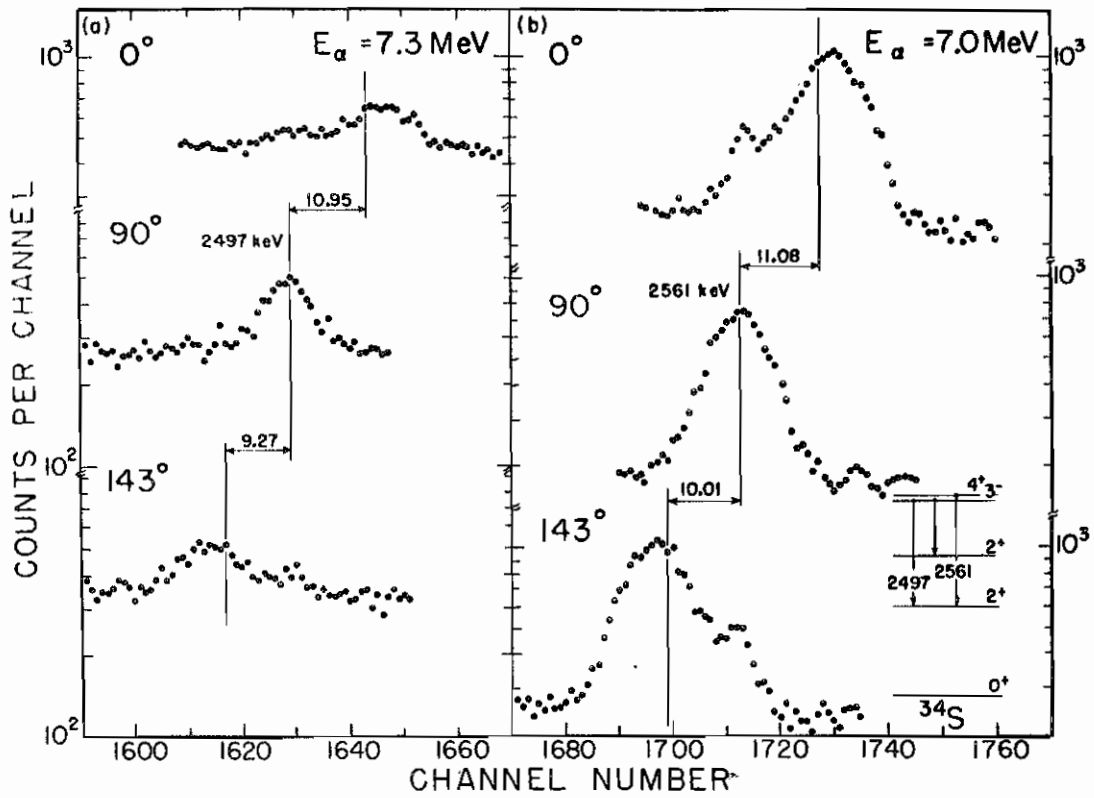

FIG. 4. The full-energy-loss peaks of the 2497- and 2561-keV γ rays corresponding respectively to the $(6 \rightarrow 1)$ and $(7 \rightarrow 1)$ transitions in ^{34}S. The spectra were recorded with the detector at 0, 90, and 143°. In (a) the bombarding energy was 7.3 MeV, and the dispersion is 0.7834 keV/channel. In (b) the bombarding energy was 7.0 MeV, and the dispersion is 0.745 keV/channel.

this level. The $(5 \rightarrow 1)$ branch was not analyzed because the energy was approximately the same as the $(6 \rightarrow 1)$ single escape energy.

Doublet at 4.65 MeV

Sample spectra of the $(6 \rightarrow 1)$ and $(7 \rightarrow 1)$ branches of the 4.62- and 4.69-MeV states are shown in Fig. 4. The spectra in Fig. 4(a) were obtained at $E_\alpha = 7.3$ MeV. The 10% branch from the 5.69- to the 4.62-MeV level was neglected in analyzing these spectra, and the sixth excited state was studied at energies up to 7.3 MeV. The spectra in Fig. 4(b) were recorded at $E_\alpha = 7.0$ MeV. At this energy there is no evidence of a 1.0-MeV γ ray due to the 65% branch to this level from the 5.69-MeV state. However, at $E_\alpha = 7.3$ MeV there was a γ ray with an energy of ~1.0 MeV, which may have been due to the 65% branch. The value of $F_{\exp}(\tau)$ was slightly smaller at this higher bombarding energy, therefore, the results obtained at $E_\alpha = 7.3$ MeV were not used.

Sample spectra of the $(6 \rightarrow 2)$ branch of the 4.62-MeV state are shown in Fig. 5. These spectra were recorded at $E_\alpha = 7.3$ MeV. The values of $F_{\exp}(\tau)$ for this branch in Table I were calculated using only the 90 and 143° data, since at 0° the 1.32-MeV γ ray and the γ ray from the first excited state of ^{60}Ni are not separated.

Doublet at 4.9 MeV

The $(8 \rightarrow 2)$ and $(9 \rightarrow 2)$ branches of the 4.88- and 4.89-MeV levels were analyzed to determine values of $F_{\exp}(\tau)$. The states were weakly populated, therefore, the uncertainties in $F_{\exp}(\tau)$ are large. However, three sets of runs at two different beam energies give similar values of the lifetimes. The lifetimes in Table I are in parentheses to show that they are tentative, and a more conservative statement would be that both levels have mean lifetimes <80 fsec.

DISCUSSION

During the course of this work we became aware of a similar measurement of the lifetimes of the levels of ^{34}S by Greene *et al.*[17] The agreement between their results and those of the present experiment is, in general, very good. All the lifetimes

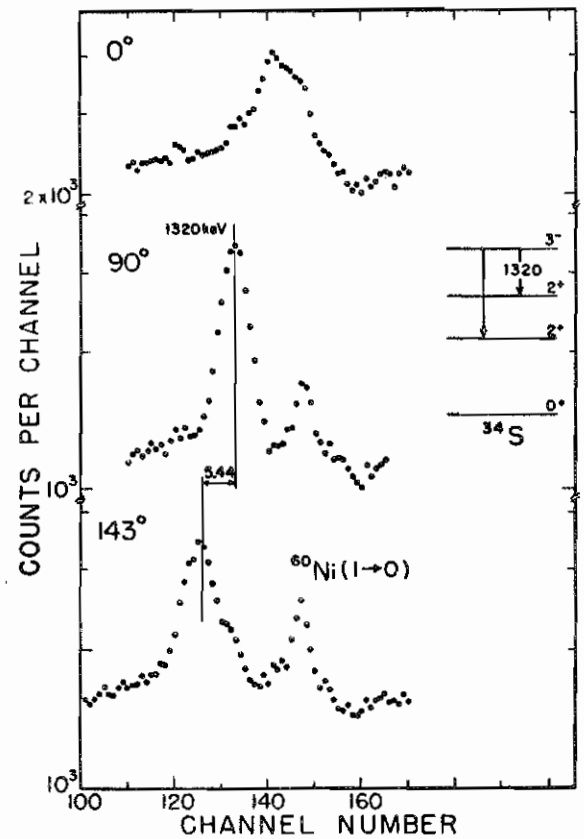

FIG. 5. The full-energy-loss peak of the 1320-keV γ ray corresponding to the (6 → 2) transition in ^{34}S. The level was populated by bombarding a GaP target on a Ni backing with 7.3-MeV α particles. The spectra were recorded with the detector at 0, 90, and 143° and with a dispersion of 0.779 keV/channel. The experimental shift in keV between 90 and 143° is indicated. In the spectrum recorded at 0°, the 1320-keV γ ray has been Doppler shifted into the 1332-keV γ ray resulting from the (1 → 0) transition in ^{60}Ni, and the shift of the centroid cannot be determined.

agree within the errors, but the present experiment gives slightly shorter lifetimes for the lowest two states and slightly longer lifetimes for the rest of the states.

Table II gives the calculated values of the electromagnetic transition strengths in Weisskopf units[18](W. u.) for the first nine excited states of ^{34}S. For the cases where $E(L+1)$ and $M(L)$ radiations compete, the strengths were not calculated unless the mixing ratio was known. Greene *et al.*[17] have pointed out that the large $E2$ strengths for the (1 → 0) and the (3 → 1) transitions suggest that these are vibrational states. However, more mixing ratios in ^{34}S are needed before the vibrational character of some of the levels can be definitely established.

Note added in proof. Grawe and Lieb[21] have also measured the lifetimes of the 2.13- and 3.30-MeV levels of ^{34}S.

APPENDIX

The Doppler-shift attenuation factor $F(\tau)$ is related to the mean lifetime τ of a nuclear level by the equation

$$F(\tau)=\frac{1}{v(0)\tau}\int_0^\infty e^{-t/\tau}v(t)\langle\cos\phi(t)\rangle dt, \qquad (1)$$

where $v(t)$ is the velocity of the recoiling nucleus, and $\langle\cos\phi(t)\rangle$ is the average value of the cosine of the scattering angle as defined in Eq. (15) of Blaugrund.[12] A computer program using a method similar to the one described by Broude[19] was written to evaluate $F(\tau)$ as a function of τ.

The program uses the expressions of Lindhard, Scharff, and Schiøtt[20] to evaluate $(d\epsilon/d\rho)_{\text{electronic}}$ and $(d\epsilon/d\rho)_{\text{atomic}}$. Using Eq. (5a) and (15) of Blaugrund, the time t and $\langle\cos\phi(t)\rangle$ can be evaluated as a function of ϵ. The integral in Eq. (1) can be

TABLE II. Electromagnetic transition strengths in ^{34}S.

Transition	J_i^π	J_f^π	δ	Multipole	$\lvert M\rvert^2$ (Weisskopf units)
(1 → 0)	2^+	0^+		$E2$	7.16
(2 → 0)	2^+	0^+		$E2$	0.91
(2 → 1)	2^+	2^+	0.126[a]	$M1$	0.055
				$E2$	2.47
(3 → 1)	0^+	2^+		$E2$	(3.61)
(4 → 0)	1^+	0^+		$M1$	$>9.78\times10^{-3}$
(5 → 0)	2^+	0^+		$E2$	0.77
(6 → 1)	3^-	2^+	0[b]	$E1$	1.1×10^{-4}
(6 → 2)	3^-	2^+	−0.02[a]	$E1$	2.27×10^{-3}
				$M2$	2.39
(9 → 0)	2^+	0^+		$E2$	(0.55)

[a] Ref. 13.
[b] Assumed.

converted to an integral over ϵ by using Eq. (5a) of Blaugrund and becomes

$$F(\tau) \propto \frac{1}{v(0)\tau} \int_0^{\epsilon(0)} e^{-t(\epsilon)/\tau} v(t) \frac{\langle \cos\phi(\epsilon) \rangle}{\epsilon^{\frac{1}{2}} (d\epsilon/d\rho)} d\epsilon . \quad (2)$$

Since ϵ is proportional to the energy of the recoiling ion and the energy range is quite large (~1000 keV), it is convenient to convert the integral in Eq. (2) to an integral over $y = \ln \epsilon$. Equation (2) thus becomes

$$F(\tau) \propto \frac{1}{v(0)\tau} \int_{-\infty}^{y(0)} e^{-t(y)/\tau} v(y) \frac{\langle \cos\phi(\epsilon) \rangle \epsilon^{1/2}}{(d\epsilon/d\rho)} dy. \quad (3)$$

Simpson's rule is then used to evaluate the integral by evaluating the integrand at 401 equally spaced values of y. In practice, a lower limit of ~ −6.0 can be used in evaluating the integral.

In order to take the target thickness into account, the target is divided into 10 layers, and $F(\tau)$ is calculated for each layer. The cross section for the reaction is assumed to be uniform throughout the target, and the average $F(\tau)$ is computed. In evaluating $F(\tau)$ for each layer of the target, the quantity

$$R_z = \int_0^{t(y)} v(t) \langle \cos\phi(t) \rangle dt$$

is evaluated at each value of $t(y)$. This quantity is compared with the target thickness D_l for that layer. If $R_z > D_l$ then the ion is assumed to have entered the backing, and the stopping parameters for the backing are then used to compute the integrand of Eq. (3) for the remaining values of y.

---

†Work supported in part by the U. S. Atomic Energy Commission.

[1]P. W. M. Glaudemans, G. Wiechers, and P. J. Brussaard, Nucl. Phys. 56, 529 (1964); 548 (1964).
[2]F. C. Erné, Nucl. Phys. 84, 91 (1966).
[3]P. W. M. Glaudemans, B. H. Wildenthal, and J. B. McGrory, Phys. Letters 21, 427 (1966).
[4]P. W. M. Glaudemans, A. E. L. Dieperink, R. J. Keddy, and P. M. Endt, Phys. Letters 28B, 645 (1969).
[5]P. W. M. Glaudemans, P. M. Endt, and A. E. L. Dieperink, to be published.
[6]G. A. P. Engelbertink, and P. W. M. Glaudemans, Nucl. Phys. A123, 225 (1969).
[7]A preliminary version of this work was presented at a recent American Physical Society meeting: C. E. Ragan, III, N. R. Roberson, C. E. Moss, R. V. Poore, G. P. Lamaze, G. E. Mitchell, and D. R. Tilley, Bull. Am. Phys. Soc. 14, 1203 (1969).
[8]C. E. Ragan, III, C. E. Moss, R. V. Poore, N. R. Roberson, G. E. Mitchell, and D. R. Tilley, Phys. Rev. 188, 1806 (1969).
[9]N. R. Roberson, R. V. Poore, F. Seibel, and J. Joyce, Columbia University Report No. CONF 690301 (unpublished), pp. 276–281.
[10]E. K. Warburton, J. W. Olness, and A. R. Poletti, Phys. Rev. 160, 938 (1967).
[11]J. B. Marion, Nucl. Data A4, 301 (1968).
[12]A. E. Blaugrund, Nucl. Phys. 88, 501 (1966).
[13]C. E. Moss, R. V. Poore, N. R. Roberson, and D. R. Tilley, to be published.
[14]G. Becker-Bender, W. Dehnhardt, W. Kutschera, D. Pelte, B. Povh, and B. Schürlein, Max-Planck Institute, Heidelberg, Germany, Report No. MPIH-1968/B/1, p.83.
[15]P. M. Endt and C. Van der Leun, Nucl. Phys. A105, 1 (1967).
[16]R. A. I. Bell, J. L'Ecuyer, R. D. Gill, B. C. Robertson, I. S. Towner, and H. J. Rose, Nucl. Phys. A133, 337 (1969).
[17]M. W. Greene, A. N. James, P. R. Alderson, D. C. Bailey, J. L. Durell, L. L. Green, and J. F. Sharpey-Schafer, in Proceedings of the International Conference on Properties of Nuclear States Montreal, Canada, 1969, edited by M. Harvey *et al.* (Presses de L'Université de Montréal, Canada, 1969), p. 114.
[18]D. H. Wilkinson, in Nuclear Spectroscopy, edited by F. Ajzenberg-Selove (Academic Press Inc., New York, 1960), Part B, p. 862 ff.
[19]C. Broude, Can. J. Phys. 45, 3415 (1967).
[20]J. Lindhard, M. Scharff, and H. E. Schiøtt, Kgl. Danske Videnskab, Selskab. Mat.-Fys. Medd. 33, No. 14 (1963).
[21]H. Grawe and K. P. Lieb, Nucl. Phys. A127, 13 (1969).

PHYSICAL REVIEW C VOLUME 2, NUMBER 2 AUGUST 1970

Mean Lifetime of the 2.94-MeV Level in ^{33}S†

C. E. Ragan, III, C. E. Moss,* C. R. Gould, and N. R. Roberson
Duke University and Triangle Universities Nuclear Laboratory, Durham, North Carolina 27706
and
G. E. Mitchell and D. R. Tilley
North Carolina State University, Raleigh, North Carolina 27607
and Triangle Universities Nuclear Laboratory, Durham, North Carolina 27706

(Received 20 April 1970)

The mean lifetime of the 2.94-MeV level in ^{33}S has been measured by the recoil distance method using the $^{30}Si(\alpha,n)^{33}S$ reaction. The lifetime was found to be 40.5 ± 2.0 psec.

INTRODUCTION

A previous measurement[1] at this laboratory of the mean lifetime of the $\frac{7}{2}^-$ level at 2.94 MeV in ^{33}S, using the Doppler-shift attenuation method (DSAM), yielded a lower limit of 4 psec. Other measurements by Cummings and Donahue[2] and van Middelkoop and Engelbertink[3] using the DSAM give lower limits of 1.4 and 7 psec, respectively. On the basis of a preliminary measurement which yielded a lifetime <300 psec, it was decided that the recoil distance method (RDM),[4] and not electronic timing, would be best suited for determining the lifetime of this level.

The present paper[5] describes the measurement of the lifetime of the 2.94-MeV level in ^{33}S using the RDM. The level was populated using the $^{30}Si(\alpha,n)^{33}S$ reaction at α-particle energies only slightly above the threshold energy (7.3 MeV).

EXPERIMENTAL PROCEDURE

A schematic drawing of the experimental setup is shown in Fig. 1. The plunger consists of a stainless-steel tube which slides inside a brass tube. The diameters of the two tubes differ by less than 5 μ. The dial indicator reads in units of 10 μ over a 1-cm range and measures the distance between the target and the silver stopper.

In preparing the targets, a procedure similar to the one described by Jones *et al.*[4] was employed to ensure that the target surface was flat. An O-ring was used to stretch a 1-μ Ni foil until it was mirror flat to the eye. SiO_2 (enriched to 95% in ^{30}Si) was then evaporated onto the downstream side of the foil. Two different target thicknesses were used: one ~35 $\mu g/cm^2$ (thin) and one ~125 $\mu g/cm^2$ (thick).

A beam of 0.2–0.3 μA of $^4He^{++}$ particles from the Triangle Universities Nuclear Laboratory FN Tandem was used at bombarding energies of 8.1 and 8.7 MeV. The effective beam energies (after correcting for the ~300-keV energy loss in the 1-μ Ni foil) were 7.8 and 8.4 MeV. Since the effective energy was 0.5–1.1 MeV above threshold, the re-

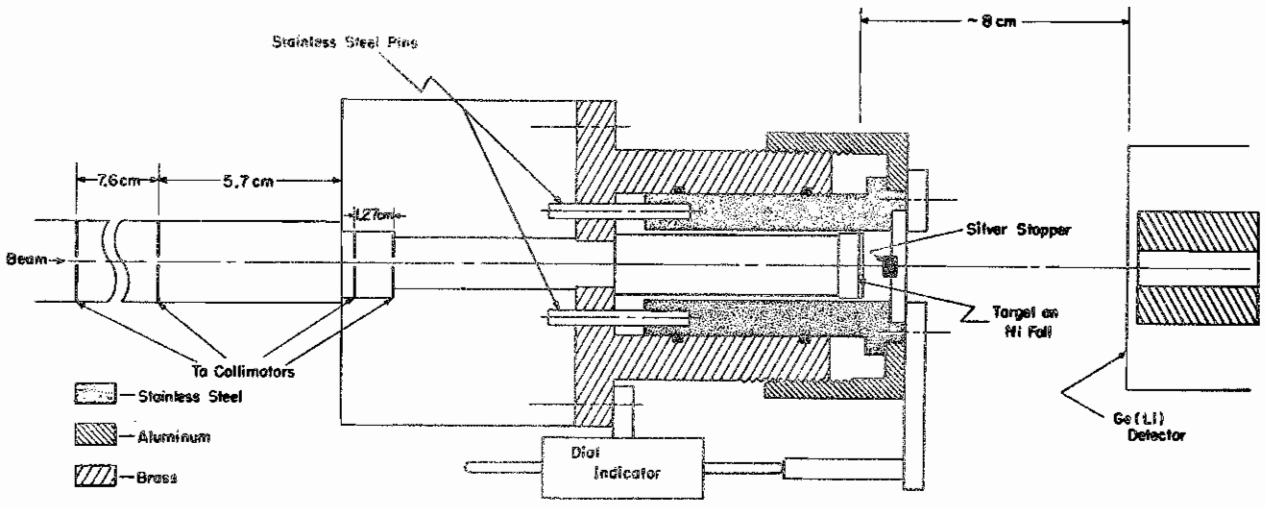

FIG. 1. Schematic drawing of the experimental setup showing the plunger, the collimating system, and the 30-cc Ge(Li) detector. The stainless-steel pins keep the stainless-steel tube from rotating as the plunger is being moved.

coiling nuclei were confined to a narrow cone about the beam axis with a half-angle <10°. These excited nuclei emerged from the target with some average velocity $\bar{v}$ and recoiled a variable distance D in a vacuum before being stopped by the plunger.

The γ rays from the excited nuclei were detected with a 30-cc Ge(Li) detector placed ~8 cm from the target and at 0° with respect to the beam direction. The resolution of the detector for 1.33-MeV γ rays was ~2.7 keV full width at half maximum. The data were recorded at various target-to-stopper distances using a 2048-channel ADC in conjunction with an on-line computer.[6]

ANALYSIS AND RESULTS

Sample spectra of the narrow unshifted peak and the broadened Doppler-shifted peak of the 2.94 – 0 MeV transition are shown in Fig. 2. These spectra were recorded using the thick target at a bombarding energy of 8.7 MeV. The intensities of the unshifted peaks I_0 and those of the Doppler-shifted peaks I_s were obtained by fitting the data with a function consisting of two Gaussians plus a quadratic background. The widths of the peaks were held constant from preliminary fits. The solid curves in the figure are examples of these fits. The intensities I_0 and I_s were used to obtain the experimental values of $R \equiv I_0/(I_0+I_s)$.

The average recoil velocity was calculated from the energy difference between the two peaks. The spread in the velocity was obtained from the width w_2 of the Doppler-shifted peak after subtracting the detector resolution as obtained from the width w_1 of the unshifted peak. The sums of all the data for each of the two experimental conditions are shown in Fig. 3. In Fig. 3(a), the spread in the velocity is very small because the beam energy is close to threshold and the target is thin. In Fig. 3(b), the thick target was used. The average recoil velocity is less than in Fig. 3(a), and the spread in the velocity is greater. The value of $\bar{v}/c$ in percent, as determined from the energy difference, is 0.703 ± 0.014 in part (a) and 0.604 ± 0.008 in part (b). Both of these values are consistent with those calculated from the kinematics assuming an isotropic angular distribution in the center of mass and taking the target thickness into account.

The experimental ratio R as a function of D is shown in Fig. 4. These data points were obtained

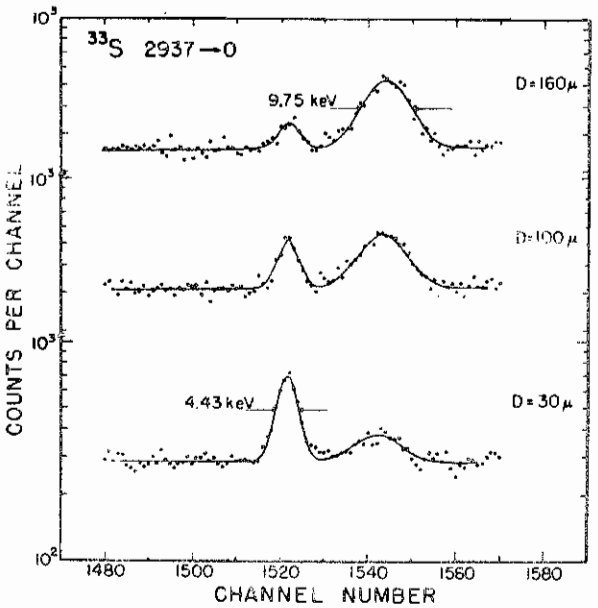

FIG. 2. The full-energy peak of the 2.94-MeV γ ray correspond to the 2.94-MeV → 0 transition in ^{33}S viewed at 0°. The level was populated in the ^{30}Si$(\alpha, n)^{33}$S reaction at E_α = 8.7 MeV using a 125-μg/cm^2 target. The narrow peak corresponds to the unshifted γ ray of energy $E_{\gamma 0}$, and the broadened peak corresponds to the Doppler-shifted peak of energy $E_{\gamma 0}(1+\bar{v}/c)$. The widths (full width at half maximum) of the two peaks are shown. The energy dispersion is 0.820 keV/channel. These representative spectra were recorded at three different target-to-plunger distances, and the dependence of the relative intensities on the distance is evident. The solid lines represent fits to the data.

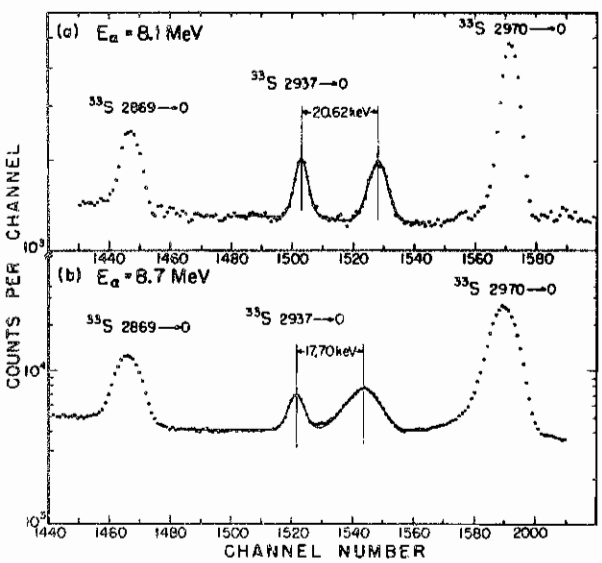

FIG. 3. Sum spectra for each of the two experimental conditions. In (a) the bombarding energy was 8.1 MeV and a 35-μg/cm^2 target was used. In (b) the bombarding energy was 8.7 MeV and a 125-μg/cm^2 target was used. The full-energy peaks of all three members of the ground-state branches of the triplet at 2.9 MeV are shown. The solid lines represent fits to the data for the two components of the 2.94-MeV γ ray. The energy dispersion in (a) is 0.817 keV/channel and in (b) is 0.820 keV/channel.

using the thin target at $E_\alpha = 8.1$ MeV. The boxes around the data points indicate the statistical uncertainty in R as well as an estimated uncertainty of ± 2 μ in the value of D. A least-squares fit was made to the data with the function

$$R = e^{-(D-D_0)/\bar{D}_m}, \quad (1)$$

where D_0 is the value of D at which $R = 1$, and D_M is the distance in which $1/e$ of the nuclei decay. The solid line in Fig. 4 represents this fit. The values of $\bar{D}_M$ and D_0 obtained from the fit are 94.45 ± 9.98 μ and 2.7 ± 6.0 μ, respectively, and correspond to a mean lifetime of 44.8 ± 4.8 psec.

A similar plot of R versus D is shown in Fig. 5. These points were obtained using the thick target at $E_\alpha = 8.7$ MeV. The dashed line represents a least-squares fit of the function in Eq. (1) to the data. This fit corresponds to a mean lifetime of 40.3 ± 1.9 psec. In order to include the large variation in the recoil velocity, a least-squares fit was made with the function

$$R = \sum A_n e^{-(D-D_0)/C_n\bar{D}_m}, \quad (2)$$

where $C_n = v_n/\bar{v}$, and v_n is a component of the recoil velocity. A_n is the fraction of the recoils that have the velocity v_n, and is determined by assuming that the velocity has a Gaussian distribution about $\bar{v}$ with a width $(w_2^2 - w_1^2)^{1/2}$. The solid line in Fig. 5 represents a fit of the function in Eq. (2) to the data. The values of $\bar{D}_m$ and D_0 obtained from the fit are 72.21 ± 3.18 μ and 1.8 ± 2.6 μ, respectively, and correspond to a mean lifetime of 39.9 ± 1.9 psec. No velocity-spread correction was necessary for the thin-target data.

The weighted average of the thin-target and thick-target results is 40.5 ± 1.8 psec. Additional corrections have been discussed in detail by Jones *et al.*[4] Briefly, the combined correction due to the contraction of the solid angle for recoiling ions, and the variation in the efficiency for the two peaks is ~0.5% and was neglected. The correction for the variation in the distance D is ~1% and is included in the final error.

No measurements were made on the attenuation of the angular distribution of the γ rays. Assuming that the attenuation is no larger than that observed by Jones *et al.*,[4] then an additional 2% uncertainty must be included in the lifetime. The mean lifetime including all of the above errors is 40.5 ± 2.0 psec.

DISCUSSION

The 2.94-MeV level in ^{33}S γ decays by two branches of approximately equal intensities. The branch to the ground state ($J^\pi = \frac{3}{2}^+$) is a mixture of $E3/M2$ radiations, while the branch to the state at 1.97 MeV ($J^\pi = \frac{5}{2}^+$) is a mixture of $M2/E1$ radiations. The mixing ratios given by Becker *et al.*[7]

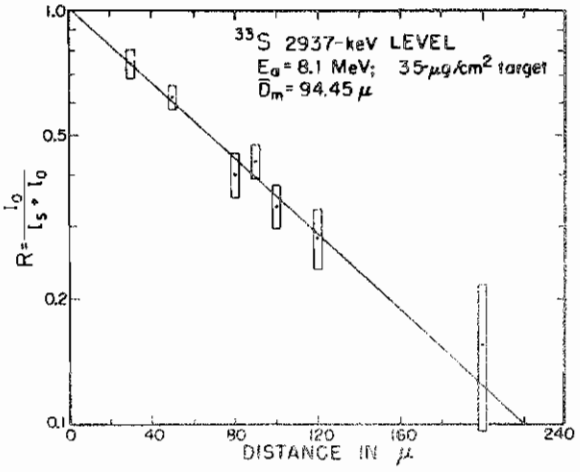

FIG. 4. The decay curve for the 2.94-MeV level in ^{33}S obtained under the conditions indicated. The ratio $I_0/(I_0+I_s)$ is plotted as a function of the plunger distance D. $\bar{D}_m = 94.45 \pm 9.98$ μ is the mean displacement from which the mean lifetime is found. The solid line represents a least-squares fit using the average recoil velocity $\bar{v}$. The mean lifetime determined from these data is 44.8 ± 4.8 psec.

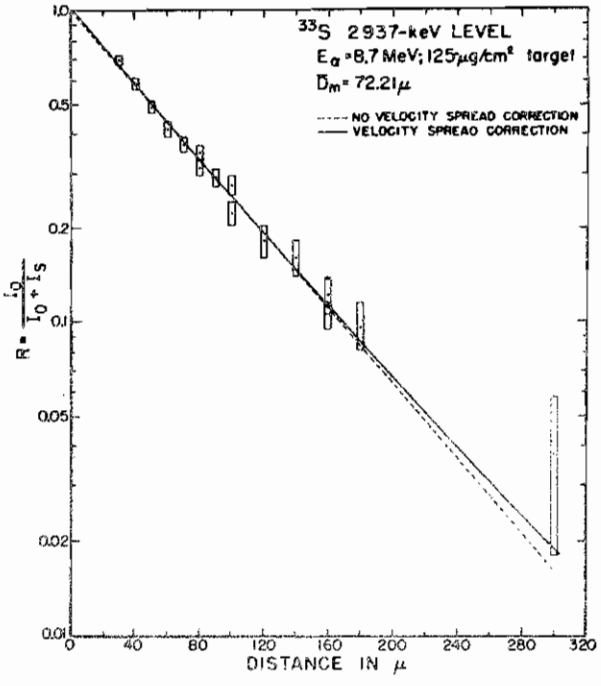

FIG. 5. The decay curve for the 2.94-MeV level in ^{33}S obtained under the conditions indicated. The ratio $I_0/(I_0+I_s)$ is plotted as a function of the plunger distance D. The dashed line represents a least-squares fit to the data using the average velocity $\bar{v}$ and corresponds to a mean lifetime of 40.3 ± 1.9 psec. The solid curve is a fit that includes the spread in the velocity. From the latter fit $\bar{D}_m = 72.21 \pm 3.18$ μ. This value of $\bar{D}_m$ corresponds to a mean lifetime of 39.9 ± 1.9 psec.

and by O'Dell *et al.*[8] are consistent with pure $E1$ for the branch to the second excited state. This branch thus has an $E1$ strength of 1.3×10^{-5} Weisskopf units[9] (W.u.). The average $E1$ strength given by Skorka, Hertel, and Retz-Schmidt[10] for $20 \leq A \leq 40$ is 1.5×10^{-3} W.u. The $E1$ strength for the 2.94 – 1.97-MeV transition in ^{33}S is, therefore, 2 orders of magnitude smaller than this average strength.

The mixing ratio for the 2.94 – 0 transition was not determined uniquely in either Ref. 7 or 8. The smaller mixing ratios from Ref. 7 (0.09 ± 0.27) and Ref. 8 (0.48 ± 0.09) yield $E3$ strengths between 0 and 40 W.u. The larger mixing ratios give $E3$ strengths >100 W.u.

During the course of this work we became aware of a measurement of the lifetime of this level by Brandolini and Signorini[11] using the DSAM with a Kr gas stopper. The value of τ from the DSA work is 38 ± 11 psec and is consistent with the present measurement. Jones *et al.*[4] obtained lifetimes in ^{22}Na using the RDM which were ~50% greater than those obtained from DSA measurements[12] using a C_2F_6 gas stopper. They pointed out that in some cases shielding effects may occur in polyatomic stopping gases. The DSA work by Brandolini and Signorini[11] was done with a monoatomic stopping gas. The agreement with the present result is much better than in the cases where the polyatomic stopper C_2F_6 was used.

ACKNOWLEDGMENTS

The authors would like to thank A. W. Lovette of the Duke University Instrument Shop for his help in designing and building the plunger. Thanks are also extended to Professor D. B. Fossan for a helpful discussion concerning the details of the RDM. One of the authors (N.R.R.) wishes to thank C. Signorini for communications regarding the work done at Padua, Italy.

---

†Work supported in part by the U. S. Atomic Energy Commission.

*Present address: University of Colorado, Boulder, Colorado.

[1]C. E. Ragan, III, C. E. Moss, R. V. Poore, N. R. Roberson, G. E. Mitchell, and D. R. Tilley, Phys. Rev. 188, 1806 (1969).

[2]J. E. Cummings and D. J. Donahue, private communication; Nucl. Phys. A142, 609 (1970).

[3]G. van Middelkoop and G. A. P. Englebertink, Nucl. Phys. A138, 601 (1969).

[4]K. W. Jones, A. Z. Schwarzschild, E. K. Warburton and D. B. Fossan, Phys. Rev. 178, 1773 (1969).

[5]C. E. Ragan, III, N. R. Roberson, C. E. Moss, C. R. Gould, G. E. Mitchell, and D. R. Tilley, Bull. Am. Phys. Soc. 15, 600 (1970).

[6]N. R. Roberson, R. V. Poore, F. Seibel, and J. Joyce, U. S. Atomic Energy Commission Report No. TID-4500, 1969 (unpublished), pp. 276 – 281.

[7]J. A. Becker, L. F. Chase, Jr., D. B. Fossan, and R. E. McDonald, Phys. Rev. 146, 761 (1966).

[8]J. M. O'Dell, R. W. Krone, and F. W. Prosser, Jr., Nucl. Phys. 82, 574 (1966).

[9]D. H. Wilkinson, in *Nuclear Spectroscopy*, edited by F. Ajzenberg-Selove (Academic Press Inc., New York, 1960), Part B, p. 862 ff.

[10]S. J. Skorka, J. Hertel, and T. W. Retz-Schmidt, Nucl. Data A2, 347 (1966).

[11]F. Brandolini and C. Signorini, Phys. Letters 30B, 342 (1969).

[12]A. E. Blaugrund, A. Fisher, and A. Schwarzschild, Nucl. Phys. A107, 411 (1968).

LIST OF REFERENCES

LIST OF REFERENCES

1. R. D. Evans, The Atomic Nucleus (McGraw-Hill Book Co., Inc., New York, 1955). Historical developments of the shell model are discussed in references 1 and 2. The development of the collective model is discussed in reference 3.
2. W. E. Meyerhof, Elements of Nuclear Physics (McGraw-Hill Book Co., Inc., New York, 1967).
3. V. H. Webb, unpublished Ph. D. dissertation, Duke University (1966).
4. A. Marelius, P. Sparrman, and T. Sundström in Hyperfine Structure and Nuclear Radiations, Editors: E. Matthias and D. A. Shirley (John Wiley and Sons, Inc., New York, 1968).
5. S. Devons, G. Manning, and D. St. Bunbury, Proc. Phys. Soc. (London) A68, 18 (1955).
6. D. St. Bunbury, S. Devons, G. Manning, and J. H. Towle, Proc. Phys. Soc. (London) A69, 165 (1956).
7. S. Devons, G. Manning, J. H. Towle, Proc. Phys. Soc. (London) A69, 173 (1956).
8. H. Fiedler and O. Tench, Germanium (Li) Gamma Spectrometer Systems (Camberra Industries, Inc., U. S. A., 1968).
9. P. W. M. Glaudemans, P. M. Endt, and A. E. L. Dieperink, to be published in Ann. Phys. (1970).
10. A. E. L. Dieperink and P. J. Brussaard, Nucl. Phys. A128, 34 (1969).
11. F. Tabakin, Ann. Phys. 30, 51 (1964).

12. C. E. Ragan, III, C. E. Moss, R. V. Poore, N. R. Roberson, G. E. Mitchell, and D. R. Tilley, Phys. Rev. 188, 1806 (1969).
13. C. E. Ragan, III, R. V. Poore, N. R. Roberson, G. E. Mitchell, and D. R. Tilley, Phys. Rev. 1C, 2012 (1970).
14. C. E. Ragan, III, C. E. Moss, C. R. Gould, N. R. Roberson, G. E. Mitchell, and D. R. Tilley, Phys. Rev. 2C, 557 (1970).
15. P. M. Endt and C. Van der Leun, Nucl. Phys. A105, 1 (1967).
16. B. Rosner and E. J. Schneid, Phys. Rev. 139, B66 (1965).
17. K. V. K. Iyengar, S. K. Gupta, B. Lal, and E. Kondaiah, Nucl. Phys. 76, 433 (1966).
18. D. R. Goosman and R. W. Kavanagh, Phys. Letters 24B, 507 (1967).
19. W. J. Naude, A. Bottega, and W. R. McMurray, Nucl. Phys. A114, 551 (1968).
20. P. W. M. Glaudemans, P. J. Brussaard, and G. A. P. Engelbertink, Bull. Am. Phys. Soc. 10, 92 (1965).
21. L. C. Biedenharn, G. B. Arfken, and M. E. Rose, Phys. Rev. 83, 586 (1951).
22. A. E. Litherland and A. J. Ferguson, Can. J. Phys. 39, 788 (1961).
23. A. E. L. Dieperink, private communication (1970).
24. B. H. Wildenthal, private communication (1970).
25. T. T. S. Kuo and G. E. Brown, Nucl. Phys. 85, 40 (1966).
26. K. W. Jones, A. Z. Schwarzschild, E. K. Warburton, and D. B. Fossan, Phys. Rev. 178, 1773 (1969).
27. J. Lindhard, M. Scharff, and H. E. Schiøtt, Kgl. Danske Videnskab. Selskab, Mat.-Fys. Medd. 33, No. 14 (1963).
28. J. Lindhard and M. Scharff, Phys. Rev. 124, 128 (1961).
29. E. K. Warburton, D. E. Alburger, and D. H. Wilkinson, Phys. Rev. 129, 2180 (1963).
30. E. K. Warburton, J. W. Olness, K. W. Jones, C. Chasman, R. A. Rastinen, and D. H. Wilkinson, Phys. Rev. 148, 1072 (1966).

31. J. W. Olness and E. K. Warburton, Phys. Rev. 151, 792 (1966).
32. E. K. Warburton, J. W. Olness, and A. R. Poletti, Phys. Rev. 160, 938 (1967).
33. A. E. Blaugrund, Nucl. Phys. 88, 501 (1966).
34. H. W. Lewis, Phys. Rev. 78, 526 (1950).
35. W. M. Currie, Nucl. Instr. Methods, 73, 173 (1969).
36. Nuclear Diodes, Inc., P. O. Box 135, Prairie View, Illinois 60069.
37. Camberra Industries, 50 Silver St., Middletown, Connecticut 06457.
38. Northern Scientific, Inc., 2551 West Beltline, P.O. Box 66, Middleton, Wisconsin 53562
39. N. R. Roberson, R. V. Poore, F. Seibel, and J. Joyce, U. S. Atomic Energy Commission Report No. TID-4500, 1969 (unpublished), pp. 276-281.
40. W. Whaling, in Handbuch der Physik, edited by S. Flügge (Springer-Verlag, Berlin, 1958), Vol. 34, p. 193.
41. G. R. Meredith and D. C. Camp, Bull. Am. Phys. Soc. 15, 478 (1970), and private communication.
42. F. Ingebretsen, T. K. Alexander, O. Häusser, and D. Pelte, Can. J. Phys. 47, 1295 (1969).
43. Nuclear Data, Editor: K. Way, B2, 5-85 (1968).
44. E. H. Auerbach, Brookhaven National Laboratory, unpublished report BNL 6562 (1962).
45. F. Perey and B. Buck, Nucl. Phys. 32, 353 (1962).
46. B. Buck and F. Perey, Phys. Rev. Letters 8, 444 (1962).
47. H. J. Rose and D. M. Brink, Rev. Mod. Phys. 39, 306 (1967).
48. A. A. Pilt, D. M. Sheppard, and P. J. Twin, University of Alberta unpublished report UAE-NPL-14 (1969).
49. W. G. Winn and D. G. Sarantites, Nucl. Instr. Methods 66, 61 (1968).
50. J. H. Ormrod and H. E. Duckworth, Can. J. Phys. 41, 1424 (1963).
51. J. H. Ormrod, J. R. MacDonald, and H. E. Duckworth, Can. J. Phys. 43, 275 (1965).

52. B. Fastrup, P. Hvelplund, and C. A. Sautter, Kgl. Danske Videnskab. Selskab, Mat.-Fys. Medd. 35, No. 10 (1966).
53. P. Hvelplund and B. Fastrup, Phys. Rev. 165, 408 (1968).
54. D. H. Wilkinson in Nuclear Spectroscopy, edited by F. Ajzenberg-Selove (Academic Press, Inc., New York, 1960) Part B, p. 852ff.
55. S. J. Skorka, J. Hertel, and T. W. Retz-Schmidt, Nucl. Data A2, 347 (1966).
56. P. W. M. Glaudemans, G. Wiechers, and P. J. Brussaard, Nucl. Phys. 56, 529 (1964); 56, 548 (1964).
57. P. W. M. Glaudemans, B. W. Wildenthal, and J. B. McGrory, Phys. Letters 21, 427 (1966).
58. R. Arvieu and S. A. Moszkowski, Phys. Rev. 145, 830 (1966).
59. B. H. Wildenthal, J. B. McGrory, E. C. Halbert, and P. W. M. Glaudemans, Phys. Letters 27B, 611 (1968).
60. P. W. M. Glaudemans, P. J. Brussaard, and B. H. Wildenthal, Nucl. Phys. A102, 593 (1967).
61. P. W. M. Glaudemans, A. E. L. Dieperink, R. J. Keddy, and P. M. Endt, Phys. Letters 28B, 645 (1969).
62. F. C. Erné, Nucl. Phys. 84, 91 (1966).
63. S. Maripuu and G. A. Hokken, Nucl. Phys. A141, 481 (1970).
64. G. A. P. Engelbertink and P. W. M. Glaudemans, Nucl. Phys. A123, 225 (1969).
65. E. K. Warburton and J. W. Olness, private communication (1968).
66. S. Goudsmit and J. L. Saunderson, Phys. Rev. 57, 24 (1940); 58, 36 (1940).
67. IBM System/360, Scientific Subroutine Package, Version II, unpublished, No. H20-0205-2 (1967).
68. J. Singer, Elements of Numerical Analysis (Academic Press, Inc., New York, 1964), pp. 281-293.

BIOGRAPHY

Charles E. Ragan, III

Personal:	Born October 19, 1944, Charleston, South Carolina
	Married; One Son; One Daughter
Education:	B.S. in Physics, The Citadel (1966)
Positions:	NDEA Fellow, Duke University, 1966-1969
	Research Assistant, Duke University 1969-1970
Memberships:	American Physical Society

Publications:

1. Mean Lifetimes and Branching Ratios of Low-Lying Levels in ^{33}S (with C. E. Moss, R. V. Poore, N. R. Roberson, G. E. Mitchell, and D. R. Tilley) Phys. Rev. 188, 1806 (1969).

2. Mean Lifetimes of Low-Lying Levels of ^{34}S (with R. V. Poore, N. R. Roberson, G. E. Mitchell, and D. R. Tilley) Phys. Rev. 1C, 2012 (1970).

3. Mean Lifetime of the 2.94-MeV Level in ^{33}S (with C. E. Moss, C. R. Gould, N. R. Roberson, G. E. Mitchell, and D. R. Tilley) Phys. Rev. 2C, 557 (1970).

Abstracts:

1. Lifetime Measurements of Low-Lying States in ^{33}S (with N. R. Roberson, C. E. Moss, R. V. Poore, G. P. Lamaze, G. E. Mitchell, and D. R. Tilley) Bull. Am. Phys. Soc. 14, 629 (1969).

2. Lifetime Measurements on Low-Lying States in ^{34}S (with N. R. Roberson, C. E. Moss, R. V. Poore, G. P. Lamaze, G. E. Mitchell, and D. R. Tilley) Bull. Am. Phys. Soc. 14, 1203 (1969).

3. Lifetime Measurement of the 2937-keV Level in ^{33}S (with N. R. Roberson, C. E. Moss, C. R. Gould, G. E. Mitchell, and D. R. Tilley) Bull. Am. Phys. Soc. 15, 600 (1970).